

รายงานวิจัยฉบับสมบูรณ์

โครงการ "การศึกษาโครงสร้างเชิงอิเล็กทรอนิกส์ของ
อุปกรณ์โมเลกุลด้วยการตรวจสอบแผ่นฟิล์มบางอินทรีย์
และคอมพิวเตอร์โมเดลลิง"

โดย ผศ.ดร.ธนากร โอสถจันทร์ และ คณะ

30 พศจิกายน 2553

รายงานวิจัยฉบับสมบูรณ์

โครงการ "การศึกษาโครงสร้างเชิงอิเล็กทรอนิกส์ของ
อุปกรณ์โมเลกุลด้วยการตรวจสอบแผ่นฟิล์มบางอินทรีย์
และคอมพิวเตอร์โมเดลลิง"

ผศ.ดร. ธนากร โอสถจันทร์ ผศ.ดร. ธีรเกียรติ์ เกิดเจริญ ผศ.ดร. เติมศักดิ์ ศรีคิรินทร์

ดร.อุดม รอบคอบ

หน่วยสร้างเสริมศักยภาพทางนาโนศาสตร์และนาโนเทคโนโลยี
ภาควิชาฟิสิกส์ คณะวิทยาศาสตร์ มหาวิทยาลัยมหิดล
สนับสนุนโดยสำนักงานกองทุนสนับสนุนการวิจัย
(ความเห็นในรายงานนี้เป็นของผู้วิจัย สกว. ไม่จำเป็นต้องเห็นด้วยเสมอไป)

กิตติกรรมประกาศ

งานวิจัยนี้ได้รับการสนับสนุนโดย สำนักงานกองทุนสนับสนุนการวิจัย

Project Code: BRG/21/2544

Project Title: A Study of Electronic Structures of Molecular Devices by Organic Thin Film

Examination and Computer Modeling

Investigator : Asst.Prof. Tanakorn Osotchan

Asst.Prof. Teerakiat Kerdcharoen

Asst.Prof. Toemsak Srikirin,

Dr. Udom Robkob

Capability Building Unit for NanoScience and Nanotechnology, Mahidol University

E-mail Address: sctos@mahidol.ac.th

Project Period: 15 June 2001 to 30 November 2010

In this research project, the electronic structure of molecular devices for carbon nanotube was investigated by molecular computer simulation. The effect of end of nanotube was evaluated. Hydrogen bonds were added in case of open end while the half sphere surface similar to that in C60 molecule was used at the end of capped nanotube. The carbon bond lengths in these open and capped carbon nanotubes were modified depending on the chiral vector index (n,m). In order to understand the application of carbon nanotube in high efficiency lithium ion battery, the interactions between a lithium ion or lithium atom and carbon nanotube was examined by placing the lithium ion or atom at various positions both inside and outside carbon nanotube. It was found that along the radius direction there are some particular positions which exhibit relatively low energy. This position can probably be the place for trapping the lithium ion with carbon nanotube. By varying the position along the nanotube axis, it indicates the possibility of transfer the lithium ion or atom in and out carbon nantube.

This research project was also studied the electronic structure of highly molecular order thin film which prepared by LB technique. The highly molecular order can be achieved by the hydrophobic and hydrophilic behaviors at each end of the molecule. However in order to achieve the applicable thin film fabrication process and applicable products, the electrical conduction in conjugated polymer molecules was investigated for their potential application in new marketing of plastic electronics. The thin film was prepared by spin coating technique which can be applied to the mass production in the industrial scale. Polyphenelene-vinylene, polyfluorene and its copolymer were conjugate polymer molecules used in this study. During the current pass through these polymer layers, the red and blue light can emit from these polymer molecules, respectively. The calculated electronic structure of conjugated polymer can be used to determine the wavelength of emitted light. The molecular modeling can also be used to indicate the stability of these polymer molecules.

Keywords: Electronic structure, Molecular Device, Organic thin film

รหัสโครงการ : BRG/21/2544

ชื่อโครงการ : การศึกษาโครงสร้างเชิงอิเล็กทรอนิกส์ของอุปกรณ์โมเลกุลด้วยการตรวจสอบแผ่นฟิล์ม

บางอินทรีย์และคอมพิวเตอร์โมเดลลิง

ชื่อนักวิจัย :ผศ.ดร. ธนากร โอสถจันทร์ ผศ.ดร. ธีรเกียรติ์ เกิดเจริญ

ผศ.ดร. เติมศักดิ์ ศรีคิรินทร์ ดร.อุดม รอบคอบ

หน่วยสร้างเสริมศักยภาพทางนาโนศาสตร์และนาโนเทคโนโลยี คณะวิทยาศาสตร์ มหาวิทยาลัยมหิดล ระยะเวลาโครงการ: 15 มิถุนายน 2544 ถึงวันที่ 30 พฤศจิกายน 2553

ในโครงการวิจัยนี้ ได้ทำการศึกษาโครงสร้างเชิงอิเล็กทรอนิกส์ของท่อคาร์บอนนาโนด้วยการ คำนวณแบบจำลองโมเลกุลด้วยคอมพิวเตอร์ ได้มีการศึกษาผลของปลายท่อที่มีลักษณะเปิดด้วยการเพิ่ม พันธะไฮโดรเจนและการสร้างท่อปลายปิดด้วยโครงสร้างคล้ายครึ่งทรงกลมของโมเลกุล C60 ได้พบว่า การปิดและเปิดปลายท่อมีผลต่อความยาวพันธะคาร์บอนภายในของท่อนาโนและโครงสร้างเชิง อิเล็กทรอนิกส์ก็มีการเปลี่ยนแปลงด้วย ซึ่งขึ้นกับดัชนี (n, m) ของท่อคาร์บอนนาโน จากนั้นจึงได้ ศึกษาอันตรกิริยาของลิเทียมอะตอมและลิเทียมอิออนที่วางในตำแหน่งต่าง ๆ ทั้งข้างนอกและข้างในท่อ คาร์บอนนาโนเพื่อช่วยทำให้มีความเข้าใจในการประยุกต์ใช้ท่อคาร์บอนนาโนเป็นตัวเก็บประจุไฟฟ้าใน ลิเทียมแบตเตอรี่ประสิทธิภาพสูง โดยพบว่าการวางตามแนวรัศมีของท่อนาโนจะมีตำแหน่งเฉพาะบาง ค่าที่จะทำให้ท่อคาร์บอนนาโนมีพลังงานต่ำกว่าบริเวณอื่น ซึ่งน่าจะเป็นตำแหน่งที่สามารถกักเก็บ ลิเทียมอิออนในโครงสร้างท่อคาร์บอนนาโนได้ การศึกษาตำแหน่งของลิเทียมในแนวแกนโมเลกุลท่อ คาร์บอนนาโนจะทำให้สามารถทราบความเป็นไปได้ของการเลื่อนเข้าออกของลิเทียมใด้

ในโครงการวิจัยนี้ยังได้มีการศึกษาโครงสร้างเชิงอิเล็กทรอนิกส์ของอุปกรณ์โมเลกุลด้วยการ ตรวจสอบสมบัติของแผ่นฟิล์มบางอินทรีย์ที่เตรียมให้มีการเรียงตัวของโมเลกุลอย่างเป็นระเบียบด้วย เทคนิคการเตรียมฟิล์มแบบ LB ซึ่งมีการควบคุมการจัดเรียงตัวของโมเลกุลด้วยสมบัติการชอบและไม่ ชอบน้ำในปลายแต่ละด้านของโมเลกุล ทำให้สามารถกำหนดจำนวนและทิศทางของการจัดวางโมเลกุล ได้ อย่างไรก็ตามในการประยุกต์ใช้ได้จริงได้มีการศึกษาสมบัติการนำไฟฟ้าของโมเลกุลสายโช่คอนจู เกตพอลิเมอร์ที่สามารถนำไฟฟ้าได้ด้วยการเตรียมฟิล์มบางโดยวิธีสปินเคลือบ ซึ่งเป็นวิธีการที่สามารถ ประยุกต์ใช้ได้กับระบบการผลิตในอุตสาหกรรม โดยได้ศึกษาการนำไฟฟ้าของคอนจูเกตพอลิเมอร์ฟินิ ลีนวินิลีน และพอลิฟูลออรีน รวมทั้งพอลิเมอร์ประกอบ ซึ่งชั้นฟิล์มบางพอลิเมอร์เหล่านี้เมื่อมีการนำไฟฟ้าจะสามารถเปล่งแสงสีแดงและสีน้ำเงินออกจากโมเลกุลเหล่านี้ได้ตามลำดับ การคำนวณ โครงสร้างเชิงอิเล็กทรอนิกส์ของโมเลกุลพอลิเมอร์เหล่านี้ จะสามารถใช้ประมาณความยาวคลี่นของแสง ที่เปล่งออกมาได้จากค่าความแตกต่างระหว่างระดับพลังงาน นอกจากนั้นการคำนวณแบบจำลอง โมเลกุลยังใช้เป็นตัวกำหนดความเสถียรของโมเลกุลพอลิเมอร์เหล่านี้ได้อีกด้วย คำหลัก : โครงสร้างเชิงอิเล็กทรอนิกส์ อุปกรณ์โมเลกุล ฟิล์มบางอินทรีย์



การเปล่งแสงจากอุปกรณ์อินทรีย์เปล่งแสงซึ่งทำด้วยฟิล์มบางคอนจูเกต พอลิเมอร์ชนิดต่างเป็นแพทเทิร์น สกว หลังจาการผ่านกระแสไฟฟ้า

บทน้ำ

ในโครงการวิจัยการศึกษาโครงสร้างเชิงอิเล็กทรอนิกส์ของอุปกรณ์โมเลกุลนี้ ได้ทำการศึกษา โครงสร้างเชิงอิเล็กทรอนิกส์ของหลายระบบอุปกรณ์โมเลกุล โดยได้ศึกษาโครงสร้างเชิงอิเล็กทรอนิกส์ของท่อคาร์บอนนาโนด้วยการคำนวณแบบจำลองโมเลกุลด้วยคอมพิวเตอร์ ได้ศึกษาโครงสร้างเชิง อิเล็กทรอนิกส์และการนำไฟฟ้าของโมเลกุลที่มีการจัดเรียงอย่างมีระเบียบในฟิล์มบางอินทรีย์ และได้มี การศึกษาโครงสร้างเชิงอิเล็กทรอนิกส์ของสายโซ่โมเลกุลคอนจูเกตพอลิเมอร์ทั้งจากการนำไฟฟ้าและ การเปล่งแสง

ในการดำนวณแบบจำลองโมเลกุลของท่อคาร์บอนนาโนด้วยคอมพิวเตอร์นั้น โดยข้อจำกัดของ
การคำนวณจึงต้องทำการประมาณสมบัติท่อคาร์บอนนาโนขนาดยาวอนันต์ด้วยท่อคาร์บอนนาโนที่มี
หน่วยย่อยซ้ำ ๆ กันจำนวนเพิ่มขึ้นเรื่อย ๆ ได้มีการศึกษาผลของปลายท่อที่มีลักษณะเปิดด้วยการเพิ่ม
พันธะไฮโดรเจนและการสร้างท่อปลายปิดด้วยโครงสร้างคล้ายครึ่งทรงกลมของโมเลกุล C60 ได้พบว่า
การปิดและเปิดปลายท่อมีผลต่อความยาวพันธะคาร์บอนภายในของท่อนาโนและโครงสร้างเชิง
อิเล็กทรอนิกส์ก็มีการเปลี่ยนแปลงด้วย ซึ่งขึ้นกับดัชนี (n, m) ของท่อคาร์บอนนาโนที่ค่าต่าง ๆ กัน
ด้วย จากนั้นจึงได้ศึกษาอันตรกิริยาของลิเทียมอะตอมและลิเทียมอิออนที่มีต่อท่อคาร์บอนนาโนเพื่อ
ช่วยทำให้มีความเข้าใจในการประยุกต์ใช้ท่อคาร์บอนนาโนเป็นตัวเก็บประจุไฟฟ้าในลิเทียมแบตเตอรี่
ประสิทธิภาพสูง โดยได้ศึกษาผลของการวางลิเทียมอะตอมและอิออนในดำแหน่งต่าง ๆ ทั้งข้างนอก
และข้างในท่อคาร์บอนนาโน โดยพบว่าการวางตามแนวรัศมีของท่อนาโนจะมีตำแหน่งเฉพาะบางค่าที่
จะทำให้ท่อคาร์บอนนาโนมีพลังงานต่ำกว่าบริเวณอื่น ซึ่งน่าจะเป็นตำแหน่งที่สามารถกักเก็บลิเทียมอิออนในโครงสร้างท่อคาร์บอนนาโนได้ การศึกษาตำแหน่งของลิเทียมในแนวแกนโมเลกุลท่อคาร์บอนนาโนจะทำให้สามารถทราบความเป็นไปได้ของการเลื่อนเข้าออกของลิเทียมได้ ในการศึกษาแบบจำลอง
ให้ใกล้เคียงกับสภาวะจริงได้มีการขยายการศึกษาอันตรกิริยาของระบบกลุ่มลิเทียมอิออนที่วางใน

ตำแหน่งต่าง ๆ ทั้งในและรอบท่อคาร์บอนนาโน พร้อมทั้งคำนวณหาระยะห่างระหว่างลิเทียมแต่ละอิออ นด้วย

ในส่วนการศึกษาโครงสร้างเชิงอิเล็กทรอนิกส์ของอุปกรณ์โมเลกุลด้วยการตรวจสอบสมบัติของ
แผ่นฟิล์มบางอินทรีย์ ได้ศึกษาสมบัติการนำไฟฟ้าของโมเลกุลในแผ่นฟิล์มบางอินทรีย์ที่เตรียมให้มีการ
เรียงตัวของโมเลกุลอย่างเป็นระเบียบตัวยเทคนิคการเตรียมฟิล์มแบบ LB ซึ่งมีการควบคุมการจัดเรียง
ตัวของโมเลกุลด้วยสมบัติการชอบและไม่ชอบน้ำในปลายแต่ละด้านของโมเลกุล ทำให้สามารถกำหนด
จำนวนและทิศทางของการจัดวางโมเลกุลได้ อย่างไรก็ตามเพื่อให้สามารถนำการศึกษาการเตรียมฟิล์ม
บางอินทรีย์และการตรวจวัดนี้ไปประยุกต์ใช้ได้จริงจึงมีการศึกษาสมบัติการนำไฟฟ้าของโมเลกุลสายโช่
คอนจูเกตพอลิเมอร์ที่สามารถนำไฟฟ้าได้ด้วยการเตรียมฟิล์มบางโดยวิธีสปินเคลือบ ซึ่งเป็นวิธีการที่
สามารถประยุกต์ใช้ได้กับระบบการผลิตในอุตสาหกรรม โดยได้ศึกษาการนำไฟฟ้าของคอนจูเกตพอลิ
เมอร์ฟินิลีนวินิลีน และพอลิฟูลออรีน รวมทั้งพอลิเมอร์ประกอบ ซึ่งชั้นฟิล์มบางพอลิเมอร์เหล่านี้เมื่อมี
การนำไฟฟ้าจะสามารถเปล่งแสงสีแดงและสีน้ำเงินออกจากโมเลกุลเหล่านี้ได้ตามลำดับ การคำนวณ
โครงสร้างเชิงอิเล็กทรอนิกส์ของโมเลกุลพอลิเมอร์เหล่านี้ จะสามารถใช้ประมาณความยาวคลื่นของแสง
ที่เปล่งออกมาได้จากค่าความแตกต่างระหว่างระดับพลังงาน LUMO และ HOMO ได้ นอกจากนั้นการ
คำนวณแบบจำลองโมเลกุลยังใช้เป็นตัวกำหนดความเสถียรของโมเลกุลพอลิเมอร์เหล่านี้ได้อีกด้วย

โครงสร้างเชิงอิเล็กทรอนิกส์ของท่อคาร์บอนนาโน

ท่อคาร์บอนนาโนจะประกอบด้วยโครงข่ายหกเหลี่ยมของอะตอมคาร์บอน ที่ม้วนโค้งเป็นผิวท่อ
ขนาดเล็กเส้นผ่านศูนย์กลางไม่กี่นาโนเมตร ท่อคาร์บอนนาโนที่มีการเตรียมได้ส่วนมากจะเกิดจากการ
ม้วนของโครงข่ายคาร์บอนจำนวนหลายชั้น และสามารถมีความยาวได้หลายไมโครเมตร การคำนวณ
โครงสร้างเชิงอิเล็กทรอนิกส์สามารถประมาณได้จาการพิจารณาท่อคาร์บอนนาโนมีขนาดยาวอนันต์
โดยมีลักษณะเหมือนโครงผลึกในแนวหนึ่งมิติ ที่มียูนิตเซลซ้ำ ๆ กันไปตามแนวท่อคาร์บอนนาโน ด้วย
การพิจารณาเป็นโครงสร้างผลึกหนึ่งมิติจะทำให้สามารถใช้ทฤษฎีแถบพลังงานประยุกต์ในการ
คำนวณหาโครงสร้างแถบพลังงานของท่อคาร์บอนนาโนได้

เมื่อพิจารณาการม้วนท่อคาร์บอนนาโน จากแผ่นระนาบโครงข่ายคาร์บอนหกเหลี่ยม พบว่า จะ สามารถสร้างท่อคาร์บอนนาโนให้มีโครงสร้างได้แตกต่างกัน ตามมุมเอียงของการบรรจบรอบของการ ม้วน มุมเอียงของการม้วนบรรจบนี้จะใช้เป็นพารามิเตอร์ในการกำหนดโครงสร้างของท่อคาร์บอนนาโน ด้วยคู่ลำดับ (n, m) ตัวอย่างเช่น ท่อคาร์บอนนาโน (9, 0) จะเกิดจากการม้วนโครงสร้างแกรไฟต์ใน แนวตั้งฉาก โดยมีวงคาร์บอนหกเหลี่ยมจำนวน 9 วง ตามแนวผิวรอบท่อ ในขณะที่ท่อคาร์บอนนาโน (5, 5) จะเกิดจากการม้วนโครงสร้างแกรไฟต์ในแนวซิกแซก ที่มีวงหกเหลี่ยมคาร์บอนในแนวตั้งฉากและ แนวขนานกับการม้วน เป็นจำนวนแนวละ 5 วง ด้วยโครงสร้างท่อนาโนที่มีค่า (n, m) ต่างๆ จะทำให้ ได้ท่อคาร์บอนนาโนที่มีสมบัติทางโครงสร้างอิเล็กทรอนิกส์ที่แตกต่างกัน จากการคำนวณโครงสร้าง แถบพลังงานของท่อคาร์บอนนาโนโดยใช้พารามิเตอร์ค่าเดียวกับในโครงสร้างผลึกแกรไฟต์ ได้แสดงให้ เห็นว่า ท่อคาร์บอนนาโน (10, 0) และ (11, 0) ประพฤติตัวเป็นสารกึ่งตัวนำที่มีช่องแถบพลังงาน ประมาณ 0.2 eV ในขณะที่ท่อคาร์บอนนาโน (9, 0) และ (12, 0) จะไม่มีช่องว่างแถบพลังงาน นั้นคือ

จะประพฤติตัวเหมือนแถบพลังงานในโลหะ และมีลักษณะแถบที่ใกล้พลังงานศูนย์นี้เป็นแนวเส้นตรงที่จุด สมมาตราสูงในมิติเวกเตอร์คลื่น ท่อคาร์บอนนาโน (9, 9), (10, 10) และ (11, 11) แสดงช่องว่างแถบ พลังานเป็นศูนย์เช่นกันแต่เกิดขึ้นในตำแหน่งที่ไม่ใช่ตำแหน่งที่มีสมมาตราสูงดังเช่นในท่อคาร์บอนนาโน (9, 0), (10, 0)

การคำนวณโครงสร้างเชิงอิเล็กทรอนิกส์ของท่อคาร์บอนนาโน ด้วยทฤษฎีของแถบพลังงาน จะ ให้ผลสอดคล้องกับกรณีของท่อคาร์บอนนาโนที่มีโครงสร้างผลึกสมบูรณ์ตลอดความยาวท่อที่ยาวอนันต์ แต่ในท่อคาร์บอนนาโนที่สังเคราะห์ได้มีความยาวจำกัดและความยาวของพันธะอาจมีค่าแตกต่างกัน โดยเฉพาะการนำท่อคาร์บอนนาโนมาใช้เป็นอุปกรณ์โมเลกุล จำเป็นต้องมีการศึกษาสมบัติและ โครงสร้างของท่อคาร์บอนนาโนในลักษณะความยาวจำกัด

ในงานวิจัยนี้ได้ดำเนินการศึกษาโครงสร้างเชิงอิเล็กทรอนิกส์ของท่อคาร์บอนนาโนที่มีความ จำกัด โดยใช้ทฤษฎีฟังก์ชั่นความหนาแน่น ซึ่งเป็นทฤษฎีที่ใช้ฟังก์ชั่นความหนาแน่นในการคำนวณค่า พลังงานของโมเลกุลแทนการใช้ฟังก์ชั่นคลื่น ทำให้สามารถลดจำนวนเทอมที่ใช้ในฟังก์ชั่นเมื่อต้อง คำนวณระบบที่มีจำนวนอิเล็กตรอนจำนวนมากได้ นอกจากนี้การคำนวณด้วยทฤษฎีดังกล่าวจะไม่ได้ใช้ พารามิเตอร์ที่มาจากการวัดสมบัติของโมเลกุล หากแต่มีการกำหนดเพียงจำนวนอิเล็กตรอนที่มีในแต่ละ ชาตุเท่านั้น ทำให้ได้ผลการคำนวณที่เป็นที่ยอมรับแต่ต้องใช้เวลาในการคำนวณนานมาก จึงเป็น ข้อจำกัดให้ไม่สามารถคำนวณโมเลกุลท่อคาร์บอนนาโนที่มีขนาดยาวมากได้

ในชั้นต้นได้ศึกษาความยาวพันธะที่เปลี่ยนแปลงไป ในบริเวณปลายท่อของโมเลกุล โดยได้ ศึกษาในกรณีที่โมเลกุลท่อคาร์บอนนาโน มีปลายปิดด้วยโครงข่ายคาร์บอนครึ่งทรงกลม ลักษณะคล้าย กับในโครงสร้างโมเลกุลของ C60 ซึ่งต้องประกอบด้วยโครงข่ายห้าเหลี่ยม เพื่อให้เกิดการโค้งปิด โครงข่ายคาร์บอนห้าเหลี่ยมเหล่านี้จะทำให้เกิดความบกพร่องในโครงสร้างเชิงอิเล็กทรอนิกส์ของโมเลกุล และทำให้ความยาวพันธะในโครงข่ายหกเหลี่ยม ในส่วนของท่อนาโนทรงกระบอกเปลี่ยนไป ด้วย นอกจากนั้นได้ศึกษาโมเลกุลท่อคาร์บอนนาโนที่มีปลายเปิด ที่ทำการสมดุลพันธะของอะตอมคาร์บอนที่ ปลายโมเลกุลท่อด้วยอะตอมไฮไดรเจน เนื่องจากในสภาวะการเตรียมท่อคาร์บอนนาโนส่วนมากจะมี

ไอโดรเจนในบรรยากาศโดยรอบ ซึ่งอาจจะมาจากแกสไฮโดรเจนที่ใส่เข้าไปโดยตรง หรือจากการ
แยกตัวจากแกสไฮโดรดาร์บอนต่างๆ ที่ใช้เป็นแหล่งกำเนิดอะตอมคาร์บอน โมเลกุลปลายเปิดเหล่านี้
จะเกิดความบกพร่องบริเวณพันธะระหว่างคาร์บอนกับไฮโดรเจนบริเวณปลายท่อ ทำให้โดรงสร้างเชิง
อิเล็กทรอนิกส์และความยาวพันธะมีลักษณะที่เปลี่ยนไป เนื่องจากท่อดาร์บอนนาโนมีโดรงสร้างการ
จัดเรียงอะตอมที่แตกต่างกันตามมุมเอียง (n, m) จึงได้ศึกษาผลของปลายปิดและปลายเปิดที่มีต่อ
โครงสร้างเชิงอิเล็กทรอนิกส์ และโดรงสร้างความยาวพันธะในโมเลกุลท่อดาร์บอนนาโนที่มีพารามิเตอร์
มุมเอียงต่างๆ ได้ศึกษาโครงสร้างเหล่านี้ในโมเลกุลท่อดาร์บอน ที่มีเส้นผ่านศูนย์กลางต่างๆที่มีมุมเอียง
ในแนวเดียวกัน และเปรียบเทียบโครงสร้างที่มุมเอียงต่างกันแต่มีเส้นผ่านศูนย์กลางใกล้เคียงกันด้วย
ผลจากการคำนวณระดับพลังงานในโมเลกุลท่อดาร์บอนนาโนที่เปลี่ยนความยาวท่อ พบว่าระดับพลังงาน
ของสถานะ LUMO และ HOMO จะมีค่าลู่เข้า ค่าของช่องว่างแถบ พลังงานที่เต่กต่างกัน เมื่อ
ความยาวของโมเลกุลท่อยาวน้อยกว่า 5 ยูนิตเซล และความยาวของพันธะจะมีค่าเปลี่ยนไปใน
บริเวณปลายท่อประมาณ 3 – 4 ยูนิตเซลจากปลายท่อ โดยท่อปลายเปิดจะมีความยาวพันธะที่
เปลี่ยนไปมากกว่าโมเลกุลท่อคาร์บอนนาโนปลายปิด

การประยุกต์อย่างหนึ่งของท่อคาร์บอนนาโนนั้น ได้มีการเสนอให้ใช้เป็นตัวเก็บประจุลิเทียมใน แบตเตอรี่ที่มีประสิทธิภาพสูง ในงานวิจัยนี้จึงได้ขยายการศึกษาโครงสร้างเชิงอิเล็กทรอนิกส์ของท่อ คาร์บอนนาโน มาศึกษา ผลของโครงสร้างต่อลิเทียมอิออนที่กระจายอยู่ในท่อคาร์บอนนาโน โดย ได้ศึกษาอันตรกิริยาของลิเทียมอิออนที่ตำแหน่งต่าง ๆ ใน และ บริเวณข้างโมเลกุลท่อคาร์บอนนาโน ใน แนวรัศมีที่ระยะต่าง ๆ จากแนวกลางท่อไปยังผิวของท่อ และ ทะลุออกไปบริเวณรอบนอกของท่อ คาร์บอนนาโน แนวการเลื่อนที่สมมาตราได้กำหนดตามแนวผ่านทะลุแนวกลางวงหกเหลี่ยมของ เครือข่ายคาร์บอนและผ่านตามแนวพันธะของเครือข่ายคาร์บอน ซึ่งพบว่าบริเวณใกล้ๆ กับผิวผนังท่อ จะมีบริเวณที่พลังงานต่ำกว่าบริเวณอื่น ซึ่งน่าจะเป็นตำแหน่งที่สามารถกักเก็บลิเทียมอิออนใน โครงสร้างโมเลกุลท่อคาร์บอนนาโนได้

นอกจากการศึกษาอันตรกิริยาในแนวรัศมีของท่อคาร์บอนนาโนแล้ว ยังได้ศึกษาอันตรกิริยา ระหว่างลิเทียมอิออนที่วางไว้ตามตำแหน่งต่าง ๆ ในแนวแกนโมเลกุลท่อคาร์บอนนาโน เพื่อศึกษา ความเป็นไปได้ของการเลื่อนเข้าของลิเทียมอิออน เข้ามายังตำแหน่งกลางโมเลกุลท่อคาร์บอนนาโน ทั้งนี้ได้ศึกษาอันตรกิริยาที่เกิดขึ้นในโมเลกุลคาร์บอนนาโนที่มีขนาดและมุมเอียงต่าง ๆ

จากการศึกษาอันตรกิริยาของลิเทียมอิออนกับท่อคาร์บอนนาโนในเบื้องต้นนั้น เป็นการศึกษา ลิเทียมอิอนเดียว แต่ในสภาวะจริงจำเป็นต้องมีการกักเก็บลิเทียมอิอนจำนวนมากในหนึ่งโมเลกุลท่อ คาร์บอนนาโน จึงได้ขยายการศึกษาในระบบที่ประกอบด้วยลิเทยมสองอิออนในตำแหน่งต่างๆ ทั้งใน และบริเวณรอบข้างท่อคาร์บอนนาโน เพื่อศึกษาอันตรกิริยาทั้งระหว่างอิออนลิเทียมกับโมเลกุลท่อ คาร์บอนนาโน และระหว่างอิออนลิเทียมทั้งสองที่ระยะห่างระหว่างลิเทียมอิออนต่างๆ

โครงสร้างเชิงอิเล็กทรอนิกส์และการนำไฟฟ้าของ

โมเลกุลที่จัดเรียงอย่างเป็นระเบียบ

การประยุกต์ที่สำคัญของอุปกรณ์โมเลกุลนั้น มีความมุ่งมั่นที่จะประยุกต์ใช้สมบัติการนำไฟฟ้า ของแต่ละโมเลกุล งานวิจัยในส่วนนี้จึงได้ศึกษาโครงสร้างเชิงอิเล็กทรอนิกส์ของโมเลกุลที่มีสมบัติการ ให้และ/หรือรับอิเล็กตรอน แล้วทำการศึกษาการตรวจวัดการนำไฟฟ้าของโมเลกุลเหล่านี้ด้วยเทคนิค การวัดแบบต่าง ๆ โดยได้ศึกษาการเตรียมฟิล์มบางของชั้นโมเลกุลที่กำหนดแนวการวางตัวของโมเลกุล ได้ ด้วยเทคนิคการเตรียมฟิล์มแบบ LB โดยการเติมโมเลกุลสารจำนวนน้อย ๆ ลงบนน้ำ แล้วเลื่อน แผ่นปาดโมเลกุลที่ลอยน้ำ ให้เรียงตัวแน่น ด้วยการตรวจวัดแรงดันพื้นผิว

ความเสถียรของโมเลกุลสามารถตรวจสอบได้ด้วยการยึดแผ่นเลื่อนให้คงที่ และวัดการ เปลี่ยนแปลงของแรงดันพื้นผิวตลอดระยะเวลาหนึ่ง เพื่อให้แน่ใจว่าระหว่างการย้ายฟิล์มจากบนผิวน้ำลง บนแผ่นฐานรองนั้น โมเลกุลจะไม่ลัม และ/หรือมีความหนาแน่นของโมเลกุลพอดี การเลื่อนแผ่นปาดให้ แคบเกินไปจะทำให้โมเลกุลซ้อนทับเป็นชั้นที่สอง จึงต้องปรับไม่ให้มีการเลื่อนที่มากกว่าแรงดันผิวค่านี้ แผ่นฐานรองต้องมีการเตรียมพื้นผิวให้สภาวะการชอบหรือไม่ชอบน้ำตามแต่ลักษณะฟิล์มที่ต้องการก่อน

โดยปกติถ้าต้องการวัดสมบัติทางไฟฟ้าของโมเลกุล แผ่นฐานรองจะเคลือบด้วยวัสดุนำไฟฟ้า เช่นอลูมิเนียมหรือทองคำ หรือใช้แผ่นผลึกซิลิกอนที่ได้โดปให้สามารถนำไฟฟ้าได้ดี ขั้วไฟฟ้า ด้านบนสามารถทำได้โดยการระเหยโลหะนำไฟฟ้าเหล่านี้ ในระบบสุญญากาศที่ป้องกันไม่ให้ชั้นฟิล์ม ได้รับความร้อนมากเกินไป จำนวนชั้นของโมเลกกุลสามารถควบคุมได้ ด้วยการกำหนดขั้นตอนและ

จำนวนครั้งของการจุมแผ่นฐานรองลงไประบบ การตรวจสอบจำนวนชั้นโมเลกุลสามารถวัดได้ ด้วย เครื่องวัดการเลี้ยวเบนรังสีเอ็กซ์

การวัดการนำไฟฟ้าสามารถทำได้โดยตรง โดยต่อขั้วโดยตรงจากขั้วไฟฟ้าด้านล่างและด้านบน ด้วยเครื่องวัดอิเล็กโตรมิเตอร์ที่มีค่าอิมพิแดนซ์ขาเข้าสูง ในการวัดการนำไฟฟ้าโดยตรงที่แต่ละโมเลกุล จะทำได้โดยการวัดโดยตรงด้วยตัวเข็มของกล้องจุลทรรศน์แรงอะตอม โดยใช้เข็มที่สามารถนำไฟฟ้าได้ ไปแตะยังชั้นฟิล์มโมเลกุลนี้ แล้ววัดปริมาณกระแสที่ไหลผ่านเมื่อให้แรงดันไบแอสที่เข็มและขั้วไฟฟ้า ด้านล่าง การวัดการนำไฟฟ้าในโมเลกุลนี้จำเป็นทำการวัดซ้ำหลายครั้ง เพื่อลดผลความผิดพลาดจาก จุดสัมผัส ชั้นออกไซด์ฉนวนไฟฟ้าที่อาจเกิดขึ้นระหว่างโมเลกุลและเข็ม การวัดการนำไฟฟ้าของ ฟิลม์บางของชั้นโมเลกุลเมื่อมีจำนวนชั้นโมเลกุลเพิ่มขึ้น จะทำให้ได้ข้อมูลการนำไฟฟ้าเนื่องจากชั้น โมเลกุลเอง เนื่องจากสามารถประมาณให้ผลของขั้วไฟฟ้าเกิดขึ้นเช่นเดียวในตัวอย่างที่มีจำนวนชั้นโมเลกุลต่างกัน

การนำกระแสไฟฟ้าในโมเลกุล สามารถอธิบายได้ด้วยโครงสร้างอิเล็กทรอนิกส์ของโมเลกุล ได้ ทำการคำนวณโครงสร้างโมเลกุลของสารที่ใช้ และได้แยกคำนวณโมเลกุลออกเป็นส่วน ๆ ที่เกี่ยวข้องกับ การรับ หรือ การให้อิเล็กตรอน ออกจากกัน แล้วคำนวณระดับพลังงานในแต่ละส่วนนั้นแยกกัน ได้ อธิบายและเปรียบเทียบการย้ายตำแหน่งของกลุ่มอิเล็กตรอนไปยัง กลุ่มโมเลกุลที่มีความสามารถในการ รับ หรือ จ่ายอิเล็กตรอนที่มีประสิทธิภาพและความแรงต่าง ๆ กัน เพื่อศึกษากลไกการย้ายอิเล็กตรอน ในโมเลกุล และอิทธิพลการย้ายอิเล็กตรอนต่อระดับพลังงานที่เปลี่ยนแปลงไป มีความเป็นไปได้ที่จะ นำแนวความคิดกลไกการอธิบายสมบัติการย้ายอิเล็กตรอนในโมเลกุลนี้ ไปออกแบบสร้างโมเลกุล ที่มี สมบัติที่ดีในการใช้เป็นอุปกรณ์โมเลกุล ความเข้าใจที่ได้จากการศึกษาผลของปัจจัยต่าง ๆ ในการ ประกอบโมเลกุล จะทำให้สามารถสร้างโมเลกุลที่ประยุกต์ใช้ในอุปกรณ์โมเลกุลใหม่ ๆ ได้

การอธิบายการนำไฟฟ้าในโมเลกุล ด้วยแบบจำลองการนำไฟฟ้าในอุปกรณ์สารกึ่งตัวนำ โดยทั่วไป จะใช้ได้อย่างไม่ครอบคลุม เนื่องจากทฤษฎีดังเดิมได้มีการประมาณการเคลื่อนที่ของ อิเล็กตรอนในผลึกสารกึ่งตัวนำด้วยทฤษฎีแถบพลังงาน แล้วประมาณความสัมพันธ์ของความเร็วและ

พลังงานด้วยพารามิเตอร์มวลยังผล ใช้หลักการประมาณด้วยกลศาสตร์ดังเดิมพิจารณาการเคลื่อนที่ด้วย
แรงจากสนามไฟฟ้าภายนอก และจากการแพร่เนื่องจากการกระจายความหนาแน่นของพาหะอิสสระ
แต่ในอุปกรณ์โมเลกุลการเคลื่อนที่ของอิเล็กตรอนนี้อยู่ในสเกลขนาดที่เล็กมาก ไม่สามารถใช้กลศาสตร์
ดังเดิมอธิบายได้อย่างถูกต้อง หากแต่ต้องมีการพิจารณาแนวคิดใหม่ในการอธิบายการขนส่งในระบบ
ควอนตัม

โดยทั่วไปในกลศาสตร์ควอนตัมจะทำการพิจารณาระบบที่อยู่แต่ในระบบปิด ดังเช่นหากมีการ พิจารณาอัตรากิริยาระหว่างอิเล็กตรอนและอะตอมจำเป็นต้องสร้างขอบเขตของระบบให้รวมทุกอย่างที่ สนใจ และมีผลต่อระบบเป็นระบบปิด จึงจะสามารถเขียนฟังก์ชั่นคลื่นเพื่ออธิบายพฤติกรรมของระบบ นั้นได้ แต่ในการอธิบายการเคลื่อนที่ของอิเล็กตรอนผ่านโมเลกุลนั้น เป็นระบบเปิด ที่มีอิเล็กตรอนไหล เข้าออกตลอดเวลา จึงต้องหาแนวทางในการอธิบายพฤติกรรมดังกล่าวด้วยระบบควอนตัม

อีกปัญหาหนึ่งที่ต้องพิจารณาในการเคลื่อนที่ของอิเล็กตรอนในโมเลกุลนั้น เป็นปัญหาของการที่ ระบบที่มีการเคลื่อนที่ของอิเล็กตรอนนี้เป็นระบบที่ไม่อยู่ในสมดุล หากแต่มีระดับพลังงานเฉลี่ยทางด้าน ที่อิเล็กตรอนไหลเข้าและออกแตกต่างกัน ซึ่งโดยทั่วไปอธิบายได้โดยใช้ระดับพลังงานเสมือนสมดุล ซึ่ง จะมีค่าไม่เท่ากันทั้งสองด้าน ดังนี้จึงต้องพิจาณาระบบควอนตัมที่อยู่ในภาวะที่ไม่สมดุลนี้ด้วย

ได้มีงานวิจัยเสนอการอธิบายระบบเหล่านี้หลายวิธี และในงานวิจัยนี้ได้ประยุกต์วิธีการใช้ พังก์ชันกรีนของสภาวะไม่สมดุลมาใช้ในการอธิบายการไหลของอิเล็กตรอน โดยในขั้นแรกได้คำนวณ ผลของตัวแปรที่ควบคุมความแรงของอันตรกิริยาระหว่าง ขั้วไฟฟ้ากับโมเลกุล โดยพิจารณาจากการ ประยุกต์โครงสร้าง n+/ n/ n+ ต่อมาจึงได้ศึกษากรณีการอธิบายการนำไฟฟ้าในโมเลกุลด้วย โครงสร้างทรานซิลเตอร์สนามไฟฟ้า ซึ่งสามารถอธิบายได้ด้วยการพิจารณาความน่าจะเป็นของการย้าย สถานะระหว่างสถานะของอิเล็กตรอนจากขั้วโลหะด้านหนึ่งผ่านสถานะที่เป็นไปได้ทั้งหมดในโมเลกุลไป ยังสถานะขั้วไฟฟ้าอีกด้านหนึ่ง โดยได้ขยายการคำนวณจากการพิจารณาสถานะของอิเล็กตรอนเดียว เป็นการย้ายสถานะระหว่างสถานะในอิเล็กตรอนหลายตัว แล้วเปรียบเทียบกับการจำลองการเคลื่อนที่ ของอิเล็กตรอนด้วยการพิจารณาผลของเปลี่ยนแปลงฟังก์ชั่นคลื่นที่มีต่อศักย์ไฟฟ้าที่ไบแอสจาก

ภายนอก ซึ่งต้องมีการคำนวณย้อนกลับระหว่างการกระจายประจุกับศักย์ไฟฟ้าและศักย์ไฟฟ้ากับ ฟังก์ชันคลื่นจนกว่าจะได้ผลที่สอดคล้องกันทั้งสองความสัมพันธ์ ซึ่งผลการคำนวณด้วยวิธีทั้งสองจะมีค่า ใกล้เคียงกัน เมื่อให้ค่าความแรงของอัตรากิริยาระหว่างสองอิเล็กตรอนมีค่าไม่มาก แต่ถ้า ค่าพารามิเตอร์นี้มีค่ามากจะทำให้ได้ความสัมพันธ์กระแสแรงดันมีความแตกต่างกันมาก

โครงสร้างเชิงอิเล็กทรอนิกส์ของสายโซ่โมเลกุลคอนจู

เกตพอลิเมอร์

คอนจูเกตพอลิเมอร์เป็นโมเลกุลสายโซ่ ที่แต่ละสายโซ่ประกอบด้วยพันธะคู่สลับกับพันธะเดี่ยว
ทำให้มีอิเล็กตรอนอิสสระเหลือ และสามารถเคลื่อนที่ได้ตามแนวสายโซ่พอลิเมอร์ จึงทำให้โมเลกุลพอลิ
เมอร์เหล่านี้ประพฤติตัวคล้ายสารกึ่งตัวนำ ที่สามารถนำไฟฟ้าได้บ้าง และสามารถปลดปล่อยแสง
ออกมาได้ถ้ามีการกระตุ้นด้วยแสงที่มีพลังงานมาก และ/หรือ เกิดการถ่ายเทพลังงานจากการร่วมตัวกัน
ของพาหะโฮลและอิเล็กตรอน ในงานวิจัยนี้ได้ศึกษาโครงสร้างเชิงอิเล็กทรอนิกส์ของคอนจูเกตพอลิ
เมอร์ พอลิฟินีลีนวินิลีนและพอลิฟูลออรีน ซึ่งจะสามารถเปล่งให้แสงสีแดงและสีน้ำเงินตามลำดับ
นอกจากนั้นยังได้ขยายการศึกษาไปยังโคพอลิเมอร์ระหว่างพอลิฟูลออรีนและแอนทราซีลอีกด้วย

ก่อนการคำนวณหาโครงสร้างเชิงอิเล็กทรอนิกส์ของโมเลกุลคอนจูเกต จะต้องหาโครงสร้างที่
ถูกต้องของโมเลกุลเหล่านี้ก่อน โดยการคำนวณหาพลังงาน แล้วขยับโครงสร้างจนได้โครงสร้างโมเลกุล
ที่ให้ค่าพลังงานที่ต่ำที่สุด เนื่องจากโมเลกุลสายโซ่พอลิเมอร์นี้ ไม่ได้มีโครงสร้างการต่อระหว่างสายโซ่
ที่แข็งแน่นนอน จึงต้องมีการศึกษาพลังงานที่ต้องใช้เมื่อมีการบิดของโครงสร้างของแต่ละหน่วยโซ่
โมเลกุล จากการเปรียบเทียบค่าพลังงานที่ต้องใช้ในการบิดหมุนสายโซ่นี้ จะทำให้สามารถประมาณ
ความเสถียรของโมเลกุลได้ นั้นคือหากต้องใช้พลังงานในการบิดหมุนสายโซ่มากแสดงว่าโมเลกุลนั้นมี
ความเสถียรมาก เมื่อได้โครงสร้างโมเลกุลที่มีพลังงานรวมต่ำสุดแล้ว จึงจะคำนวณโครงสร้างเชิง
อิเล็กทรอนิกส์ด้วยทฤษฎีพังก์ชั่นความหนาแน่น เนื่องจากโมเลกุลสายโซ่ฟอลิเมอร์นั้นจะประกอบด้วย
หน่วยโมเลกุลย่อยจำนวนมาก ต่อกันเป็นสายโซ่โมเลกุล แต่ในการคำนวณไม่สามารถคำนวณ

โครงสร้างที่มีจำนวนโมเลกุลหน่วยย่อยจำนวนมากได้ เพราะใช้เวลานานมาก จึงจำเป็นต้องประมาณ ระดับพลังงานด้วยการคำนวณระดับพลังงานที่มีจำนวนโมเลกุลน้อย ๆ และเพิ่มขึ้นตามลำดับ แล้วทำ การเขียนกราฟระหว่าง ระดับพลังงานที่คำนวณได้กับส่วนกลับของจำนวนหน่วยโมเลกุล ซึ่งพบว่าค่า ระดับพลังงานจะสู่เข้าสู่ค่าหนึ่งเมื่อค่าส่วนกลับของจำนวนหน่วยโมเลกุลมีค่าเป็นศูนย์ หรือเท่ากับ จำนวนหน่วยโมเลกุลมีค่าเป็นอนันต์ ค่าความต่างของระดับพลังงานที่สู่เข้าของระดับพลังงาน LUMO และ HOMO จะสามารถใช้ประมาณค่าความยาวคลื่นแสงสูงสุดที่จะถูกดูดกลืนได้ด้วยโมเลกุลคอนจูเกต นี้ อย่างไรก็ตามการคำนวณประมาณค่าความยาวคลื่นที่ปลดปล่อยจากโมเลกุลพอลิเมอร์เหล่านี้ จำเป็นต้องมีการคำนวณหาโครงสร้างโมเลกุลที่เสถียรในสถานะที่ถูกกระตุ้นด้วย โดยการขยับ โครงสร้างโมเลกุลในสภาวะที่ถูกกระตันนี้ ให้มีพลังงานรวมค่ำที่สุดอีกครั้งหนึ่งก่อนคำนวณหาระดับ พลังงาน LUMO และ HOMO ใหม่ ซึ่งจะได้ความต่างของระดับพลังงานที่น้อยกว่า ทำให้ได้ความ ยาวคลื่นที่ปลดปล่อยออกมามีค่ามากกว่าความยาวคลื่นที่ถูกดูดกลืน

ในกรณีของการศึกษาโครงสร้างเชิงอิเล็กทรอนิกส์ของ โมเลกุลสายโซ่โคพอลิเมอร์นั้น ได้ศึกษา
ผลของการจัดเรียงสำดับโมเลกุลย่อยต่อระดับพลังงานที่คำนวณได้ด้วย เนื่องจากการผสมหน่วย
โมเลกุลอีกชนิดหนึ่ง ลงไปในสายโซ่คอนจูเกตโมเลกุลชนิดหนึ่ง จะทำให้ความยาวของช่วงคอนจูเกตที่
อิเล็กตรอนจะสามารถเคลื่อนที่ได้อย่างอิสสระนั้นมีระยะที่สั้นลง ทำให้ความต่างของระดับพลังงานมีค่า
มากขึ้นด้วย ซึ่งผลการลดความยาวของช่วงคอนจูเกตนี้ สามารถแสดงได้ด้วยการกระจายตัวของออร์
บิทัล การเปรียบเทียบการเรียงสำดับของหน่วยโมเลกุล เช่น การเรียงสลับโมเลกุล A และ B ที่
อัตราส่วน 33% สามารถพิจารณาได้เป็นกลุ่ม ABBBBA, ABBBAB, BABBAB, BABABB, BBAABB
ซึ่งจากการศึกษาการกระจายของออร์บิทัล ในระดับ LUMO และ HOMO ทำให้เข้าใจผลของแทรกของ
หน่วยโมเลกุลอีกชนิดในโครงสร้างโคพอลิเมอร์ได้ อย่างไรก็ตาม เนื่องจากหน่วยโมเลกุล ที่นำมา
ประกอบเป็นโมเลกุลโคพอลิเมอร์นี้ มีสมบัติปลดปล่อยแสงด้วย การประมาณการเปล่งแสงจากโมเลกุล
พอลิเมอร์นี้จึงต้องพิจารณาผลที่เป็นสมบัติเฉพาะของตัวหน่วยโมเลกุลนี้ด้วย

บทวิจารณ์

จากการดำเนินงานวิจัยในโครงการศึกษาโครงสร้างเชิงอิเล็กทรอนิกส์ของอุปกรณ์โมเลกุลด้วย
การตรวจสอบแผ่นฟิล์มบางอินทรีย์และคอมพิวเตอร์โมเดลลิงนี้ ทำให้หน่วยสร้างเสริมศักยภาพทางนา
โนศาสตร์และนาโนเทคโนโลยี คณะวิทยาศาสตร์ มหาวิทยาลัยมหิดล ได้พัฒนาความรู้และความ
เชี่ยวชาญทั้งทางด้านเทคโนโลยีการเตรียมฟิล์มบางอินทรีย์ด้วยเทคนิคการเตรียมฟิล์มแบบต่าง ๆ
เรียนรู้เทคนิคการสังเคราะห์และพัฒนาวัสดุอินทรีย์และวัสดุพอลิเมอร์ชนิดต่าง ๆ พัฒนาเทคนิคการ
ประกอบฟิล์มบางเป็นอุปกรณ์ต่าง ๆ และพัฒนาศักยภาพการคำนวณแบบจำลองโมเลกุลซึ่งเป็น
เครื่องมือที่สำคัญต่อการศึกษางานวิจัยในระดับนาโนเมตรนี้ เป็นผลให้ทางหน่วยสร้างเสริมศักยภาพ
ทางนาโนศาสตร์และนาโนเทคโนโลยีสามารถประดิษฐ์อุปกรณ์เปล่งแสงอินทรีย์ อุปกรณ์ตรวจวัดแก็ส
และกลิ่นต่าง ๆ และพัฒนาการสังเคราะห์วัสดุและวัสดุผสมนาโนเพื่อการประยุกต์ใช้ในงานต่าง ๆ ซึ่ง
ได้เกิดความร่วมมือกับโรงงานอุตสาหกรรมในระยะต่อมา ในระหว่างการดำเนินโครงการวิจัยนี้ได้มี
นักศึกษาทั้งในระดับปริญญาโทและปริญญาเอกเข้าร่วมพัฒนาเทคนิคและศึกษาปัจจัยต่าง ๆ ที่มีผลใน
งานวิจัย ทำให้โครงการเป็นส่วนสำคัญที่สามารถสร้างนักวิจัยใหม่ให้มีทักษะความชำนาญในการ
ค้นคว้าวิจัยทั้งทางอุปกรณ์โมเลกุลและนาโนเทคโนโลยีด้วย

ผลลัพธ์จากโครงการวิจัย

1. ผลงานตีพิมพ์ในวารสารวิชาการนานาชาติ

Anurak Udomvech, Teerakiat Kerdcharoen, Tanakorn Osotchan, "First principles study of Li and Li+ adsorbed on carbon nanotube: Variation of tubule diameter and length," Chemical Physics Letters 406 (2005) 161–166.

Anurak Udomvech, Teerakiat Kerdcharoen, Vudhichai Parasuk, Yuthana

Tantirungrotechhai and Tanakorn Osotchan, "Electronic Structure of the Finite-Sized

Single-walled Carbon Nanotubes," International Journal of Nanoscience Vol. 2, No. 3

(2003) 141-152.

2. การนำผลงานวิจัยไปใช้ประโยชน์

- <u>เชิงวิชาการ</u> ในระหว่างการดำเนินโครงการวิจัยนี้ได้มีนักศึกษาทั้งในระดับปริญญาโทและ ปริญญาเอกเข้าร่วมพัฒนาเทคนิคและศึกษาปัจจัยต่าง ๆ ที่มีผลในงานวิจัย ทำให้โครงการเป็น ส่วนสำคัญที่สามารถสร้างนักวิจัยใหม่ให้มีทักษะความชำนาญในการค้นคว้าวิจัยทั้งทางอุปกรณ์ โมเลกุลและนาโนเทคโนโลยีด้วย
- <u>เชิงสาธารณะ</u> จากการดำเนินงานวิจัยในโครงการศึกษาโครงสร้างเชิงอิเล็กทรอนิกส์ของอุปกรณ์ โมเลกุลด้วยการตรวจสอบแผ่นฟิล์มบางอินทรีย์และคอมพิวเตอร์โมเดลลิงนี้ ทำให้หน่วยสร้าง เสริมศักยภาพทางนาโนศาสตร์และนาโนเทคโนโลยี คณะวิทยาศาสตร์ มหาวิทยาลัยมหิดล ได้ พัฒนาความรู้และความเชี่ยวชาญทั้งทางด้านเทคโนโลยีการเตรียมฟิล์มบางอินทรีย์ด้วยเทคนิค การเตรียมฟิล์มแบบต่าง ๆ เรียนรู้เทคนิคการสังเคราะห์และพัฒนาวัสดุอินทรีย์และวัสดุพอลิเม

อร์ชนิดต่าง ๆ พัฒนาเทคนิคการประกอบฟิล์มบางเป็นอุปกรณ์ต่าง ๆ และพัฒนาศักยภาพ การคำนวณแบบจำลองโมเลกุลซึ่งเป็นเครื่องมือที่สำคัญต่อการศึกษางานวิจัยในระดับนาโน เมตรนี้ เป็นผลให้เกิดเครือข่ายความร่วมมือในการวิจัยพัฒนากับหน่วยงานวิจัยของรัฐและกับ นักวิจัยในมหาวิทยาลัยอื่นในช่วงต่อมา

- <u>เชิงพาณิชย์</u> จากการดำเนินงานวิจัยในโครงการทำให้หน่วยสร้างเสริมศักยภาพทางนาโน ศาสตร์และนาโนเทคโนโลยีสามารถประดิษฐ์อุปกรณ์เปล่งแสงอินทรีย์ อุปกรณ์ตรวจวัดแก็ส และกลิ่นต่าง ๆ และพัฒนาการสังเคราะห์วัสดุและวัสดุผสมนาโนเพื่อการประยุกต์ใช้ในงาน ต่าง ๆ ซึ่งได้เกิดความร่วมมือกับโรงงานอุตสาหกรรมในระยะเวลาต่อมา
- 3. ผลงานตีพิมพ์ในวารสารวิชาการ

Areefen Rassamesard, Toemsak Srikhirin, Teerakiat Kerdcharoen and Tanakorn Osotchan, Scanning Probe Microscope Investigation of Electrical Characteristics and Surface Morphology of Side Chain Liquid Crystalline Copolymers," Chiang Mai J. Sci. 32 (2005) 543-548.

4.

- Rassamesard, T. Srikhirin, T. Kerdcharoen, T. Osotchan, "Molecular Electronic Device from Monolayer Films", Proceedings of the 2005 Electrical Engineering/Electronics,
 Computer, Telecommunications, and Information Technology International Conference,
 12-13 May 2005, Asia Pattaya Beach Hotel, Pattaya, Thailand.
- Kanchana Sivalertporn and Tanakorn Osotchan "Hopping and Drift-Diffusion Currents in Organic Devices" Proceedings of the 2nd IEEE International Conference on Nano/
 Micro Engineered and Molecular Systems, January 16-19,2007, Bangkok, Thailand, pp.830-833

- Udomvech, T. Osotchan, T. Kerdcharoen, "Energetic and Structural Properties of Liintercalated Ultra-Small Diameter Single-Walled Carbon Nanotubes", 10th Annual
 National Symposium for Computational Science and Engineering, 22-24 March 2006,
 Chiang Mai University 17-22.
- Udomvech, T. Kerdcharoen, "Theoretical Study of Lithium Atoms Insertion into Smallest Diameter Carbon Nanotubes", 9th Annual National Symposium for Computational Science and Engineering, 23-25 March 2005, Mahidol University, 534.
- Kanchana Sivalertporn and Tanakorn Osotchan "Simulation of One Dimensional Carrier Hopping Transport in Alq3 organic Devices", 10th Annual National Symposium for Computational Science and Engineering, 22-24 March 2006, Chiang Mai University. 28-32.
- Rassamesard, T. Taveecharoenkool, S. Krongsuk, T. Srikhirin, T. Kerdcharoen, T.
 Osotchan, "Dynamic and Electronic Structure of Side Chain Liquid Crystalline
 Copolymers", 9th Annual National Symposium for Computational Science and
 Engineering, 23-25 March 2005, Mahidol University.
- T. Maturos, T. Srikhirin, T. Kerdcharoen, T. Osotchan, "Electronic Structure of Copolymerization of 9,9-Di(2'-ethylhexyl) 2,7 dibromofluorene (BEH-PF) and dibromo(anthracene)", 9th Annual National Symposium for Computational Science and Engineering, 23-25 March 2005, Mahidol University, 404-410.
- Kriengsak Sriwichitkamol, Teerakiat Kerdcharoen, Tanakorn Osotchan and Supa
 Hannongbua, "Quantum Chemical Calculations of Electronic Structures and Electronic
 Properties of Polyfluorene and its derivatives," 7th Annual National Symposium for
 Computational Science and Engineering, Chulalongkorn University, 2003.

- Thanyarat Udommaneethanakit, Teerakiat Kerdcharoen, Toemsak Srikhirin,
- Vudthichai Parasuk, and Supa Hannongbua, "Photoisomerization of 4-(4' Hydroxyphenylazo)nitrobenzene," 7th Annual National Symposium for Computational
 Science and Engineering Chulalongkorn University, 2003.
- Chantasri and T. Osotchan "Quantum Transport Through Single Molecule with N-Electron Model," Siam Physics Conference 2007 (SPC2007), Nakorn Pathom, Thailand
- Tanakorn Osotchan, "Concept of Electronic Devices in Nanotechnology; Electron
 Transport Approach" The 32rd Congress on Science and Technology of Thailand (f.32),
 10-12- October -06, pp.44
- Yingyot Infahsaeng, Tanakorn Osotchan and Toemsak Srikhirin, "Simulation of Electrical Properties in Single Layer Organic Device," 31st Congress on Science and Technology of Thailand, 18-20 October 2005, Suranaree University of Technology, Nakhon Ratchasima D_0044
- Areefen Rassamesard, Tanakorn Osotchan, Toemsak Srikhirin, "Electrical characteristic of monolayer film of a side chain liquid crystal copolymers studied by scanning tunneling microscopy and atomic force microscopy," 30th Congress on Science and Technology of Thailand D0033.
- T. Maturos, P. Srisongkam, S. Maneetoon, A. Udomvech, T. Kerdcharoen,
 "Conformation and Electronic Structure Relate Emission Spectra for Polyfluorene and
 Anthracene Copolymer", 31st Congress on Science and Technology of Thailand, 18-20
 October 2005, Suranaree University of Technology, Nakhon Ratchasima D_0033.

- Areefen Rassamesard, Tanakorn Osotchan, Toemsak Srikhirin, Phatcharin
 Thamasirianunt, "Molecular rectifier," 29th Congress on Science and Technology of Thailand.
- Udomvech, T. Kerdcharoen, "First Principle Study of Lithium Atoms Insertion into Ultrasmall Diameter Carbon Nanotubes", 31st Congress on Science and Technology of Thailand, 18-20 October 2005, Suranaree University of Technology, Nakhon Ratchasima.
- Anurak Udomvech1,2, Tanakorn Osotchan1,2 and Teerakiat Kerdcharoen,
 "THEORETICAL INVESTIGATION OF Li+/Li and Li CLUSTERS INSERTION INTO
 SINGLE-WALLED CARBON NANOTUBES," 30th Congress on Science and Technology of Thailand D0048.

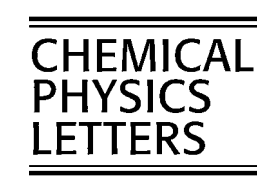
ภาคผนวก



Available online at www.sciencedirect.com







www.elsevier.com/locate/cplett

First principles study of Li and Li⁺ adsorbed on carbon nanotube: Variation of tubule diameter and length

Anurak Udomvech, Teerakiat Kerdcharoen *, Tanakorn Osotchan

Department of Physics and Capability Building Center for Nanoscience and Nanotechnology, Faculty of Science, Mahidol University, Rama 6 Road, Bangkok 10400, Thailand

> Received 12 December 2004; in final form 22 February 2005 Available online 19 March 2005

Abstract

We have performed first principles calculations of Li and Li⁺ adsorbed on the sidewall of carbon nanotubes. Density functional theory based on the B3LYP functional and all-electron basis set centered on atoms was employed. Carbon nanotubes were modeled by varying the diameter ranging from the chiral vector (6,0) to (12,0), and by varying the tubule length for the nanotubes having chiral vector (9,0) from 1 to 3 unit cells. Based on the study of potential energy surface, it was found that the Li atom and cation prefer to localize near the carbon nanotube sidewall and that surface diffusion of Li/Li⁺ can easily take place along the internal sidewall, while being hindered for the external sidewall. Binding energies tend to depend on the configuration, i.e., on being odd or even for the chiral vector (*m*,0), rather than on the diameter size. In addition, they depend on the tubule length but converge rapidly after 3 unit cells. The atomic net charge (natural bond orbital and Mulliken population analysis) on the lithium inside carbon nanotube does not depend on whether the Li–CNT is neutral or charged. The results of this study may be helpful for understanding the fundamentals of how the Li-ion carbon nanotube battery works.

© 2005 Elsevier B.V. All rights reserved.

1. Introduction

After its discovery by Iijima [1] in 1991, research on carbon nanotube (CNT) reaches a critical mass in many areas of physics and chemistry. Synthesis methods have been rapidly improved, making it possible to produce large amount of size-controlled CNT for commercial applications [2]. CNT has two types of structure: (1) the single-walled carbon nanotube (SWNT) which is a single rolled graphene sheet; (2) the multi-walled carbon nanotube (MWNT) in which each CNT is encapsulated by the others based on the Russian-Doll model. Carbon nanotube can adsorb a number of atomic and molecular species, e.g., alkali metals (i.e., Li [3], K [4], Rb [5] and Cs [6]) and hydrogen [7], nitrogen [8], oxygen [9] and

methane [10] gases. The adsorption properties provide the opportunities for applications such as hydrogen and other gases storage [11], gas sensor [12], catalyst [13] and Li-ion batteries [14].

Recently, nano-structured materials for anode has drawn interest from the battery industry since the engineering limit has been reached using conventional electrodes such as carbonaceous materials and metal oxides [15]. The hope is that the optimization of the device performance, i.e., charge—discharge cycles and reversibility, can be achieved on the basis of the CNT. The CNT is a prospect candidate for uses in Li-ion batteries since the large numbers of nanoscale sites for intercalant atoms on the CNT exceed those found on the commonly used graphite electrode, LiC₆. As a replacement for the graphite on the negative electrodes of the Li-ion batteries, the CNT will release the intercalant Li as Li⁺ into the electrolytic medium. The metal ions will later accept electron and deposit at vacant position on

^{*} Corresponding author. Fax: +66 2 2015843. E-mail address: sctkc@mahidol.ac.th (T. Kerdcharoen).

the positive electrode (i.e., Li_xCoO_2). Theoretical studies on interactions between Li and Li^+ with CNT will therefore be helpful in understanding the fundamentals of how such a battery will work.

In this Letter, we have studied the interaction between Li and Li⁺ with the CNT as a function of distance of the metal from the CNT, as well as the variation of the CNT's diameter for the nanotubes having chiral vector ranging from (6,0) to (12,0). Tubule length of the CNT is also varied on some specific structures in order to study the effect of length on the potential energy surface.

2. Methodology

Since a typical CNT is very large molecule, a compromise between the level of method and the details of the molecular model has to be made. In principles, one can employ either a low level of calculation (e.g., semiempirical methods) with the largest possible molecular system [16-18] (e.g., cluster or periodic nanotube), or a high level of calculation (e.g., correlated methods) with the smallest molecular model [19,20] (e.g., benzene). The availability of methods with small scaling law such as DFT allows reasonable accuracy for sufficiently large model system. For examples, Zhao et al. [21] has performed SCF pseudopotential plane-wave calculation based on local density approximation (LDA) on a periodic Li₅C₄₀ system that represents Li-intercalated CNT ropes. Yang and co-workers employed LDA calculations using an electron core potential to study Li₂C₁₂₀, Li₂C₁₃₂ and Li₂C₁₂₀H₁₂ that model the Li intercalation in open, closed and H-saturated CNTs, respectively. In the present work, we employed a generalized gradient approximation (GGA) method based on B3LYP parameterization to study Li and Li⁺ intercalation in CNT. A standard all-electron basis set (6-31G) was chosen for our calculations.

All of the SWNT employed in this study is of the zigzag type, which are denoted by the chiral vector (m,0), where m = 6-12. Since the CNTs in this study are finite-sized, hydrogen atoms are used to cap the dangling carbon atoms at the two open ends of the nanotube. All CNTs, except for (9,0), are modeled by one unit-cell cylinder (1UC, see Fig. 1 for definition) and have the corresponding chemical formula $C_{4m}H_{2m}$. This type of carbon nanotube model, called 'cyclacene', has been theoretically well studied within the perspectives of organic chemistry [22–24]. In our previous study, we have found that modeling the finite-length CNT by extending the radius and length of cyclacene structures can be very useful [25]. The geometric parameters were also found to be dependent on how the terminal end is capped (fullerene capping or hydrogen capping), though exponentially converged with increasing tubule length.

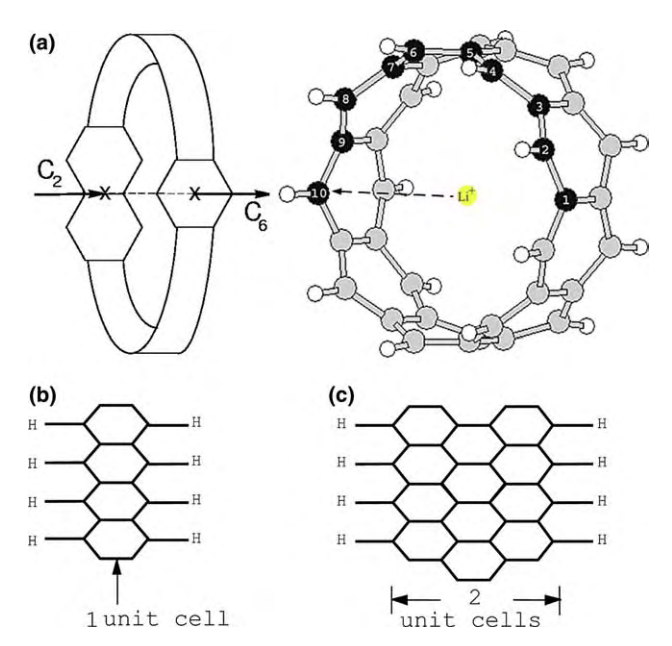


Fig. 1. Definition of (a) C_2 and C_6 trajectories of Li/Li⁺, (b) 1UC, and (c) 2UC carbon nanotube models.

For the (9,0), the length is varied from 1 to 3 unit cells (1UC–3UC), in order to study the effect of tubule length. The largest system studied in this work is Li⁺C₁₀₈H₁₂. Our previous study, based on AM1 semi-empirical method has found that the capping hydrogen atoms affect both the geometric structure and the electronic structure. This effect rapidly converges when the tubule length extends beyond 6 unit cells. In that study, it was also found that the open (H-capped) and the closed carbon nanotubes have similar HOMO–LUMO energy gap after the removal of the defected states caused by the capping hydrogen.

The potential energy surface (PES) of the M-CNT system (where M = Li and Li⁺, respectively) is investigated by inserting a metal into the CNT from the sidewall and plotting the binding energy as a function of the distance along the cross-section. The structures of the model CNT obtained by geometry optimization are kept fixed after the insertion of Li/Li⁺. Penetration of Li/Li⁺ through the nanotube sidewall has been done on the basis of two trajectories: C₂ for which the ion penetrates through C-C bond and C₆ where the metal pass through the middle of the hexagon (see Fig. 1).

3. Results and discussion

Potential energy surfaces for Li–CNT and Li⁺–CNT were investigated for model SWNT by varying the diameters from (6,0) to (12,0), as illustrated in Fig. 2a–b. The cluster model of these nanotubes has only 1 unit cell length (1UC). The binding energies and distances from the Li and Li⁺ to the centers of the C–C bond

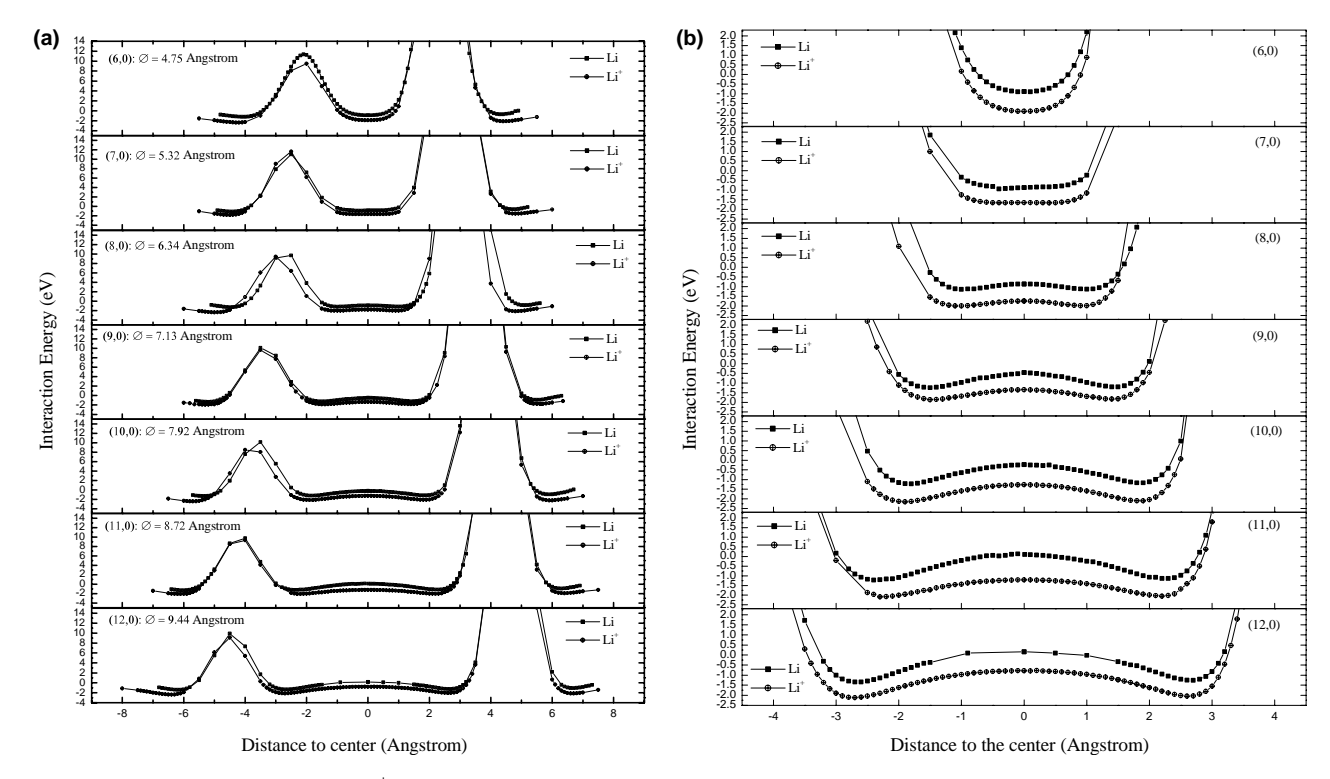


Fig. 2. Potential energy surface of Li/Li^+ -CNT: (a) overall trajectory and (b) zoom-in trajectory inside CNT. The positive and negative x axes represent C_2 and C_6 trajectories (see Fig. 1), respectively.

 $(C_2 \text{ trajectory})$ and hexagon $(C_6 \text{ trajectory})$ at the energy minima are tabulated in Table 1.

Li atom and cation can be adsorbed on both the interior and exterior of the nanotube's sidewall. The PES has double-well shape inside the tube, except for the (6,0) and (7,0) structures, because both the Li and Li⁺ prefer to bind to the side of the nanotube. The diameter of the (6,0) tube $(\sim 4.7 \text{ Å})$ is so small that the energy minimum is located at the center of the tube. The bind-

ing site requires Li and Li⁺ to separate by about 2 Å from the sidewall, which will be discussed later. It is not clear whether the double-well PES starts to develop in the (7,0) nanotube as the potential well is rather flat. Detailed evaluation of the energy minimum has found that the potential barrier height separating the two minima is less than 0.01 eV, below the marginal accuracy of the method employed. For the (8,0)–(12,0), the barrier heights inside the tube are 0.28/0.25, 0.78/0.52,

Table 1
Binding energies (eV) for Li/Li⁺-CNT (1 unit cell model) at the local minima calculated for trajectories C₂ and C₆ (see Fig. 1)

Structure	C ₂ direction		C ₆ direction		
	Internal wall	External wall	Internal wall	External wall	
(6,0)	0.89/1.90	0.69/2.11	0.89/1.90	1.21/2.36	
		(1.95)/(2.02)		(1.75)/(1.78)	
(7,0)	0.87/1.66	0.61/1.55	0.87/1.66	1.09/1.83	
		(2.06)/(2.04)		(1.66)/(1.71)	
(8,0)	1.14/1.99	0.83/2.12	1.15/2.00	1.26/2.34	
	(2.13)/(2.18)	(1.97)/(2.01)	(2.05)/(2.18)	(1.74)/(1.82)	
(9,0)	1.20/1.83	0.91/1.77	1.24/1.86	1.33/1.93	
	(2.12)/(2.13)	(1.98)/(2.08)	(2.02)/(2.06)	(1.68)/(1.75)	
(10,0)	1.17/2.10	0.96/2.22	1.22/2.16	1.32/2.43	
	(2.01)/(2.02)	(1.99)/(1.99)	(2.02)/(2.05)	(1.66)/(1.76)	
(11,0)	1.14/2.05	0.93/1.90	1.21/2.08	1.31/2.08	
	(2.01)/(2.11)	(1.99)/(2.09)	(1.91)/(2.03)	(1.69)/(1.87)	
(12,0)	1.26/2.05	1.06/2.13	1.34/2.12	1.41/2.37	
	(2.09)/(2.08)	(2.00)/(2.04)	(1.90)/(1.92)	(1.72)/(1.76)	

Distances (Å) between Li/Li⁺ to the center of C-C bond and C₆ hexagon are in parentheses.

0.99/0.88, 1.32/0.88 and 1.50/1.33 eV, respectively, for Li/Li⁺. They are high enough to define the double-well shape. As the tubule diameter increases, Li/Li⁺ is more likely to be located near the tubule wall rather than at the center.

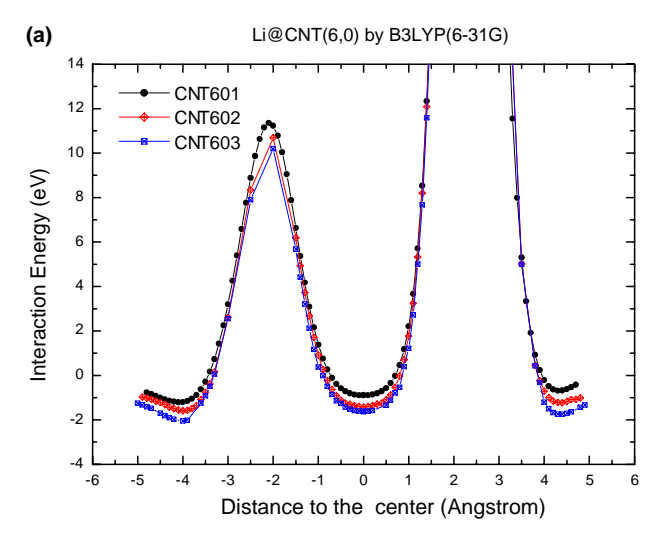
In this study, two types of binding sites have been investigated, C-C bond (C₂) and hexagon (C₆). From Table 1, we could see that Li/Li+ prefer to be adsorbed at C₆ than C₂ sites even if the binding energies between these two sites in the tube's interior differ only slightly (0.00/0.00, 0.00/0.00, 0.01/0.01, 0.04/0.03, 0.05/0.05,0.07/0.04 and 0.08/0.07 eV for the structure (6,0)(12,0), respectively). Preferential adsorption of Li/Li⁺ on the C₆ site has more contrast for the exterior of the tubes (differences are 0.52/0.25, 0.48/0.27, 0.43/0.22, 0.42/0.16, 0.36/0.21, 0.38/0.18 and 0.35/0.23 eV for the structure (6,0)–(12,0), respectively). To elucidate visually, single cylindrical potential well is formed along the internal sidewall, whereas a cluster of local minima covers the external sidewall with each minimum being separated from other minima by six saddle points (C₂ sites) with a barrier of around 0.4-0.5 eV for Li and 0.2–0.3 eV for Li⁺. Although the barrier between C₂ and C₆ binding sites for Li is higher than Li⁺ indicating that Li⁺ has higher mobility than Li along the external tubule wall, the binding energies for Li⁺ are larger. (1.09–1.41 eV for Li and 1.83–2.43 eV for Li⁺).

Surface diffusion may easily take place along the internal sidewall, while it is hindered for the external sidewall. Frontera and co-workers [26] studied molecular interaction potential between Li⁺ and small-diameter arm-chair SWNT based on ab initio wave function, thus observing a channel that would allow ion mobility inside the nanotube. Visually, if we fill a CNT by Li or Li⁺, it is expected that the atom or ions will tend to localize on the hexagons along the nanotube's external sidewall, while freely moving along the sidewall for the inside. For rechargeable Li-ion battery, nanotubes can be made open allowing for the intercalated Li/Li⁺ to migrate into and out of the tubes. A first principles calculation by Yang et al. [27] suggests that there is no insertion barrier for Li⁺ into the nanotube's terminal end if the opening carbons are saturated with hydrogen atoms. Since the Li atom and cation prefer to localize near the carbon nanotube sidewall, small-diameter carbon nanotubes may be better advantageous than the larger ones for use as batteries.

Adsorption on the external wall is more stabilized than on the internal wall for all nanotubes. The reason for this is that the external pi orbitals are pointing away from each others, as opposed to the internal ones. Therefore, the orbital interactions between Li/Li⁺ and CNT would be more efficient for the external adsorption. Dubot and Cenedese [16] have studied Li atom adsorption on CNT by semi-empirical AM1 method and found that there is preferential adsorption on the

external sidewall. Liu et al. [28] also observed similar trend on arm-chair SWNT using LDA density functional method. The equilibrium metal- C_6 hexagon distances are also shorter for the external adsorptions (\sim 1.7–1.9 versus 1.9–2.2 Å). Binding energies for (m,0) when m is even are always higher than those for odd m's. For instances, the binding energies at the external adsorption sites for the even m's will be about 0.4 eV larger than the odd m's. Such behavior can be attributed to the orbital symmetry, being enhanced in the even cases.

Interaction energies upon variation of tubule length for (9,0) nanotube are plotted in Fig. 3. For Li, the internal binding energy increases from 1.24 to 1.77 eV and the external binding energy increases from 1.33 to 1.88 eV, as the tubule length increases from 1UC to 3UC (43% and 41% change, respectively). For Li⁺, the internal binding energy increases from 1.86 to 2.44 eV and the external binding energy increases from 1.93 to 2.58 eV, as the tubule length increases from 1UC to 3UC (31% and 34% change, respectively). As can be seen, the finite-length effect has a stronger influence on



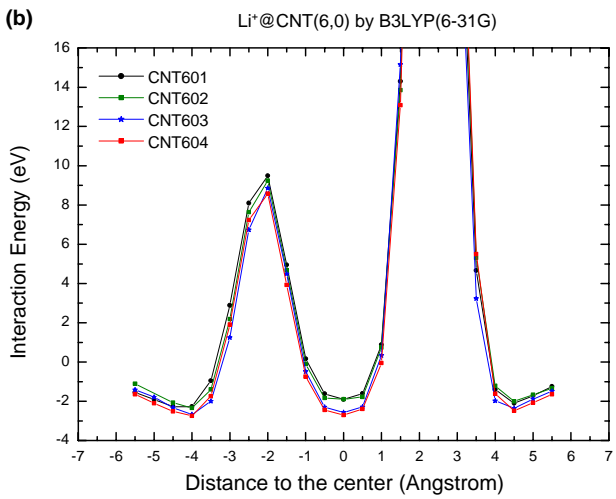
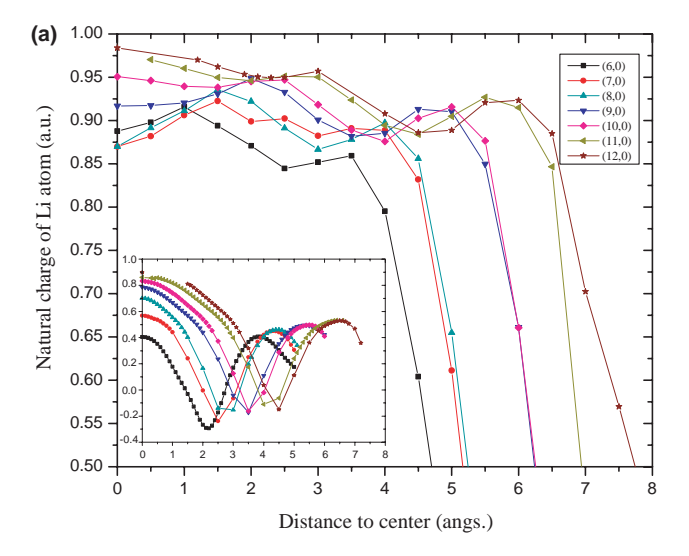


Fig. 3. Dependence of potential energy surface on the tubule length of (a) Li–CNT and (b) Li⁺–CNT.

Li than that on Li⁺. Our study on smaller system such as (6,0) nanotube indicates that the binding energies between Li/Li⁺ with the tube is likely to converge when the tube is 5 unit-cell long [29]. The same study also revealed that the finite-length effect is stronger for the Li than for the Li⁺ intercalated system.

Penetration of the Li/Li⁺ through the C₆ hexagon of all structure (1UC models of (6,0)–(12,0)) requires energies averaging 9.0/9.6 eV. Previous study found that the energy barrier for Li⁺ penetration through the center of a benzene ring ranges from 11 to 15 eV, as determined by various levels of calculations (HF, DFT, MP2) and basis functions (e.g., STO3G, 6-31G*, 6-311++G**) [20]. The larger energy barrier for the case of benzene arises from higher electron density which is gained from six hydrogen atoms as electron donor. The lower electron density of the nanotube cylinder considered in our study comes from the fact that there are only two hydrogen atoms per C₆ hexagon. Increase of the tubule length in case of (9,0) nanotube from 1UC to 3UC leads to the reduction of this effect. This results in a lower energy barrier (from 10.13/ 9.62 to 9.58/9.32 eV for Li/Li⁺ as shown in Fig. 3). Such behavior is also seen in case of (6,0) tube. Therein, the energy barrier is reduced from 9.49 to 8.57 eV upon the increasing length from 1UC to 4UC [29].

Dependence of the atomic net charge of Li/Li⁺ on tubule diameter and length have been investigated based on the natural bond orbital (NBO) and Mulliken population analysis, as illustrated in Fig. 4. Atomic net charge value on the intercalant lithium does not depend on whether it is a neutral atom or an ion. For instances, the NBO atomic net charge on Li/Li⁺ when they are loca ted at the center of the (6,0)–(12,0) 1UC tube is equal to 0.89/0.88, 0.87/0.87, 0.87/0.88, 0.92/0.92, 0.95/0.95, 0.97/ 0.97 and 0.98/0.98, respectively. Mulliken atomic net charge also follows the similar trend. The Mulliken charge on Li/Li⁺ when they are located at the center of the (6,0)–(12,0) 1UC tube is equal to 0.41/0.43, 0.57/0.58, 0.70/0.69, 0.79/0.78, 0.83/0.82, 0.86/0.86 and 0.90/0.88, respectively. The atomic net charge (both NBO and Mulliken) for Li atom as it moves far away from the CNT approaches zero, in contrast to singly positive charge in case of Li⁺. This indicates that the lithium atom and cation always have a positive charge when they are intercalated inside the negative electrode (CNT) in the Li-ion batteries. During the discharge process, carbon nanotube negative electrode will release the intercalant Li as Li⁺ into the electrolytic medium. The metal ions will later accept electrons and deposit at the vacant positions on the positive electrode (i.e., Li_x CoO₂). Since lithium always remains positive when it is deposited in the matrix of positive electrode (i.e., Li_x CoO_2), when it is in the electrolytic medium, or when it is intercalated in the negative electrode (CNT), all of which renders high mobility to the Li⁺, it is unbeaten as a electrical conducting material in battery.



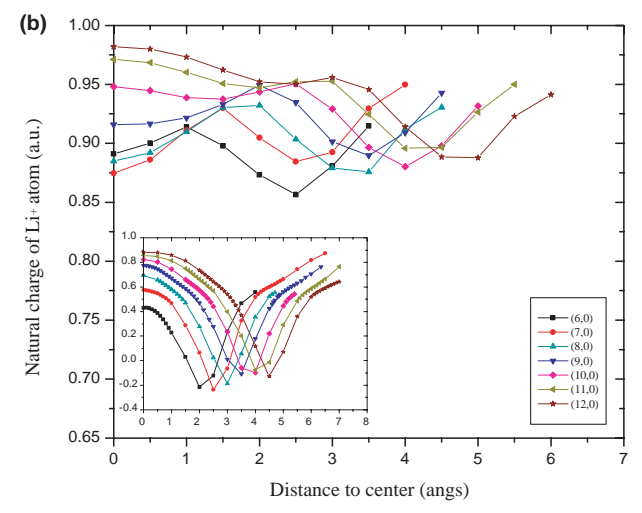


Fig. 4. Dependence of natural bond orbital (NBO) atomic net charge of (a) Li and (b) Li⁺ on the tubule diameter. Mulliken charges are also provided for comparison in the inset.

During the intercalation in CNT, the atomic charge of Li/Li⁺ is maximized (positive charge) when the intercalant is located at the center of the tube. In case of longer tube (3UC), the excessive negative charge that CNT gains from the intercalant is locally distributed over the carbons on the circumference only. As the Li/Li⁺ moves from the center of nanotube to the sidewall, the negative charge tends to localize at the carbon atoms in close proximity to the intercalant, where as the other carbon atoms have their charges neutralized. The atomic charges of all C atoms, however, shift slightly to a lesser negative value in the case of intercalated Li⁺, due to the surplus positive charge from the ion.

4. Conclusion

This work has suggested an assumption on adsorption mechanism of Li/Li⁺ onto the carbon nanotube

(CNT) surface. It was found that the intercalated Li/Li⁺ prefers to localize near the carbon nanotube sidewall, instead of being located at the tubule center. Therefore, larger carbon nanotubes which have useless space inside will be at a disadvantage compared with the small-diameter ones when used as batteries. Some characteristics of charge—discharge mechanism for Li–CNT batteries could be conjectured as follows.

- Lithium (Li/Li⁺) always preserves positive charge (close to +1) when it locates inside and close to the outside wall of CNT. Since CNT is used as the negative electrode, it is presumed that only Li⁺ will be released to the electrolyte.
- 2. Surface diffusion of Li/Li⁺ can easily take place along the internal sidewall. The potential energy surface forms a tube-shaped transporter path inside the CNT. In contrast, Li/Li⁺ preferred to localize at C₆ sites on the external surface. Therefore, storage of Li/Li⁺ inside the CNT can be facilitated by opening the terminal ends and/or the sidewall since Li/Li⁺ can move inward as more Li/Li⁺ are added into the tube.

The above-mentioned hypotheses are doubtlessly based on quite limited models employed in this study, i.e., the finite CNT with single intercalant model. Further investigation which extends this model to a higher level is being conveyed.

Acknowledgments

Financial support from Basic Research Grant of the Thailand Research Fund (BRG/21/2544) is gratefully acknowledged. A.U. expresses his gratitude to the Commission on Higher Education and Faculty of Graduate Studies at Mahidol University. We are thankful to Professor Thanh N. Truong at the University of Utah for generous support of computational resources and Professor I. Ming Tang for proofreading the manuscript.

References

- [1] S. Iijima, Nature 354 (1991) 56.
- [2] C.N.R. Rao, B.C. Satishkumar, A. Govindaraj, M. Nath, ChemPhysChem 2 (2001) 78.
- [3] N. Bendiab, E. Anglaret, J.-L. Bantignies, A. Zahab, J.L. Sauvajol, P. Petit, C. Mathis, S. Lefrant, Phys. Rev. B 64 (2001) 245424.
- [4] A.S. Claye, N.M. Nemes, A. Janossy, J.E. Fischer, Phys. Rev. B 62 (2000) R4845.
- [5] A.M. Rao, P.C. Eklund, S. Bandow, A. Thess, R.E. Smalley, Nature 388 (1997) 257.
- [6] A. Wadhawan, R.E. Stallcup II, J.M. Perez, Appl. Phys. Lett. 78 (2001) 108.
- [7] A. Cao, H. Zhu, X. Zhang, X. Li, D. Ruan, C. Xu, B. Wei, J. Liang, D. Wu, Chem. Phys. Lett. 342 (2001) 510.
- [8] Q.-H. Yang, P.-X. Hou, S. Bai, M.-Z. Wang, H.-M. Cheng, Chem. Phys. Lett. 345 (2001) 18.
- [9] X.Y. Zhu, S.M. Lee, Y.H. Lee, T. Frauenheim, Phys. Rev. Lett. 85 (2000) 2757.
- [10] S. Talapatra, A.D. Migone, Phys. Rev. B 65 (2002) 045416.
- [11] A.C. Dillon, M.J. Heben, Appl. Phys. A 72 (2001) 133.
- [12] S. Peng, K. Cho, Nanotechnology 11 (2000) 57.
- [13] J. Adelene Nisha, M. Yudasaka, S. Bandow, F. Kokai, K. Takahashi, S. Iijima, Chem. Phys. Lett. 328 (2000) 381.
- [14] J.-M. Tarascon, M. Armand, Nature 414 (2001) 359.
- [15] N. Li, C.R. Martin, B. Scrosati, J. Power Source 97–98 (2001) 240.
- [16] P. Dubot, P. Cenedese, Phys. Rev. B 63 (2001) 241402.
- [17] A. Shimizu, H. Tachikawa, Chem. Phys. Lett. 339 (2001) 110.
- [18] G. Madjarova, T. Yamabe, J. Phys. Chem. B 105 (2001) 2534.
- [19] J.M. Vollmer, A.K. Kandalam, L.A. Curtiss, J. Phys. Chem. A 106 (2002) 9533.
- [20] T. Kar, J. Pattanayak, S. Scheiner, J. Phys. Chem. A 105 (2001) 10397
- [21] J. Zhao, A. Buldum, J. Han, J.P. Lu, Phys. Rev. Lett. 85 (2000) 1706.
- [22] H.S. Choi, K.S. Kim, Angew. Chem. Int. Ed. 38 (1999) 2256.
- [23] H.S. Choi, D. Kim, P. Tarakeshwar, S.B. Suh, K.S. Kim, J. Org. Chem. 67 (2002) 1848.
- [24] H.S. Choi, S.B. Suh, S.J. Cho, K.S. Kim, Proc. Natl. Acad. Sci. USA 95 (1998) 12094.
- [25] A. Udomvech, T. Kerdcharoen, V. Parasuk, Y. Tantirungrotechai, T. Osotchan, Int. J. Nanosci. 2 (2003) 141.
- [26] C. Garau, A. Frontera, D. Quinonero, A. Costa, P. Ballester, P.M. Deya, Chem. Phys. Lett. 374 (2003) 548.
- [27] J. Yang, H.J. Liu, C.T. Chan, Phys. Rev. B 64 (2001) 085420.
- [28] Y. Liu, H. Yukawa, M. Morinaga, Comput. Mater. Sci. 30 (2004) 50.
- [29] A. Udomvech, T. Osotchan, T. Kerdcharoen, unpublished data.



ELECTRONIC STRUCTURE OF THE FINITE-SIZED SINGLE-WALLED CARBON NANOTUBES

ANURAK UDOMVECH*, † , TEERAKIAT KERDCHAROEN*, † , VUDHICHAI PARASUK ‡ , YUTHANA TANTIRUNGROTECHAI $^{\$}$, and TANAKORN OSOTCHAN*, †

*Department of Physics, Faculty of Science
Mahidol University, Bangkok 10400, Thailand

†Institute of Science and Technology for Research and Development
Mahidol University, Nakorn Pathom 71730, Thailand

‡Department of Chemistry, Faculty of Science
Chulalongkorn University, Bangkok 10300, Thailand

§Department of Chemistry, Faculty of Science
Mahidol University, Bangkok 10400, Thailand

¶sctkc@mahidol.ac.th

Received 14 March 2003 Revised 13 June 2003

The effects of tubule length and terminal capping on the geometrical and electronic properties of finite-sized zig-zag (9,0) single-walled carbon nanotubes (SWNT), which length varying from 2 up to 12 unit cells (~50 Å), were investigated using molecular mechanics, semi-empirical methods (AM1 and EHMO) and density functional theory (B3LYP). AM1 method indicates how the nanotube ends are capped affects strongly the tubule geometric parameters. Although these effects seem to decrease exponentially as the tube gets longer, the converging values for C-C bond length in the open- and closed-end structures are slightly different. It was learned that combination of low-level methods like AM1 and EHMO (which tend to overestimate and underestimate the HOMO-LUMO energy gap, respectively) together with high-level method such as DFT is efficient to estimate band gap for finite-sized nanostructures. The HOMO-LUMO energy gaps obtained from semi-empirical and DFT methods decrease as the tubule length increases. Terminal capping also affects strongly the electronic structure of finite-sized nanotube. Thus, closing the terminal ends by fullerene hemisphere broadens the energy gap of the hydrogen-saturated open-end nanotube. Although the open-end SWNT has much lower AM1 HOMO-LUMO energy gap than the closed-end SWNT, these orbitals unfortunately are localized near the capping hydrogen, thereby do not provide conducting channels for electrons. By comparing only the delocalized frontier orbitals, both structures yield closer energy gap. Analysis of the energy gap based on EHMO, AM1 and DFT results suggests that both open- and closed-end finite-sized SWNT are semiconductor, in agreement with recent scanning tunneling experiment. It was found that the slight accumulated negative charges are likely to locate at the nanotube's fullerene tips.

Keywords: Carbon nanotube; finite-sized effects; computational nanotechnology.

[¶]Corresponding authors.

1. Introduction

After its discovery by Iijima in 1991,¹ carbon nanotubes (CNT) have become a central issue in nanoscience and nanotechnology. For practical applications to be realized, efforts have been made to improve synthesis methods so that large amount of size-controlled CNT can be produced.^{2–4} CNT can be classified into two groups: (1) multiwalled carbon nanotube (MWNT) in which each nanotube is wrapped by and/or contains other tubes based on the Russian–Doll model; (2) single-walled carbon nanotube⁵ (SWNT) which is a rolled graphene sheet. MWNT is a good candidate to replace bulk carbon materials in some conventional applications, i.e., high-capacity battery⁶ and hydrogen storage⁷ for fuel cells. For more advanced applications such as nanoelectronics and nanosensors, SWNT is more appropriate since its synthesis and manipulation can be better controlled at nanoscale precision.

In general, most production processes produce CNT of micrometer length with diameters ranging from 1 to 20 nm.⁸ Therefore, most theoretical studies of CNT have been done in the infinite limit based on a quasi-one-dimensional model. Recently, cutting tools^{9,10} have become available for shortening the length of CNT to the nanometer scale, thus opening up future nanoscale mechanics and electronics applications. It is therefore necessary to gain better understanding of the characteristics of finite-length CNT. At such nanoscale regime, computational modeling becomes very important whereas simple analytical theory¹¹ can be quite nonrealistic.

A lot of theoretical work has been done on investigating the electronic structure, ^{12,13} chemisorption, ^{14,15} mechanical properties, ^{16,17} conductivity ^{18,19} and switching properties ^{20,21} of CNT. Most of the studies were done using periodic boundary condition. Otherwise they have to employ cluster model to estimate the bulk properties. Among the theoretical works on finite-length CNT with small diameter, Türker ^{22,23} has published several papers from the perspectives of organic chemistry where finite-sized CNTs are made of many "cyclacene" rings undergoing intermolecular unification process. This cyclacene tube is consequently open-end and saturated by hydrogen at both ends. Although it is still unclear how such hydrogenated open CNT generally form in most production process, theoretical works on this kind of CNT has nevertheless been very useful.

On one hand, for open-end CNT it is natural to think that dangling carbon atoms at the mouth of CNT undergo passivation by hydrogen atoms or other functional groups, depending on the controlled experimental conditions. Experimental encapsulation²⁴ of alkali metals into CNT cavity implies the diffusion of metals through the opening terminals or side-wall structural defects rather than penetrating through the closed wall. A theoretical study²⁵ even shows that the metals prefer to enter the hydrogen-capped terminal rather than a dangling open-valence one. On the other hand, for closed-end CNT opening it is possible by available cutting tools as noted earlier. Despite unsuccessful attempts to synthesis cyclacene tubules from

the bottom-up, rapid improvement in nanoprecision strategy will make this possible one day. For that reason, it is worthwhile to study properties of this candidate for possible future electronics application.

In the present work, we investigate the dependence of geometry and electronic structure on the length of finite-sized SWNT based on molecular mechanics and semi-empirical modeling. The effect of the terminal, for whether it is open or closed, is also included. Although the system size in this study prohibits full quantum mechanical methods to be employed in geometry optimization, single point calculations are carried out where possible.

2. Models and Computational Details

In the present study, finite-sized SWNT of the type denoted by chiral vector (9,0)are considered. This so-called zigzag SWNT included in this study covers both openand closed-end structures with variation of length from two unit cells (denoted by 2UC) up to 12 unit cells (denoted by 12UC). Definition of the unit cell, open-end and closed-end structures are exhibited in Fig. 1. For the open-end nanotubes, hydrogen atoms are used to saturate the dangling bonds at the terminal ends. To make a closed-end nanotube, C_{60} is bisected at its equator and the resulting two half spheres are attached to each end of the tube. The stoichiometry for the open- and closed-end nanotubes are $C_{36N}H_{18}$ and C_{36N+42} , respectively, where N is the number of unit cells. Consequently, the largest structures used in this study are $C_{432}H_{18}$ for the open-end nanotube and C_{474} for closed-end nanotube, corresponding to a length of around 40–50 Å.

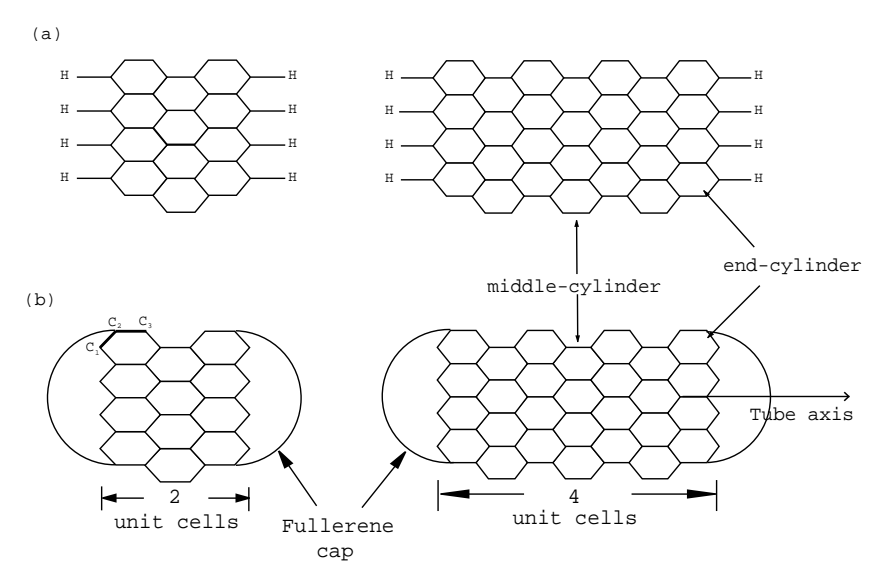


Fig. 1. Definition of (9, 0) SWNT viewed by the sidewall; (a) open-ended and (b) closed-end structures.

The geometry of the nanotubes is investigated by molecular mechanics method based on the MM3 parameterization²⁶ whereas both geometric and electronic properties are studied by semi-empirical quantum mechanics based on the AM1 Hamiltonian.²⁷ Full geometry optimizations are performed without symmetry constraint. To verify the quality of the AM1 method, results from *ab initio* Hartree–Fock and density functional theory (DFT) calculations on a single cyclacene ring (one unit-cell nanotube) are compared. DFT calculations are also employed to investigate electronic properties of short nanotubes with length up to three unit cells. Extended Hückel Molecular Orbital (EHMO) method is also performed for comparison of the electronic properties obtained from AM1 and DFT methods.

For a combination of methods, for instances Hartree–Fock single-point calculation based on $6\text{-}31\mathrm{G}$ basis following a geometry optimization by semi-empirical AM1 method, a notation of HF/ $6\text{-}31\mathrm{G}$ /AM1 is used.

3. Results and Discussion

3.1. Geometry

In practice, computational models of CNT depend on a set of atomic coordinates calculated by molecular mechanics methods or obtained from the bulk graphite because first principles optimized structure of practical system size is impossible. ^{28–30} Accordingly, all C–C bonds of CNT in these studies are assumed to have isotropic bond-length. In this study, we distinguish between C–C bond that lie in parallel with the tube axis (C2–C3) from those lying on the circumference (C1–C2), as depicted in Fig. 1. For comparison with high-level methods, optimized geometries of a single cyclacene ring (1UC) are given in Table 1. Table 2 compares two types of C–C bond lengths for the optimized structures obtained from MM3 and AM1.

From Table 1, one observes that the semi-empirical AM1 structure is in agreement with $\mathrm{HF}/6\text{-}31\mathrm{G}^*$ within 0.01 Å resolution. Both semi-empirical and first principles methods show the differences between two types of C–C bond within a range of 0.04–0.06 Å, whereas MM3 almost overlooks this. Such differences are due to small disturbance of hydrogen atoms to the electron distribution of the aromatic rings. Although replacing the full basis set $(6\text{-}31\mathrm{G}^*)$ with effective core potential

Table 1. Comparison of the bond-length, atomic net charges (on C1 and C2), HOMO, LUMO and HOMO–LUMO energy gap of the 1UC structure as obtained from computation at different level of theory (see definition in Fig. 1).

	MM3	AM1	HF/6-31G*	$\mathrm{HF}/\mathrm{CEP} ext{-}31\mathrm{G}$	B3LYP/6-31G*	B3LYP/CEP-31G
C1-C2 (Å)	1.402	1.408	1.403	1.422	1.410	1.436
C2-C3 (Å)	1.399	1.452	1.462	1.477	1.470	1.493
C1 charge (au)	_	-0.103	-0.167	-0.348	-0.252	-0.499
C2 charge (au)	_	-0.035	-0.033	0.0797	0.121	0.194
HOMO (eV)	_	-6.820	-4.808	-4.834	-3.923	-4.198
LUMO (eV)	_	-2.117	-0.163	-0.658	-2.790	-3.100
$\delta E \text{ (eV)}$	_	4.703	4.645	4.176	1.133	1.098

	Open-end				Closed-end			
	MM3		AM1		MM3		AM1	
Cells	Terminal	Middle	Terminal	Middle	Terminal	Middle	Terminal	Middle
2	[1.398]	[1.400]	[1.440]	[1.431]	[1.399]	[1.399]	[1.423]	[1.421]
	$\{1.402\}$	$\{1.407\}$	$\{1.411\}$	$\{1.420\}$	$\{1.400\}$	$\{1.405\}$	$\{1.434\}$	$\{1.432\}$
4	[1.398]	[1.397]	[1.439]	[1.426]	[1.399]	[1.397]	[1.423]	[1.420]
	$\{1.402\}$	$\{1.399\}$	$\{1.411\}$	$\{1.425\}$	$\{1.400\}$	$\{1.399\}$	$\{1.435\}$	$\{1.428\}$
6	[1.398]	[1.397]	[1.439]	[1.425]	[1.399]	[1.397]	[1.423]	[1.420]
	$\{1.402\}$	$\{1.399\}$	$\{1.411\}$	$\{1.425\}$	$\{1.400\}$	$\{1.399\}$	$\{1.435\}$	$\{1.428\}$
8	[1.398]	[1.397]	[1.439]	[1.425]	[1.398]	[1.398]	[1.423]	[1.420]
	$\{1.402\}$	$\{1.399\}$	$\{1.411\}$	$\{1.425\}$	$\{1.400\}$	$\{1.399\}$	$\{1.435\}$	{1.428}
10	[1.398]	[1.397]	[1.439]	[1.425]	[1.398]	[1.398]	[1.423]	[1.420]
	{1.402}	{1.399}	{1.412}	{1.425}	{1.402}	{1.400}	{1.435}	{1.428}

Table 2. Dependence of C1–C2 (in { }) and C2–C3 (in []) bond-lengths on the length of openand closed-end SWNT(9, 0) as obtained from geometry optimization using MM3 and AM1 techniques (see definition in Fig. 1).

basis (CEP-31G) in the first principles calculations exaggerates the C-C bond lengths, the relative difference between two C-C types is still maintained. From this observation, the use of AM1 method (which also neglect effects of the core electrons) to investigate relative difference in two types of the C-C bonds in longer CNT will be useful.

[1.425]

 $\{1.425\}$

[1.399]

 $\{1.402\}$

[1.397]

 $\{1.399\}$

[1.423]

 $\{1.435\}$

[1.420]

 $\{1.428\}$

12

[1.398]

{1.402}

[1.397]

{1.399}

[1.439]

 $\{1.412\}$

Dependence of the C1–C2 and C2–C3 bond lengths upon the increasing tubule length is listed in Table 2. Molecular mechanics does not take into account the increasing length effect for both open- and closed-end SWNTs. This method produces also almost identical C-C bond length located at the middle and terminal rings, which is independent on how the tube is capped. A relatively small variation (less than 0.005 Å) around the average value C-C of 1.40 Å is due to the tight quadratic nature of the MM3 potential energy surface.

In contrast, AM1 calculations yield different bond-length for C1–C2 and C2– C3 and is sensitive to the boundary effect on the tube geometry. Thus, the C-C bonds located at the terminal ends and at the middle cylinder are calculated to have different bond-length values. These values depend on how the tube is capped, namely whether they are open or closed. For instances, C1–C2 and C2–C3 bondlengths located at the terminal cylinder are 1.411 and 1.439 Å in the open-end structures, whereas they are 1.435 and 1.423 Å in the closed-end structures. The C-C bond-lengths located at the terminal cylinder are not dependent on the tubule length, in contrast to the ones located at the middle cylinder, which have converging values when the nanotubes grow beyond four unit cells. If the SWNT is long enough, one may expect that the C-C bond located at the middle cylinder should not depend on how the terminal ends are capped. As for the open-end 12UC structure,

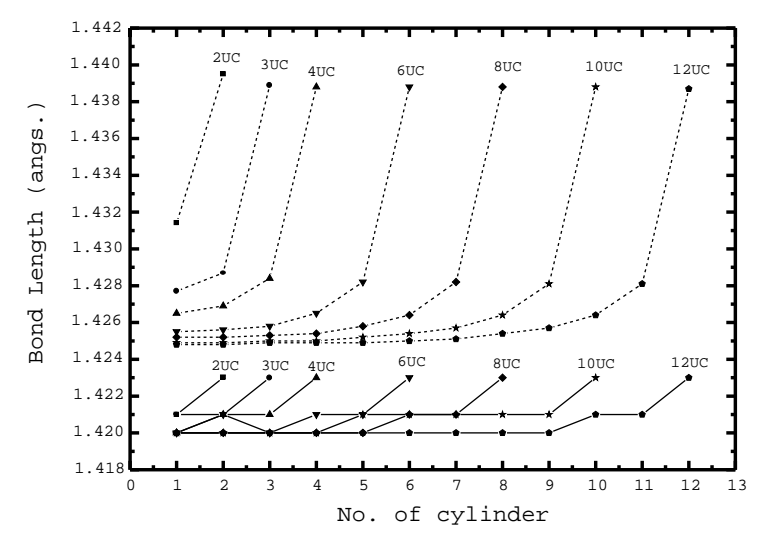


Fig. 2. Variation of C2–C3 bond length as its location changes from the middle cylinder to the tubule's end of the open-end (---) and closed-end (---) structures as the nanotube grows from 1UC to 12UC.

the middle cylinder have identical C–C bond length of 1.425 Å for both C1–C2 and C2–C3. For the closed-end 12UC structure, the C–C bond lying parallel to the tube axis is 0.008 Å shorter than those lying along the cylinder curve (1.420 Å versus 1.428 Å for C2–C3 and C1–C2, respectively). The experimental average C–C bond-length in bulk graphite and SWNT is 1.42 Å.

Figure 2 shows the variation of C2–C3 bond length as its location changes from the middle cylinder to the tubule's end. For both structures, the C2–C3 bond tends to be elongated when it is located near the tube's end. This effect is more elaborated in the case of open-end structures (up to 0.014 Å) than in the case of the closed-end ones (up to 0.003 Å only). This is probably caused by the electronegativity difference between C and H for the open-end structures, which does not exist in the closed-end SWNT. It can be seen that the terminal caps, either by hydrogen or fullerene, strongly affect the geometry only at the nearest C–C bond. For examples, the difference of the C2–C3 bond lengths between the middle cylinder (bond number 1) and the terminal cylinder (bond number 10) is 0.014 Å for the 10UC SWNT. This difference is exponentially reduced to only 0.003 Å when the terminal C2–C3 bond is just one bond into the tube (bond number 9). Thus, the boundary effect to the geometry of SWNT appears to be short-range.

3.2. Electronic properties

AM1 method is quite successful in providing structural information of carbon systems, compared to more expensive *ab initio* methods. For electronic properties, it has been however well-known that semi-empirical AM1 and *ab initio* Hartree–Fock

methods are poor in describing unoccupied molecular orbitals, leading to overestimated HOMO-LUMO energy gap. Therefore, the HOMO and LUMO from AM1 calculations will be used only for qualitative purpose, i.e., comparing electronic properties between the open- and closed-end structures. As seen from Table 1, AM1 method yields Mulliken charge and HOMO-LUMO gap in agreement with Hartree-Fock calculation for a cyclacene ring (1UC open-end SWNT). It is expected that AM1 method will give qualities comparable to Hartree–Fock method for longer nanotubes. Thus, dependence of the electronic properties on tubule length between open- and closed-end structures can be compared.

Figures 3(a) and 3(b) shows that the HOMO-LUMO energy gap is smaller as the tubule length increases for both open-end and closed-end structures, as similarly observed in finite-length conductive polymer.³¹ For the closed-end structure, HOMO has higher binding energy and becomes less stabilized when the tube becomes longer. HOMO in the open-end structures contrarily has lower binding energy and becomes more stabilized when the tubule length increases. However, the dependence of LUMO energy on the tubule length is quantitatively similar for both structures; namely, it becomes more stabilized with increasing length. The HOMO-LUMO energy gap for closed-end structure is higher than that of the open-end structure. Because of the overestimated HOMO-LUMO gap obtained from the AM1 method, it is not possible to know whether the HOMO-LUMO energy gap implies metallic or semi-conducting state. To solve this problem, we employ the Extended Hückel Molecular Orbital (EHMO) method, which is known to underestimate the molecular orbital energy. Thus, the real HOMO-LUMO energy gap is expected to locate between extreme values obtained from AM1 and EHMO methods.

From Fig. 3(b), the closed-end SWNTs have EHMO HOMO-LUMO energy gap less than 2.0 eV, with the energy gap almost vanishing (less than 0.25 eV) when the tubule length reaches 12 unit cells (50 Å long). It can also be seen that EHMO theory predicts vanishing HOMO-LUMO gap for finite-sized open-end SWNT (longer than 1UC). To estimate the real value of the HOMO-LUMO gap for the finite-sized SWNT, density functional theory (especially hybrid functionals), which is known to give HOMO-LUMO gap close to experimental values for conductive polymers, ³² is employed for 1UC-3UC structures. The energy gap of 1.7 and 0.3 eV (see Fig. 3(b)) are found for 3UC closed-end and open-end structures, respectively, which agrees with the above assumption that the practical HOMO-LUMO gap value should be between the ones yielded from AM1 and EHMO method. Thus, we can use AM1 and EHMO methods together to estimate HOMO-LUMO gap for longer structures that are impractical for DFT.

If we assume that the HOMO-LUMO energy gap is equivalent to the band gap concept in solid-state physics, the above results would suggest that finite-sized (9,0)SWNTs do not have metallic states as their counterpart does in the infinite range. Recent scanning tunneling spectroscopy also measures a band gap of 0.08 eV for nanosized (9, 0) SWNTs, as opposed to simple analytical theory.³³ Although the open-end SWNTs show smaller HOMO-LUMO gap, which may mean that they

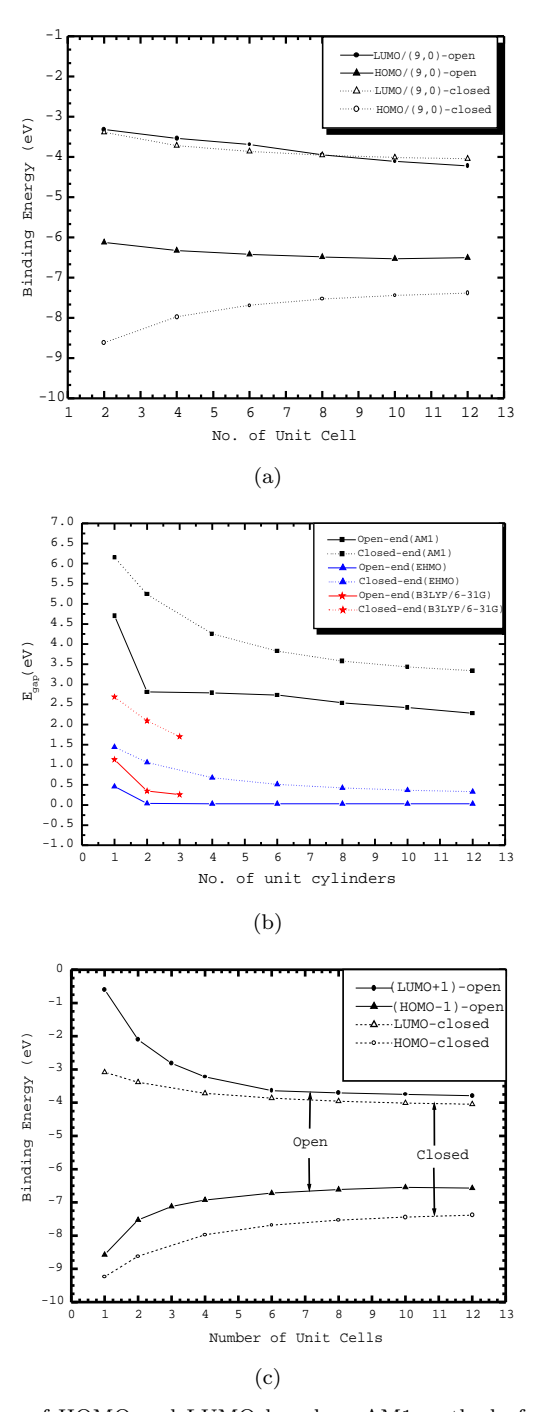


Fig. 3. (a) Dependence of HOMO and LUMO based on AM1 method of open- and closed-end structures on the length of nanotube. (b) Comparison of HOMO–LUMO energy gap obtained from EHMO, AM1 and DFT methods and its dependence on the tubule length. (c) Comparison of the delocalized frontier orbitals for the open-end (HOMO-1 and LUMO+1) and closed-end (HOMO and LUMO) structures.

have more metallic behavior than the closed-end structures, orbital analyses show that HOMO and LUMO are localized at the terminal ends in the case of the openend structures instead of the delocalized states for the case of closed-end structures. To compare the frontier orbital energy gap in the sense of solid-state physics, the delocalized states, HOMO-1 and LUMO+1, are chosen for the open-end structures.

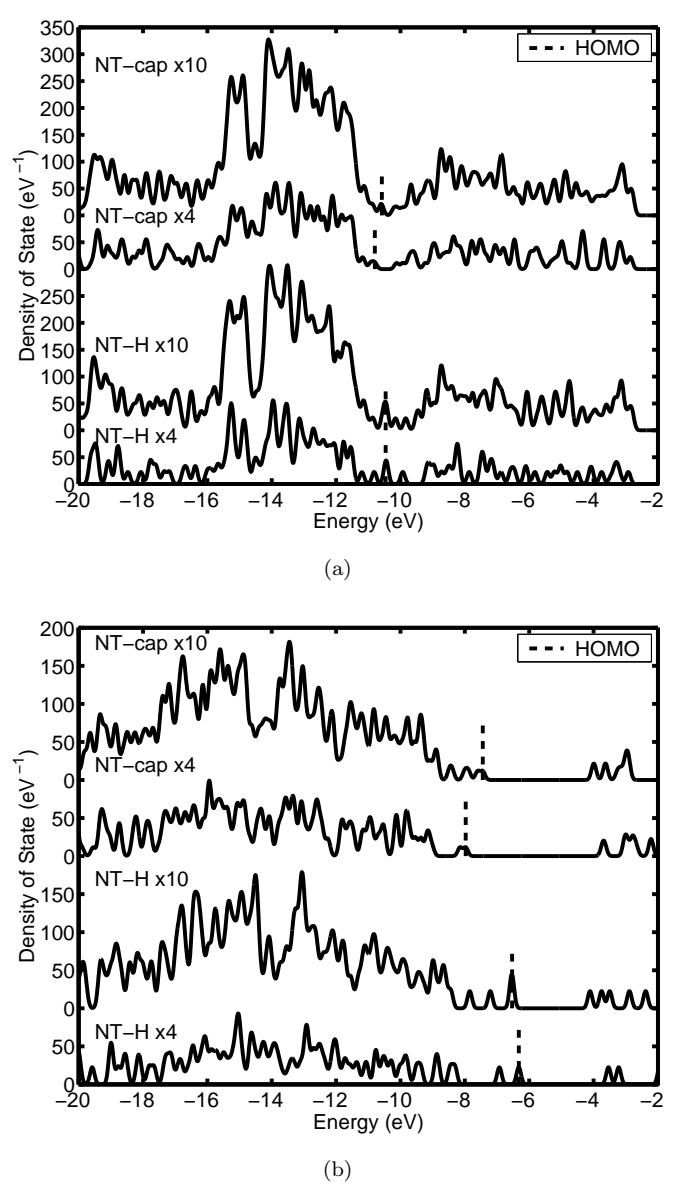


Fig. 4. Density of states for the $4\mathrm{UC}$ and $10\mathrm{UC}$ open- and closed-end structures based on (a) EHMO and (b) AM1 methods.

Figure 3(c) shows that delocalized HOMO–LUMO gap for closed-end SWNT and delocalized (HOMO-1)–(LUMO+1) gap have comparable value, which means that the conducting channel of SWNT is not affected by the boundary state.

Densities of states (DOS) based on EHMO and AM1 methods for 4UC and 10UC SWNTs are plotted in Figs. 4(a) and 4(b). It can be seen that the DOS pattern for open- and closed-end SWNTs differ only around the frontier states. Both methods illustrate that the boundary condition (whether SWNT is open or closed) does not influence the energy states below the frontier level. For examples, looking at the AM1 DOS of open- and closed-end 10UC SWNTs, we see that both structures have three bands for the occupied states (binding energy between 8–12, 12–14 and 14–20 eV). Increasing the tubule length adds more states into the level below the frontier states, but only slightly changes the pattern of the DOS and does not modify the population of the frontier states. It becomes clear that HOMO, LUMO and a few states around them can be regarded as defect states caused by the boundary condition. Based on this idea, the real energy band gap will be somewhat larger and thereby supporting the semiconducting behavior of the finite SWNT.

Table 3 displays the net atomic charge summed on a carbon cylinder located at the middle and at the terminal of SWNT. Due to the boundary effect, it can be seen that the net atomic charge inside the open-end structures is negative, as opposed to the closed-end ones where it is positive. In the case of open-end structures, carbon atoms at the terminal draw electrons from hydrogen atoms into the tube. These excessive electronic charges are shared among the other carbons in the tube. For the closed-end structures, it is surprising to observe slightly positive charge accumulated inside the nanotube. This implies that the fullerene caps draw electrons from the tube. To confirm this assumption, total net atomic charge on the fullerene caps are summed. The fullerene cap demonstrates a capability to draw electron out of the tube: it draws 0.029 electron from the two unit-cell long tube and as the tubule length increases more electronic charge is drawn out to reach maximum capacity at 0.054 electron. In a recent LDA calculation of a model (9, 0) nanotube, the charge accumulation on the nanotube's cap is related to the sharpness of the tip.³⁴

Table 3. Mulliken atomic net charge summed over all carbon atoms located at the terminal cylinder and middle cylinder. For the closed-end structures, summation over all carbons located in the fullerene cap is also shown.

	Open-end structure		Closed-end structure			
No. CNTs unit cells	Terminal	Middle	Terminal	Middle	Fullerene cap	
2	-1.268	-0.234	0.03	0.084	-0.029	
4	-1.21	-0.055	0.021	0.032	-0.045	
6	-1.211	-0.036	0.006	0.02	-0.054	
8	-1.206	-0.025	0.006	0.006	-0.054	
10	-1.201	-0.02	0.006	0.006	-0.054	
12	-1.199	-0.018	0.006	0.005	-0.054	

4. Summary

The geometrical and electronic properties of (9, 0) single-walled carbon nanotube having open-end and closed-end structure are investigated using molecular mechanics (MM3), semi-empirical AM1 method and density functional theory (B3LYP). MM3 overlooks the length of the nanotube and how it is capped at the ends by producing almost identical C-C bond-length values. Semi-empirical AM1 method is rather sensitive to the boundary conditions, though the effect is only short-range. Although these effects seem to exponentially decrease as the tube gets longer, the converging values for C-C bond length in the open- and closed-end structures are slightly different (1.425 versus 1.420 A). It was learned from this work that combination of low-level methods like AM1 and EHMO (which tend to overestimate and underestimate the HOMO-LUMO energy gap, respectively) together with high-level method such as DFT is efficient to estimate band gap and other electronic properties for finite-sized nanoscale structures, which is important for nanocircuit design. Terminal capping strongly affects the electronic structure of finite-sized nanotube. Closing the terminal ends by fullerene hemisphere broadens the energy gap of the hydrogen-saturated open-end nanotube. Although the open-end SWNT has much lower HOMO-LUMO energy gap than the closed-end SWNT (2.28 versus 3.34 eV for 12 unit-cell), these orbitals unfortunately are localized near the capping hydrogen, thereby not providing conducting channels for electrons. Comparing only the delocalized frontier orbitals, both structures yield comparable energy gap (2.78 versus 3.34 eV for 12 unit-cell). Based on the band theory model, finite-sized (9, 0) SWNT having either open or closed ends are semiconductor. Therefore, these structures are appropriate for devices (i.e., switch), not conducting wire, for nanoscale circuits.

Acknowledgments

A. Udomvech expresses his gratitude to Ministry of University Affairs. Financial support by the Thailand Research Fund is gratefully acknowledged (BRG/21/2544). The authors are thankful to Professor I. M. Tang for proofreading the manuscript.

References

- 1. S. Iijima, *Nature* **354**, 56 (1991).
- 2. P. M. Ajayan and T. W. Ebbesen, Rep. Prog. Phys. 60, 1025 (1997).
- 3. P. M. Ajayan, Chem. Rev. 99, 1787 (1999).
- 4. C. N. R. Rao, B. C. Satishkumar, A. Govindaraj, and M. Nath, Chem. Phys. Chem. **2**, 78 (2001).
- 5. S. Iijima and T. Ichihashi, *Nature* **363**, 603 (1993).
- 6. G. Maurin, Ch. Bousquet, F. Henn, P. Bernier, R. Almairac, and B. Simon, Chem. Phys. Lett. **312**, 14 (1999).
- 7. A. Cao, H. Zhu, X. Zhang, X. Li, D. Ruan, C. Xu, B. Wei, J. Liang, and D. Wu, Chem. Phys. Lett. 342, 510 (2001).
- 8. T. W. Ebbesen, Phys. Today 49, 26 (1996).

- 9. A. Rubio, S. P. Apell, L. C. Venema, and C. Dekker, Eur. Phys. J. B 17, 301 (2000).
- 10. I. Stepanek, G. Maurin, P. Bernier, J. Gavillet, A. Loiseau, R. Edwards, and O. Jaschinski, Chem. Phys. Lett. **331**, 125 (2000).
- 11. R. Saito, M. Fujita, G. Dresselhaus, and M. S. Dresselhaus, Phys. Rev. B 46, 1804 (1992).
- 12. S. Peng and K. Cho, *Nanotechnology* **11**, 57 (2000).
- 13. L. Yang and J. Han, Phys. Rev. Lett. 85, 154 (2000).
- 14. V. Meregalli and M. Parrinello, Appl. Phys. A 72, 143 (2001).
- 15. V. V. Simonyan, J. Karl Johnson, A. Kuznetsova, and J. T. Yates, Jr., J. Chem. Phys. **114**, 4180 (2001).
- 16. G. Van Lier, C. Van Alsenoy, V. Van Doren, and P. Geerlings, Chem. Phys. Lett. 326, 181 (2000).
- 17. L.-M. Peng, Z. L. Zhang, Z. Q. Xue, Q. D. Wu, Z. N. Gu, and D. G. Pettifor, Phys. Rev. Lett. 85, 3249 (2000).
- 18. J. Wu, W. Duan, B.-L. Gu, J.-Z. Yu, and Y. Kawazoe, Appl. Phys. Lett. 77, 2554 (2000).
- 19. A. N. Andriotis and M. Menon, J. Chem. Phys. 115, 2737 (2001).
- 20. A. N. Andriotis, M. Menon, D. Srivastava, and L. Chernozatonskii, Phys. Rev. Lett. **87**, 066802 (2001).
- 21. A. N. Andriotis, M. Menon, D. Srivastava, and L. Chernozatonskii, Appl. Phys. Lett. **79**, 266 (2001).
- 22. L. Türker, J. Mol. Struc. (Theochem) 490, 55 (1999).
- 23. L. Türker, J. Mol. Struc. (Theochem) **536**, 235 (2001).
- 24. G. Maurin, Ch. Bousquet, F. Henn, P. Bernier, R. Almairac, and B. Simon, Chem. Phys. Lett. 312, 14 (1999).
- 25. J. Yang, H. J. Liu, and C. T. Chan, Phys. Rev. B 64, 085420 (2001).
- 26. N. L. Allinger, Y. H. Yuh, and J.-H. Lii, J. Am. Chem. Soc. 111, 8551 (1989).
- 27. M. J. S. Dewar, E. G. Zoebisch, E. F. Healy, and J. J. P. Stewart, J. Am. Chem. Soc. **107**, 3902 (1985).
- 28. J. Han, A. Globus, R. Jaffe, and G. Deardorff, Nanotechnology 8, 95 (1997).
- 29. A. Rochefort, D. R. Salahub, and P. Avouris, J. Phys. Chem. B 103, 641 (1999).
- 30. S. Erkoc, Int. J. Mod. Phys. C 11, 175 (2000).
- 31. M. S. Wong, Z. H. Li, M. F. Shek, K. H. Chow, Y. Tao, and M. D'Iorio, J. Mater. Chem. 10, 1805 (2000).
- 32. U. Salzner, P. G. Pickup, R. A. Poirier, and J. B. Lagowski, J. Phys. Chem. A 102,
- 33. M. Ouyang, J. L. Huang, C. L. Cheung, and C. M. Lieber, Science 292, 702 (2001).
- 34. C. Kim, B. Kim, S. M. Lee, C. Jo, and Y. H. Lee, *Phys. Rev. B* **65**, 165418 (2002).

Energetic and Structural Properties of Li-intercalated the Ultra-Small Diameter Single-Walled Carbon Nanotubes

Anurak Udomvech^{1,2}, Tanakorn Osotchan¹ and Teerakiat Kerdcharoen¹
¹Center for Nanoscience and Nanotechnology, Department of Physics, Faculty of Science, Mahidol University, Rama 6 Road, Bangkok, 10400 Thailand.

²Department of Physics, Faculty of Science, Thaksin University, Songkhla, 90000 Thailand.

Abstract

The energetic and structural properties of two Li-intercalated 4 Å single-walled carbon nanotubes (SWCNTs) have been studied based on the density functional theory. The (3,3), (4,2), and (5,0) SWCNTs are used in this work. Our calculation employed the hybrid functional B3LYP and various all electrons basis set models. The binding energies indicated that Li atoms can be draw from exterior into interior of an ultra-small nanotube, while zigzag (5,0) tube has energy barrier at the open-mount. The energy profiles along the longitudinal axis of two Li inside the zigzag (5,0) and armchair (3,3) are slightly fluctuating, whereas it is rather flat for the chiral (4,2) nanotube. Zigzag (5,0) nanotube has been shown explicitly Li-Li localized near the tube-center. It probably formed a Li cluster inside the zigzag nanotube. Oppositely, each Li is located at each tube-mount of the armchair (3,3) tube. In case of (4,2) tube, no preferential location is found for two Li atoms, as described by flat potential energy profile. The intercalated atoms affect the geometric parameter of the central region structure more than the rest of the ultra-small nanotube. The structural properties of zigzag (5,0) nanotube is more sensitive to the intercalated atoms than the armchair (3,3) and chiral (4,2) structures, respectively. Both results could be used to verify the strong chiralities dependence of the ultra-small nanotubes.

1 Introduction

Since the discovery by Iijima in 1991, carbon nanotube (CNT) [1,2] have attracted much attention as a potential candidate for nanoscale devices. Particularly, single-walled carbon nanotubes (SWCNTs) [2] have more the subject of intense experimental and theoretical investigation. Therefore their unique properties are small diameter, high tensile strength [3], high chemical and thermal stabilities, heat conduction [4], and remarkable electronics [5,6,7,8], etc. An individual SWCNT can be thought of as a rolled perfect graphite single layer (or graphene). Depending on the way of rolling up graphene, various SWCNTs with different chiralities and diameters can be theoretically studied to obtain various properties and novel applications. Recently, SWCNTs are now routinely being fabricated in experiments. Especially, SWCNTs with ultra-small diameter were fabricated inside the microporous channels of zeolite AlPO₄₋₅ (AFI) single crystal.[9,10,11] These carbon nanotubes have a very small diameter of ~ 4 Å and are perfectly arranged in a close-packed hexagonal lattice.

In the present study, we have studied the intercalation of Li atoms through the opening mount of ultra-small diameter (~4Å) SWCNTs to investigate its possibility of confinement guess atoms and structural effects of 4Å SWCNTs due to Li intercalation. Li atoms inserted into different chiralities of SWCNT as a function of distance along tube axis, since the curvature effect is very strong, were examined. There are three chiralities of SWCNTs, i.e., the armchair (3,3), zigzag (5,0), and chiral (4,2).

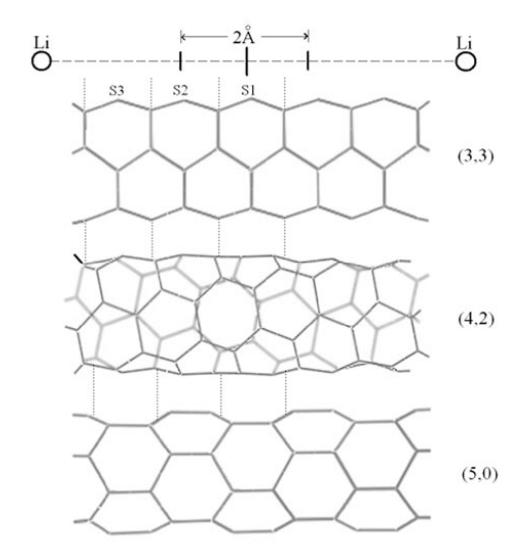


Fig.1. Model of 2Li atoms intercalated along tube-axis inside the ultra-small diameter SWCNTs

2 Computational Details and Modeling

The calculations are based on role of self-consistent field approach using density functional theory. Hybrid-functional of B3LYP [12,13] in generalized gradient approximation (GGA) was chosen. The 6-31G(d) basis set that includes a set of d-like wave functions is used in calculation of the 2Li-SWCNT rigid model. Rigid structures of SWCNT real-space cluster model are obtained from relaxed primarily SWCNT structure by B3LYP and split-valence 3-21G basis set (B3LYP/3-21G). The fully relaxation of two Li-SWCNT models are employed notation of B3LYP/3-21G//B3LYP/3-21G for observation the optimized parameters and interaction energies to verify potential surface compare with rigid model. The optimal energy of relaxed two Li-SWCNTs rigid structures are also carried out with notation of B3LYP/6-31G(d)//B3LYP/3-21G. All models are calculation on each atom, i.e., C, H, and Li atoms. The unrestricted spin wave functions are used, i.e., different orbital is played for different spins.

The finite-length SWCNTs are choose to model (see in figure 1) each type with nominal formulas $C_{66}H_{12}$, $C_{72}H_{12}$, and $C_{80}H_{10}$ for ultra-small diameter (3,3), (4,2), and (5,0) respectively. In calculation, lithium atoms are constrained movement in the distance along tube-axis. Two Li atoms are positioned to penetrate symmetrically, one on each end of the nanotube. The rims of all finite nanotube structures were saturated by hydrogen. The interaction energy of the system is defined by subtracting the sum of the total energy of undoped nanotube and the energies of the isolated Li atoms from the total energy of the complex system.

3 Results and Discussion

Practically, using the chirality effect for the energetic of Li atoms inside the ultra-small diameter nanotubes, we consider whether the alkali atoms can overcome the barrier of insertion and the ability of atoms are inside nanotube. Our previous work [14] revealed that Li atom favorably located at the center of small diameter (6,0) nanotube. We referred the longitudinal direction along nanotube-axis as a pathway for moving 2-Li atoms through the open-mount and along longitudinal direction of ultra-small diameter nanotubes.

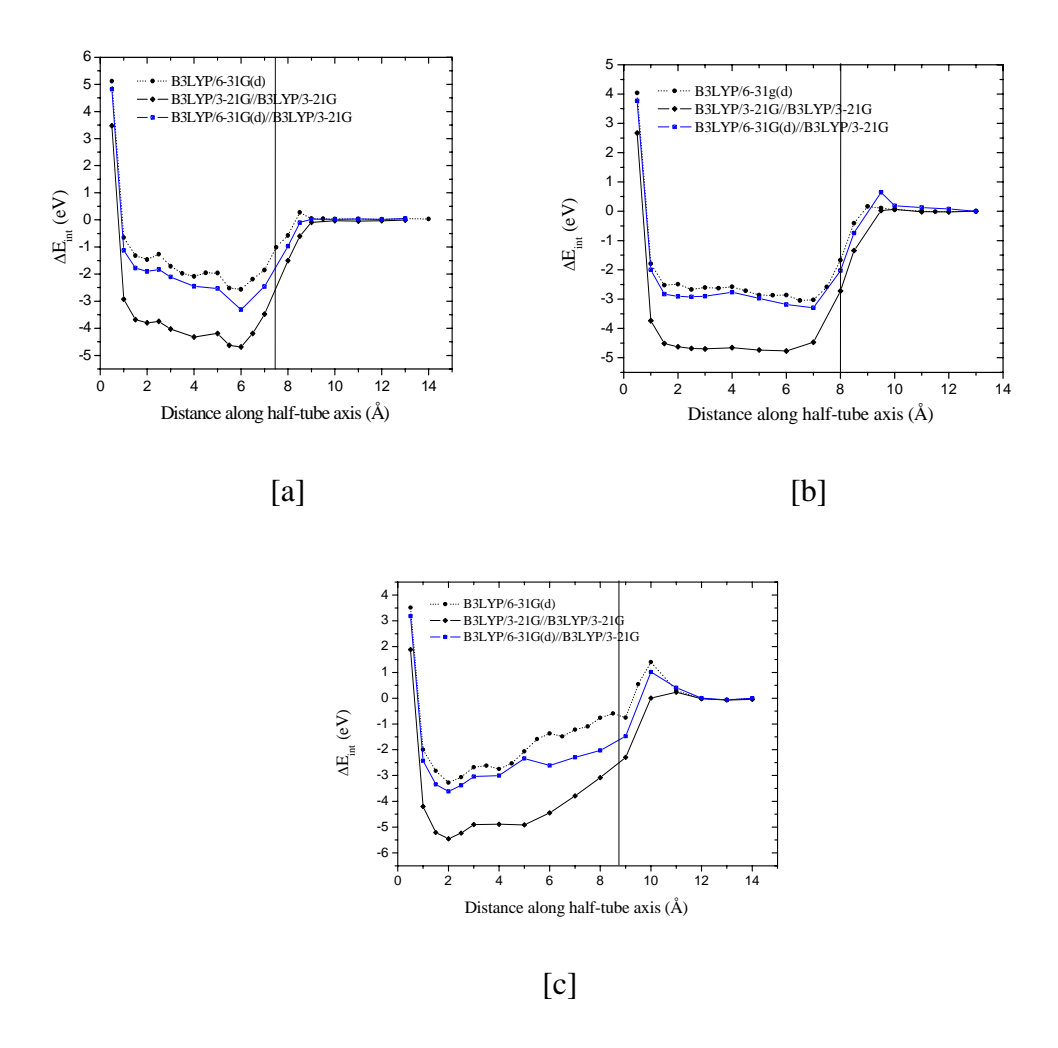


Fig.2. The interaction energies as a function of the distance measured from the geometric center of the finite-length [a] (3,3), [b] (4,2), and [c] (5,0) nanotubes. The dot-circle line is binding energy from rigid model, solid-square line is interaction energy form the model of fully optimization of two Li-SWCNTs, and triangle-blue line is interaction energy from B3LYP/6-31G(d)//B3LYP/3-21G model. The vertical solid line marks the position of the nanotube edge.

The binding energy of all models is demonstrated in Figure 2. They demonstrated the binding energy compare with the distance along half tube-axis. All models are shown the energy change as 2-Li penetrated through each open-mount of SWCNTs. It referred Li atoms have lower binding energy inside than outside. These results could confirm that Li can be draw from exterior into interior of an ultra-small nanotube. However, it appeared energy barrier at the open-mount of (5,0) chirality for non-relaxed rigid B3LYP/6-31G(d) (black-dot line) and relaxed rigid B3LYP/6-31G(d)//B3LYP/3-21G (blue line) models (see figure 2c). Even though both rigid models are not so well with (5,0) tube at open-mount, though the energy profile of rigid models are still satisfy the energy profile of fully relaxation (B3LYP/3-21G//B3LYP/3-21G) model. Because of rigid B3LYP/6-31G(d)//B3LYP/3-21G model has given the binding energy behind fully relaxation model, the quantitative binding energy exhibited deeper than non-relaxed rigid model about 22%. However, it implied that the rigid model could qualitatively used to describe the potential curve of Li atoms intercalation the ultra-small SWCNTs. For fully relaxation model (black line), the energy profile inside the fully relaxed 2-Li intercalated shortly (3,3) and (5,0) nanotubes have a slightly energy barrier fluctuation. Particularly (3,3) chirality (figure 2a), It has shown

deeper binding energy (~5 eV) when Li atoms located at each open-mount than the rest. Oppositely, (5,0) tube shown the binding energy (~5.5 eV) when Li-Li closed to nanotube center. It revealed deeper binding energy than it is located near the open-mount (see figure 2c). For (4,2) chirality has rather flat energy curve if Li atoms located inside nanotubes (see figure 2b).

The Li-Li interaction inside (3,3) has a rather long-range Coulomb repulsion than the others tubes. For (3,3) tube, the interaction shows Li atoms has strongly repulsive even though both Li atoms are as long as possible a distance inside nanotube. It would ensure that Li can not easily movement inside (3,3) structure. However, (5,0) nanotube has been shown explicitly difference of Li-Li interaction with (3,3) and (4,2) tubes. It was exhibited more attractive energy inside nanotube when two Li atoms closed together. Then, it probably formed a Li cluster at tube-center of (5,0) nanotube.

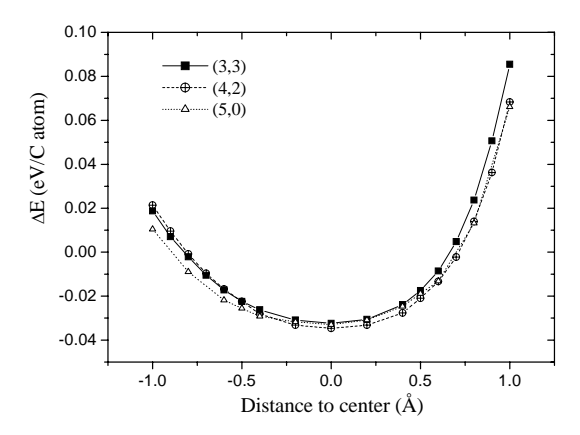


Fig.3. The binding energies per C atom as a function of the distance measured along cross-section of the finite-length (3,3), (4,2), and (5,0) nanotubes. The B3LYP/6-31G(d) energies obtained from 2-Li atom into SWCNT relaxed structures by B3LYP/3-21G

In order to determine the chirality dependence of Li-intercalated ultra-small diameter SWCNTs, the binding energies per C atom as a function of the distance measured along cross-section of the finite-length (3,3), (4,2), and (5,0) nanotubes are investigated in figure 3. In radial direction, we calculated binding energy by rigid B3LYP/6-31G(d) model in which SWCNT structures were relaxed B3LYP/3-21G technique. Li atom is moved from tube-axis in left side (or minus sign (-)) toward the center of hexagon and toward the C-C bond of opposite sidewall. It exhibited lowest energy at center of all tubes. However, the energy curve of all tubes shown a few different when Li toward the sidewall. The energy curve nearly the center of hexagon of (3,3) and (4,2) tubes almost coincide with each other, while that of (5,0) has a lower energy. Even so it has manifested the coincidence between (4,2) and (5,0) tubes if Li toward the C-C bond, while (3,3) has a higher energy. This emphasizes the interaction in radial direction of ultra-small diameter SWCNTs belief that strong curvature has affect Li-Li interaction. Both radial and longitudinal directions, there has shown strong dependence of Li-Li binding energy on the chirality of ultra-small diameter nanotubes.

Initially, the finite-length geometry of ultra-small diameter SWCNTs are obtained from the bulk graphite. All bonding have isotropic. These structures are fully relaxed by B3LYP/3-21G method. In complex systems, we optimized those structures with the same methods to obtain the bond length. To analyze the changing of bond length from pristine to 2Li-intercalated nanotube system, we divided the structure of nanotubes as section of cylinders (see figure 1). Each section is denoted by S1, S2, S3, and so on. The average C-C bond length (bl_{av}) of pristine nanotubes by 3-21G is demonstrated in Table 1.

Table 1. The average C-C bond length (bl_{av}) of pristine (3,3), (4,2), and (5,0) nanotubes. S1, S2, S3, and S4 indicated each section of nanotube along tube-axis (see model in figure 1)

model III	ngure 1)					
Chirality of					bl _{av} (Å) from
SWCNTs		bl_{av}	(Å)		LDA cal	lculation
_	S 1	S2	S 3	S4	Ref. ^a	Ref. ^b
Pristine (3,3)	1.435	1.445	1.426		1.422	1.435
Pristine (4,2)	1.435	1.438	1.430		1.425	1.430
Pristine (5,0)	1.440	1.441	1.438	1.438	1.419	1.425

^aThe structure of the 4 Å-diameter SWCNTs inside the AFI single crystal. ¹⁵

^bThe structure of the isolated 4 Å-diameter SWCNTs. ¹⁶

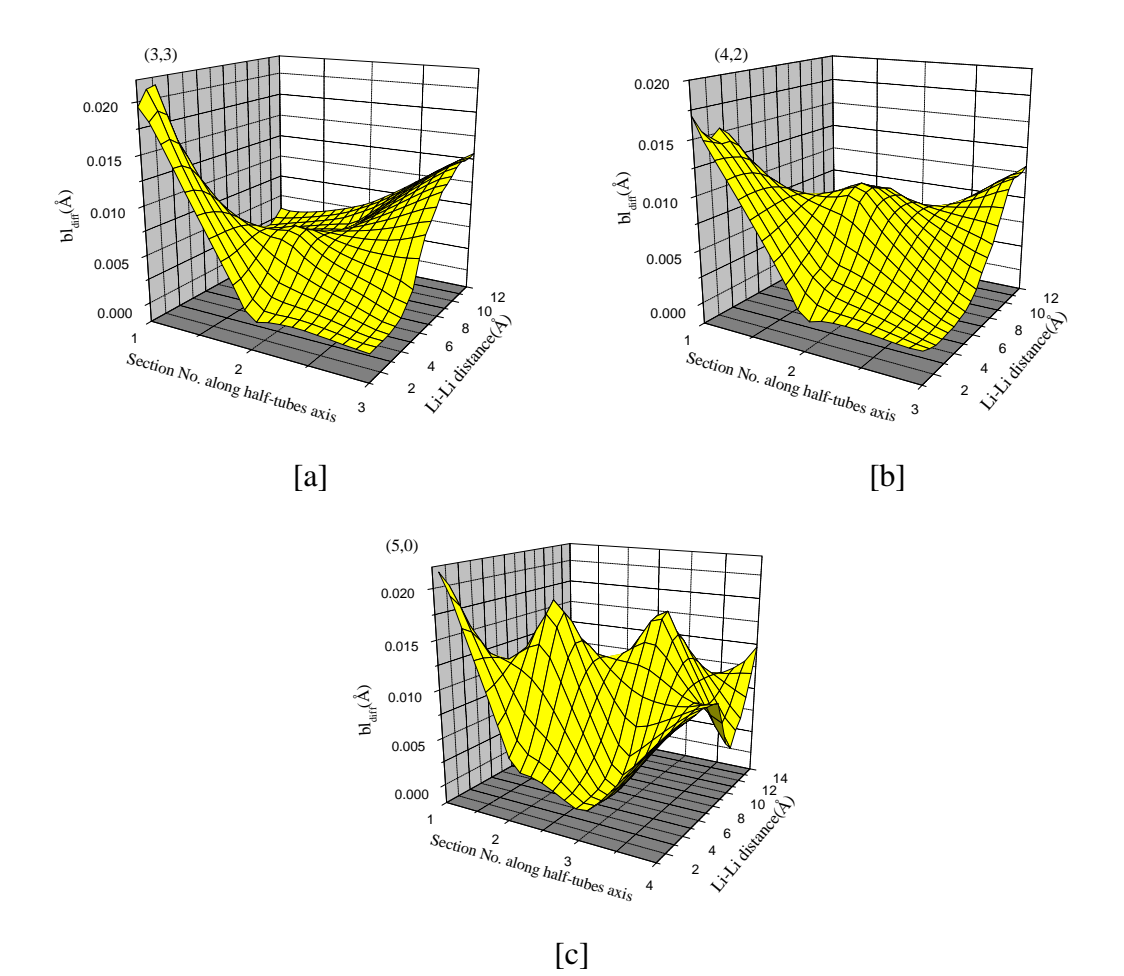


Figure 5 The C-C bond length difference (bl_{diff}) is the average C-C bond length (bl_{av}) of the intercalation 2Li atoms inside SWCNTs are relatively change to bl_{av} of pristine [a] (3,3), [b] (4,2), and [c] (5,0) nanotubes, respectively.

From Table 1, we compared the bl_{av} on each section with LDA results from Yanga [15] and Liu.[16] Our bl_{av} has rather more resolution than bl_{av} of 4 Å-diameter SWCNTs inside the AFI system. However, a periodically LDA calculation of isolated 4 Å-diameter SWCNTs is in agreement with our bl_{av} within a range of 0.01-0.02 Å. Such differences are due to hybrid B3LYP functional and the full basis set (3-21G). Each section and each type of chiralities is no identical bl_{av} . For each section, the explicitly different S2>S1>S3 of bl_{av} are found for all nanotubes. The bond length at terminal (or

S3, S4) is shortest bond length and S2 is largest bond length. For middle (or S1), bond length is the same for (3,3) and (4,2) tubes. Even so it has shown different from (5,0) tube. This is similarity with the LDA calculations that bl_{av} of (3,3) and (4,2) almost equivalence.

For intercalation system, the bond-length difference (bl_{diff}) of 2Li-intercalated ultra-small diameter SWCNTs are shown in figure 5. These bl_{diff} are measured comparison with pristine nanotubes in Table 1. All figures are plotted in 3D to perform the changing of nanotube structure when Li-Li distance is located on each configuration along tube-axis. For all nanotubes, bl_{diff} at S1 is most disturbances since Li-Li distance closed together. S2 is smallest disturbance for armchair tube (figure 5a) whereas Li-Li distance about 4-6 Å. For (4,2) tube (figure 5b), bl_{diff} of S1 and S3 is smaller disturbed than (3,3) tube. However S2 is a few more than (3,3) tube. Particularly, (5,0) tube is shown some explicitly structural effects due to Li-Li interaction (see figure 5c). All sections are strongly disturbed more than others.

4 Conclusion

In summary, Li atoms can overcome the nanotube mounts into the interior of an ultra-small nanotube, while zigzag (5,0) tube has energy barrier at the open-mount. The energy profiles along the tube-axis of two Li inside the zigzag (5,0) and armchair (3,3) has occurs slightly fluctuating, whereas it is rather flat for the chiral (4,2) nanotube. Zigzag (5,0) nanotube has been shown explicitly Li-Li localized near the tube-center. It probably formed a Li cluster inside the zigzag nanotube. Oppositely, each Li is located at each tube-mount of the armchair (3,3) tube. In case of (4,2) tube, no preferential location is found for two Li atoms, as described by flat potential energy profile. The intercalated atoms affect the geometric parameter of the central region structure more than the rest of the ultra-small nanotube. The structural properties of zigzag (5,0) nanotube is more sensitive to the intercalated atoms than the armchair (3,3) and chiral (4,2) structures, respectively. Both results could be used to verify the strong chiralities dependence of the ultra-small nanotubes.

Acknowledgments

The author expresses gratitude to the Department of Mathematic for High Performance Computing and Center for Nanoscience and Nanotechnology, Mahidol University for Computation has been done.

References

- [1] S. Iijima, *Nature (London)*, 354 (1991), 56.
- [2] S. Iijima, T. Ichibashi, *Nature (London)*, 363 (1993), 603.
- [3] Z. Tu, Ou-Yang, *Phys. Rev. B*, 65 (2002), 233407.
- [4] A.A Farajian, et.al. *Phys. Rev. B*, 67 (2003), 205423.
- [5] T. W. Odom, et.al. Nature, 391 (1998), 62-64.
- [6] A. Javey, et. al. Nature, 424 (2003), 654.
- [7] P. Avouris, Chem. Phys., 281 (2002), 429-445.
- [8] J. Kong, et. al. *Science*, 287 (2000), 287, 622.
- [9] Z.K. Tang, et.al. Appl. Phys. Lett., 73 (1998), 2287.
- [10] H. Shimoda, et.al. Phys. Rev. Lett., 88 (2002), 015502.
- [11] N. Wang, Z. K. Tang, G. D. Li, J. S. Chen, Nature (London), 408 (2000), 51.
- [12] A.D. Beck, J. Chem. Phys., 98 (1993), 5648.
- [13] C. Lee, W. Yang, R.G. Parr, Phys. Rev. B, 38 (1998), 785.
- [14] A. Udomvech, T. Osotchan, T. Kerdcharoen, Chem. Phys. Lett., 406 (2005), 161.
- [15] X.P. Yanga, et al. Eur. Phys. J. B, 32 (2003), 345.
- [16] H.J.Liu, C.T. Chan, Phys. Rev. B, 66 (2002), 115416.

THEORETICAL INVESTIGATION OF LITHIUM CLUSTERS INSERTION INTO SINGLE-WALLED CARBON NANOTUBES

Anurak Udomvech^{1,3}, Thanh N. Truong² and Teerakiat Kerdcharoen^{1,3}

¹ Department of Physics, Faculty of Science, Mahidol University, Bangkok, 10400

² Department of Chemistry, University of Utah, Salt Lake City, USA.

³ Capability Building Center for Nanoscience and Nanotechnology, Mahidol University, Bangkok, 10400

ABSTRACT: Theoretical investigations on single-walled carbon nanotubes (SWNTs) have been performed using first-principles total energy calculations to explore feasibility of doping Li atoms through the open-end of nanotubes. Our previous work has shown that Li@tube systems could enhance the capacity of lithium batteries by using both interiors and exteriors of nanotubes. The insertion of Li atoms into (6,0) single-walled carbon nanotubes have shown no insertion barrier in which the tube's mouth is passivated. The diffusion barrier is small inside the nanotube and Li atoms prefer to reside along the tube axis. For the different diameter tube, (9,0), it has shown different interaction characteristic if lithium is located at tube axis.

KEYWORDS: carbon nanotubes, single-walled, first-principle, DFT, Li, alkali-metal

1. INTRODUCTION

At the moment, carbon nanotubes have attracted much attention as materials for nanoscale applications. Therefore, they can be both metallic and semiconductor depend on their chirality (Saito 1998). The other unique properties of carbon nanotubes are high tensile strength (Tu *et al* 2002), high chemical, thermal stability and remarkable electronic conduction (Baughman *et al* 2002, Yoon *et al* 2002, Farajian *et al* 2003). They have hollow inside which can be used as storage of atoms and ions for batteries applications. Carbon nanotube can adsorb a number of atomic and molecular species, for instances alkali metals (Bendiab *et al* 2001, Claye *et al* 2000, Rao et al 1997, Wadhawan *et al* 2001) and hydrogen, nitrogen, oxygen, and methane gases. The adsorption properties provide the opportunities for applications such as hydrogen and other gases storage (Dillon *et al* 2001), gas sensor (Peng *et al* 2000), catalyst (Nisha et al 2000) and Li-ion batteries (Tarascon *et al* 2001).

In our research, we have studied the insertion of alkali-metal atoms through the opening mount of single-walled carbon nanotubes as a function of distance along tube-axis, as well as variation of nanotubes' length. The nanotube diameter is also studied in some specific structures to investigate the effects on potential energy.

2. METHOD AND DETAILS OF CALCULATIONS

In our work, the calculations have been carried out in the density functional formalism with a self-consistent manner. The insertion process is performed using a real-space cluster scheme with Becke's 3-parameter hybrid functional (Becke 1993) where the correlation functions is provided by the functional of Lee-Yang-Parr, which includes both local and non-local terms (Lee *et al* 1988, Miehlich *et al* 1989). We use a standard all-electron basis set of 6-31G to represent orbitals of C, H, and Li atoms in all calculations. Spin-unrestricted wave functions are employed for different orbitals and spins.

All the SWNT structures employed in this study are the zigzag type represented by a chirality of vector (m,0) (Saito 1998). The SWNT in this study are finite-sized by varying unit-cell cylinder along tube-axis and hydrogen atoms are used to cap the dangling carbon atoms at the two open-ends of the nanotube. The structure of nanotubes have been non-relaxing atomic coordinate, in order to save computational effort with point group symmetry of *D6H* and *C2V* for (6,0) and (9,0)

nanotubes respectively. Penetration of Li through the two open-ends of nanotube has been done based on tube-axis trajectory.

3. RESULTS AND DISCUSSIONS

Our previous work on the potential energy surface of Li atom inside (6,0) SWNT has demonstrated that Li atom prefers energy minima located at the center of nanotube (Udomvech *et al* (unpublished)) as depicted in **Figure 1.** From this point, the present works used the direction of (6,0) nanotube center as a reference path for moving Li atoms through the open-mount of nanotube. The binding energy profile of the system was defined by subtracting the total energy of the whole from the sum of the total energy of SWNTs and the energies of the isolated Li atoms.

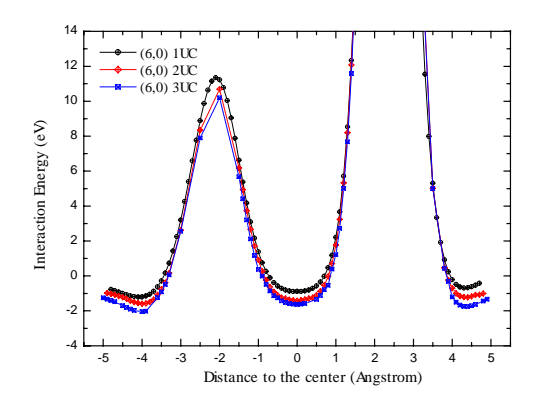
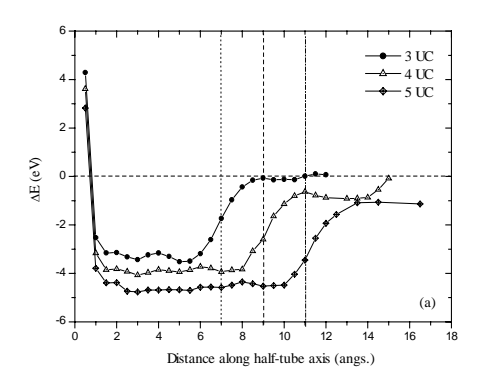


Figure 1. Demonstration of potential energy surface of Li atom and (6,0) nanotube interaction on cross section direction

With theoretical investigation using density functional approach, we found that the insertion of two Li atoms into (6,0) single-walled carbon nanotubes has no insertion barrier in which the tube mouth is passivated by H as depicted in **Figure 2**. The dot, dash and dot-dash lines indicated the rim of nanotubes of different lengths. The Li atoms have lower energy inside the nanotube than outside the nanotubes. For two Li atom-SWNT (**Figure 2a**), all structures exhibit small diffusion barrier inside the nanotube, which suggested that Li atoms prefer to reside along the tube axis and not freely moving. Particularly, the interaction of 2 Li atoms inside nanotube 3UC (~7 Å) is similar to the results of Liu and co-worker (Liu *et al* 2003). The binding energy curves for Li-C are rather smooth for nanotube length 5UC (~11 Å). These results show different binding energy from LDA approach by Yang and co-worker which suggests there is no energy barrier to docking Li atoms inside nanotubes (Yang *et al* 2001). The binding energy curves give the screened Li-Li interaction when the two Li atoms are close to each other. The Li-Li interaction is weakly repulsive at long distance of two Li atoms that will possibly push other Li atoms into the interior nanotube.



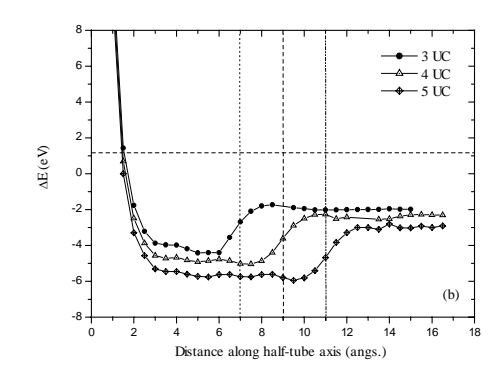
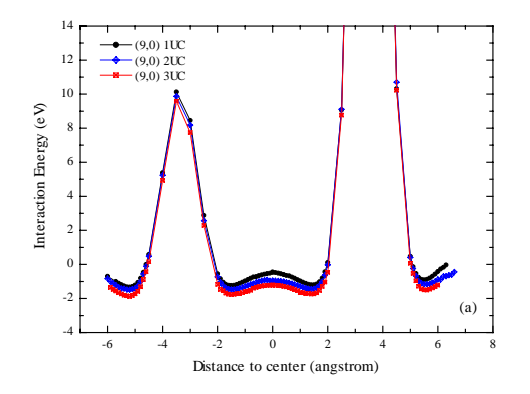


Figure 2. Binding energy as a function of the distance from the Geometric center of the (6,0) SWNT of finite length 3 UC, 4UC, and 5UC (a) 2 Li atoms-SWNT (b) 3 Li atoms-SWNT



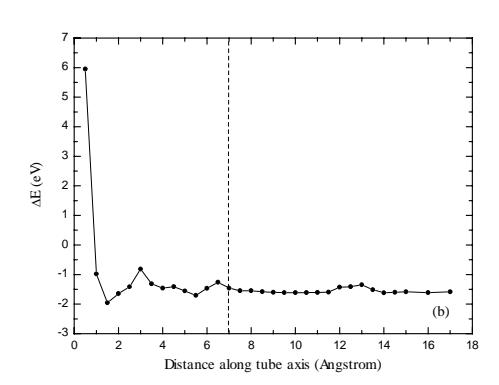


Figure 3. (a) Demonstration potential energy surface of Li atom and (9,0) nanotube interaction on cross section direction (b) Binding energy as a function of the distance from the geometric center of the (9,0) SWNT of finite length 3UC

Figure 2b shows that if 3 Li atoms are inserted into nanotubes, the binding energy will be deeper than insertion of 2 Li atoms. However, it shows unsatisfied result for lithium located far away from nanotube-mount for the reason that Kohn-Sham orbitals could not represent local electron at very far distances. For the larger diameter nanotube, (9,0), previous work revealed double-well potential shape as depicted in **Figure 3a** (Udomvech *et al* (unpublished)). Up to this point, we suggested (9,0) nanotube could be used as host material for storage number of atoms and ions more and better than (6,0) one. However, the insertion of Li atoms on tube-axis direction is important. It shows different binding energy if lithium atoms located at the tube axis as depicted in **Figure 3b**.

The interaction curve reveals that Li atoms do not prefer to located along the tube-axis direction of (9,0) nanotubes. The binding energy of the Li atoms are different from (6,0) nanotube both inside and outside. We are pursuing study of Li atoms moving in other direction, e.g. off tube-axis direction close the sidewall of nanotube.

4. CONCLUSIONS

We have found that Li atoms prefer to locate at sites along the tube-axis in (6,0) nanotube but not in (9,0). The insertions of Li atoms to SWNT have energy barrier when the open-mount are passivated. The diffusion barrier is small inside the nanotube indicating that Li atoms prefer to reside along the tube axis and not freely moving. The Li atoms have lower energy inside the nanotube than outside the nanotubes. In larger diameter of nanotube, the interaction curve shows that Li atoms do not prefer to locate at the tube-axis direction.

5. ACKNOWLEDGEMENT

A. U. expresses his gratitude to the Center of High Performance Computing, University of Utah and Capability Building Center for Nanoscience and Nanotechnology, Mahidol University for Computation has been done.

6. REFERENCES

- Baughman, R.H., Zakhidov, A.A., and de Heer, W.A. (2002). "Carbon Nanotubes--the Route Toward Applications." *Science*. Vol. 297, 787.
- Becke, A.D. (1993). "Density-Functional Thermochemistry. III. The Role of Exact Exchange." *Journal of Chemical Physics*. Vol. 98, 5648.
- Bendiab, N., Anglaret, E., Bantignies, J.-L., Zahab, A., Sauvajol, J.L., Petit, P., Mathis C., and Lefrant, S. (2001). "Stoichiometry Dependence of the Raman Spectrum of Alkali-Doped Single-Wall Carbon Nanotubes." *Physical Review B*. Vol. 64, 245424.
- Claye, A.S., Nemes, N. M., Janossy A., and Fischer, J.E. (2000). "Structure and Electronic Properties of Potassium-Doped Single-Wall Carbon Nanotubes." *Physical Review B*. Vol. 62, R4845.
- Dillon, A.C., and Heben, M.J. (2001). "Hydrogen Storage using Carbon Adsorbents: Past, Present and Future." *Apply Physics A.* Vol. 72, 133.
- Farajian, A.A. (2003). "Electronic Transport through Bent Carbon Nanotubes: Nanoelectromechanical Sensors and Switches." *Physical Review B.* Vol. 67, 205423.
- Lee, C., Yang, W., and Parr, R.G. (1988). "Development of the Colle-Salvetti Correlation-Energy Formula into a Functional of Electron Density." *Physical Review B*. Vol. 38, 785.
- Liu, H.J., Chan, C.T. (2003). "Chirality Dependence of the Energetics and Electronic Properties of Li-Intercalated 4 Å Carbon Nanotubes." *Solid State Communication*. Vol 125, 77-82.
- Miehlich, B., Savin, A., Stoll, H., and Preuss, H. (1989). "Results Obtained with the Correlation Energy Density Functionals of Becke and Lee, Yang and Parr." *Chemical Physics Letter*. Vol. 157, 200.
- Nisha, J.A., Yudasaka, M., Bandow, S., Kokai, F., Takahashi, K., and Iijima, S. (2000). "Adsorption and Catalytic Properties of Single-Wall Carbon Nanohorns." *Chemical Physics Letter*. Vol. 328, Issue 4-6, 381.
- Peng, S., and Cho, K. (2000). "Chemical Control of Nanotube Electronics." *Nanotechnology*. Vol. 11, 57.
- Rao, A.M., Eklund, P.C., Bandow, S., Thess A., and Smalley, R.E. (1997). "Evidence for Charge Transfer in Doped Carbon Nanotube Bundles from Raman Scattering." *Nature*. Vol. 388, 257.
- Saito, R., Dresselhaus, G., and Dresselhaus, M. (1998). *Physical Properties of Carbon Nanotubes*. London: Imperial College Press.
- Tarascon, J.-M., and Armand, M. (2001). "Issues and Challenges Facing Rechargeable Lithium Batteries." *Nature*. Vol. 414, 359.
- Tu, Z. and Ou-Yang, Z. (2002). "Single-Walled and Multiwalled Carbon Nanotubes Viewed as ElasticTubes with the Effective Young's Moduli Dependent on Layer Number." *Physical Review B.* Vol. 65, No. 23, 233407.
- Udomvech, A., Osotchan, T., Truong, T.N., and Kerdcharoen, T. (unpublished). "A DFT Study of Li and Li⁺ Adsorbed on Carbon Nanotube: Variation of Tubule Diameter and Length."
- Wadhawan, A., Stallcup II, R.E., and Perez, J.M. (2001). "Effects of Cs Deposition on the Field-Emission Properties of Single-Walled Carbon-Nanotube Bundles." *Apply Physics Letter*. Vol. 78, 108.

- Yang, J., Liu, H.J., Chan, C.T. (2001). "Theoretical Study of Alkali-Atom Insertion into Small-Radius Carbon Nanotubes to Form Single-Atom Chains." *Physical Review B*. Vol. 64, 08542.
- Yoon, Y.G., Delaney, P. and Louie, S.G. (2002). "Quantum conductance of multiwall carbon nanotubes." *Physical Review B*. Vol. 66, 073407.

Theoretical Investigation of Lithium Atoms Insertion into the Ultra-Small Diameter Carbon Nanotubes

Anurak Udomvech^{1,2} and Teerakiat Kerdcharoen^{1,3*}

Thailand

Abstract

Computations of Li-intercalation into ultra-small single walled carbon nanotubes have been carried out within the framework of the first principles density functional calculation. The energetic and structural properties of two Li atoms as a function of distance along the longitudinal axis of (3,3), (4,2) and (5,0) nanotubes have been calculated. It was found that Li atoms can be easily pulled into the interior of (3,3) and (4,2) nanotubes, whereas there exists a small energy barrier at the open-mount of (5,0) tube. Thus, the energy profiles along the longitudinal axis inside the zigzag (5,0) and armchair (3,3) are slightly fluctuating, whereas it is rather flat for the chiral (4,2) nanotube. The zigzag (5,0) nanotube allows Li-Li to localize near the tube center, which would probably form a Li₂ cluster inside the nanotube. In contrast, Li atoms prefer to locate near the open mounts of the armchair (3,3) tube. In case of (4,2) nanotube, no preferential location is found as described by the flat potential energy profile. The intercalated atoms affect the geometric parameters at the central region structure more than the rest of the nanotube. The structural properties of zigzag (5,0) nanotube is more responsive to the intercalated atoms than the armchair (3,3) and the chiral (4,2) structures, respectively. These results support an evidence that chirality plays a crucial role in Li-tube interactions, especially for the ultra-small nanotubes. The study also suggests that appropriate tubule chiralities are needed for using as efficient anode materials in Li battery.

Keywords: carbon nanotube, Li-battery, computational modeling, chirality

I. INTRODUCTION

Carbon nanotube (CNT) [1] has attracted much attention as a potential candidate for nanoscale devices. Particularly, single-walled carbon nanotubes (SWCNTs) have become ones of the most studied materials due to their unique properties. [2-5] An individual SWCNT can be thought of as a rolling up a flat graphene sheet. [6] Recently, SWCNTs with precise diameter and length can be synthesized and fabricated. [7-9] These carbon nanotubes have a diameter of ~ 4 Å and are perfectly arranged in a closely packed hexagonal lattice. [10-12] The adsorption property of CNTs provides the opportunities for applications such as hydrogen and gas storage [13], gas sensor [14], catalyst [15], and Li-ion batteries. [16] In case of Li-ion

¹ Department of Physics and Center of Nanoscience and Nanotechnology, Faculty of Science, Mahidol University, Rama 6 Road Bangkok 10400, Thailand

² Department of Physics, Faculty of Science, Thaksin University, Songkhla 90000, Thailand

³ NANOTEC Center of Excellence at Mahidol University, National Nanotechnology Center,

battery, the key important role to increasing the stored energy density lies in improving the electrode materials. CNT is a prospect candidate for uses in Li-ion batteries because the large numbers of nanoscale sites available for intercalant atoms on the CNT exceed those found on the commonly used graphite electrode, LiC₆. [17] For instances, higher lithium capacity up to Li_{1.6}C₆ and Li_{2.7}C₆ has been achieved in SWCNT [18]. A theoretical capacity is predicted with enhanced lithium density up to LiC₂ [19].

In the present work, we have studied the intercalation of two lithium atoms inside the ultra-small diameter SWCNT. Intuitively, the ultra-small diameter SWCNTs are ideal anode materials for Li-ion battery. The unusually high surface-volume aspect ratio could extend the storage capacity beyond presently known anode materials. The ultra-small 4-Å diameter carbon nanotubes have three possible chiralities such as the armchair (3,3), zigzag (5,0), and chiral (4,2). As a result, investigation of lithium intercalation into these structures is necessary to understand effects from chirality. The first principles density functional calculation was chosen to investigate the energetic and structural properties.

II. COMPUTATIONAL DETAILS

In the present work, Kohn-Sham density functional theory was used. The generalized gradient approximation of Beck's three-exchange parameters (B3) [20] and Lee-Yang-Parr local and non-local correlation potentials (LYP) [21] were chosen using 6-31G(d) and 3-21G Gaussian basis sets. To investigate the potential energy profile of inserting two Li atoms into the nanotubes, three models of the Li₂@SWCNT structures were proposed. The first model is denoted by "rigid Li₂@SWCNT/6-31G(d)", of which interaction energies were calculated at the 6-31G(d) level based on the Li-free SWCNT geometry optimized at the 3-21G level. This model could save a lot of computational power because it neglects geometrical relaxation of the nanotubes upon Li's insertion. The second model, as denoted by "B3LYP/3-21G//B3LYP/3-21G", represents the interaction energies calculated at 3-21G level based on the optimized Li₂-tube geometry obtained at the same level of theory. The third model, as denoted by "B3LYP/6-31G(d)//B3LYP/3-21G", is similar to the second model, for which the energy profile is calculated at 6-31G(d) but using the optimized structure obtained at the 3-21G level. Usage of various types of model would reveal dependency of the results on the computational models.

^{*} Corresponding Author: teerakiat@yahoo.com

In principles, Li intercalation is referred to adsorption of Li atoms or ions in the interior and/or at the exterior side-walls of CNTs. In the present work, we are interested in the intercalation process that brings two Lithium atoms into the nanotube's interior. For such small diameter nanotubes, Li atom is assumed to locate at the center of the tube, as also suggested by our previous study of (6,0) nanotube [22]. Fig. 1 defines the pathway for moving two Li atoms along the longitudinal axis of the nanotubes. In the calculations, two Li atoms were moved symmetrically along this path from each end of the nanotube into the interior. The high symmetry of Li₂ intercalation helps reduce computation time. The finite-length models (see Fig. 1) with the nominal formulas $C_{66}H_{12}$, $C_{72}H_{12}$ and $C_{80}H_{10}$ were chosen to represent the (3,3), (4,2) and (5,0) ultra-small diameter SWCNTs, respectively. The rims of all nanotubes were saturated by hydrogen atoms. The unrestricted spin wave functions were used. The interaction energy, ΔE , of the system is defined by subtracting the sum of the total energy of Li-free nanotube and the energies of the isolated Li atoms from the total energy of the whole complex.

III. RESULTS AND DISCUSSION

A. Energetic Properties

The potential energy profiles obtained from DFT/B3LYP calculation of all models are shown in Fig. 2, which demonstrates the energy change as two Li atoms move through each open-mount of SWCNTs. All models predict that Li atoms are stabilized inside carbon nanotubes, although some models exhibit potential barrier at the entrance of the tube's mount due to the repulsion with the hydrogen atoms capped at the tubule ends, i.e., the fixed-2Li@SWCNT model and the B3LYP/6-31G(d)//B3LYP/3-21G model of (4,2) and (5,0) nanotubes. In general, all models reproduce the same potential energy shape, although the 3-21G overestimates the potential energy. The compatibility of the potential curves generated from the "rigid Li₂@SWCNT/6-31G(d)" and the B3LYP/6-31G(d)//B3LYP/3-21G models suggests that rigid structural model, instead of the relaxed ones, can be used to reproduce the potential energy surface for Li-intercalated nanotubes, in order to minimize the computational resources.

In case of the fully optimized B3LYP/6-31G(d)//B3LYP/3-21G model, the potential energy of the full relaxation models (circle-solid line) has an analogous shape with that of Liu. [23] The energy profile inside the fully relaxed (3,3) and (5,0) nanotubes have a slight energy fluctuation. For the (3,3) tube (Fig. 2a), there is a potential well when Li atoms are located near each open-mount. In contrast, the (5,0) tube (see Fig. 2c) reveals a preferential

binding energy when Li-Li is closed to the nanotube center. The intercalated (4,2) nanotube (Fig. 2b) has a rather flat energy curve, in which the potential well does not exist at the mount, contrary to Liu's result that the potential well was found. Such contradiction may arise from the PW91 functional employed in Liu's case.

Since the Li-Li interaction inside the (3,3) tube has a rather long-range Coulomb repulsion than the others tubes, such chirality might not be a good candidate for Li host because Li atoms can reside with less packing. In contrast, the (5,0) nanotube has shown the formation of Li cluster inside the tube. Each Li binds strongly when it is facing to the hexagonal ring with Li-Li distance about 4 Å. Such potential energy shape (Fig. 2c) is useful for drawing Li atoms into the tube, allowing more packing than the (3,3) chirality. The charge-screening effect from nanotube allows Li atoms to come closely together more than bare Li atoms [24].

The above-mentioned results provide good reasons for the utilization of the ultra-small diameter nanotube as anode materials of Li battery as follows: (i) (3,3) nanotube may not be suitable because Li prefer to localize near tube-mounts, (ii) (5,0) tube may be used as host material in battery or to make single atomic chain (or nanowire) due to highly-packed cluster formation, and (iii) Li would followed charge-discharge cycle and reversibility very well in (4,2) more than other two nanotubes due to the flat potential inside the nanotube.

B. Structural Properties

In this section shall we discuss the structural properties of the bare and Li₂-intercalated nanotubes. For convenience, we divide the structure of nanotubes into different sections (S1-S4) as depicted in Fig. 1. Table I compares the average C-C bond lengths (bl_{av}) with LDA results from Yanga [25] and Liu [26]. The periodic LDA calculation of isolated 4 Å-diameter SWCNTs is in agreement with our results within a range of 0.01-0.02 Å. Each section has different bl_{av} values with a relationship S2>S1>S3 for all types of nanotubes. The average C-C bond length of the pristine tubes obtained by the 6-31G(d) basis set is in agreement with the 3-21G within 0.002 Å resolutions. Therefore, 3-21G basis set should be sufficient for describing geometry and this should justify our nanotube models employed in this work.

To demonstrate the effects of Li-intercalation on the nanotube geometry, the bond-length difference (bl_{diff}) between the intercalated and pristine tubes is plotted in Fig. 3. The plot shows that the nanotubes expand their geometry slightly in the proximity of the Li's location. For instances, Li will cause a strain at the terminal section when it starts to enter the tube and this strain moves together with the Li, as shown by the diagonal ridge of the 3-D plot

where Li is located. Thus, such geometrical distortion is more expressed in the (5,0) than the (4,2) and (3,3) chiralities (see Fig. 3(a-c)). This could be the reason that the Li₂-intercalated (5,0) nanotube has a quite fluctuating potential profile (Fig. 2). Again, the (4,2) chirality has shown its advantage for Li host over other types of ultra-small diameter SWNTs.

IV. CONCLUSION

This study supports a notion that chirality plays a crucial role in Li-tube interactions, especially for the ultra-small nanotubes, which affects the suitability of each kind of chirality as anode material in Li-battery. The results bring a conclusion that the (4,2) nanotube is the most suitable candidate among all chiralities as an efficient anode materials, based on the special characteristics as follows:

- (1) If we consider the energy profile inside the nanotubes, Li could bind with the (4,2) nanotubes more strongly than the (5,0) and (3,3) chiralities. The flat potential energy curve inside the (4,2) nanotube would allow loading and de-loading of Li atoms during the charge-discharge process to happen easily. In contrast, the local minima existing in the (5,0) and (3,3) chiralities are a disadvantage for reversibility.
- (2) Loading of Li atoms into carbon nanotubes can cause strain to the nanotubes' geometry. It was found that the (4,2) and (3,3) nanotubes have less geometrical distortion than the (5,0) nanotube.

It must be noted, however, that the above-mention hypotheses are based on limitation posed by the intercalation model that involves with only two Li atoms. Further investigation which extends this model to a higher level is in progress.

ACKNOWLEDGMENT

This work was financially supported via a Networked Laboratory grant from the National Nanotechnology Center. Career Development Grants from the Thailand Research Fund in cooperation with the Commission on Higher Education given to T.K. (RMU4880008) are acknowledged. The authors express gratitude to Prof. I. M. Tang for High Performance Computing and reading the manuscript.

References

- [1] S. Iijima, Nature (London) 354 (1991) 56.
- [2] Z. Tu, Ou-Yang, Phys. Rev. B 65 (2002) 233407.

- [3] M. Meyyappan, Carbon Nanotubes Science and Applications. CRC Press, Florida, 2005.
- [4] A.A. Farajian, B.I. Yakobson, H. Mizuseki, Y. Kawazoe, Phys. Rev. B 67 (2003) 205423.
- [5] P. Avouris, Chem. Phys. 281 (2002) 429-445.
- [6] R. Saito, G. Dresselhaus, M.S. Dresselhaus, Physical Properties of Carbon Nanotubes. Imperial College Press, London, 1999.
- [7] Z.K. Tang, H.D. Sun, J. Wang, J. Chen, G. Li, Appl. Phys. Lett. 73 (1998) 2287.
- [8] H. Shimoda, B. Gao, X.P. Tang, A. Kleinhammes, L. Fleming, Y. Wu, O. Zhou, Phys. Rev. Lett. 88 (2002) 015502.
- [9] Z. M. Li, J. P. Zhai, H. J. Liu, I. L. Li, C. T. Chan, P. Sheng, Z. K. Tang, Appl. Phys. Lett. 85 (2004) 1253.
- [10] C. Marin, M.D. Serran, N. Ya, A.G. Ostrogorsky, Nanotechnology 14 (2003) L4–L5.
- [11] M. Hulman, R. Pfeiffer, H. Kuzmany, 2004, New J. Phys. 6 (2004) 1.
- [12] Y.F. Mei, G.G. Siu, Ricky K.Y. Fu, P.K. Chu, Z.M. Li, J.P. Zhai, H.J. Liu, Z.K. Tang, C.W. Lai, H.C. Ong, Appl. Phys. Lett. 87 (2005) 213114.
- [13] A.C. Dillon, M.J. Heben, Appl. Phys. A. 72 (2001) 133.
- [14] S. Peng, K. Cho, Nanotechnology 11 (2000) 57.
- [15] J.A. Nisha, M. Yudasaka, S. Bandow, F. Kokai, K. Takahashi, S. Iijima, Chem. Phys. Lett. 328 (2000) Issue 4-6 381.
- [16] J.-M. Tarascon, M. Armand, Nature 414 (2000) 359.
- [17] N. Li, C.R. Martin, B. Scrosati, J. Power Source 97-98 (2001) 240.
- [18] M. Winter, J.O. Besenhard, M.E. Spahr, P. Novah, Adv. Mater. (Weinheim, Ger.) 10 (1998) 725.
- [19] J. Zhao, A. Buldum, J. Han, J.P. Liu, Phys. Rev. Lett. 85 (2000) 1706.
- [20] A.D. Beck, J. Chem. Phys. 98 (1993) 5648.
- [21] C. Lee, W. Yang, R.G. Parr, Phys. Rev. B. 38 (1998) 785.
- [22] A. Udomvech, T. Kerdcharoen, T. Osotchan, Chem. Phys. Lett. 406 (2005) 161.
- [23] H.J. Liu, C.T. Chan, Solid State Comm. 125 (2003) 77-82.
- [24] Unpublished data in which bare Li-Li interaction given by B3LYP/6-31G(d) calculation.
- [25] X.P. Yanga, H.M. Weng, J. Dong, Eur. Phys. J. B 32 (2003) 345.
- [26] H.J. Liu, C.T. Chan, Phys. Rev. B 66 (2002) 115416.

Table I: The average C-C bond length (bl_{av}) of pristine (3,3), (4,2), and (5,0) nanotubes was calculated by B3LYP/3-21G level. S1, S2, S3, and S4 indicated each section of nanotube along tube-axis (see model in figure 1). The average C-C bond length (bl_{av}) obtained from B3LYP/6-31G(d) calculation, is shown in [...]

					bl _{av} (Å)	from
		bl_{av}	(Å)		LD	PΑ
-	S1	S2	S 3	S4	ref. ^a	ref. ^b
(3,3)	1.435 [1.431]	1.445 [1.443]	1.426 [1.426]		1.422	1.435
(4,2)	1.435	1.438	1.430		1.425	1.430

	[1.436]	[1.436]	[1.428]			
(5,0)	1.440	1.441	1.438	1.438	1.419	1.425
	[1.439]	[1.440]	[1.437]	[1.428]		

aThe structure of the 4 Å-diameter SWCNTs inside the AFI single crystal. The structure of the isolated 4 Å-diameter SWCNTs. The structure of the isolated 4 Å-diameter SWCNTs. The structure of the isolated 4 Å-diameter SWCNTs.

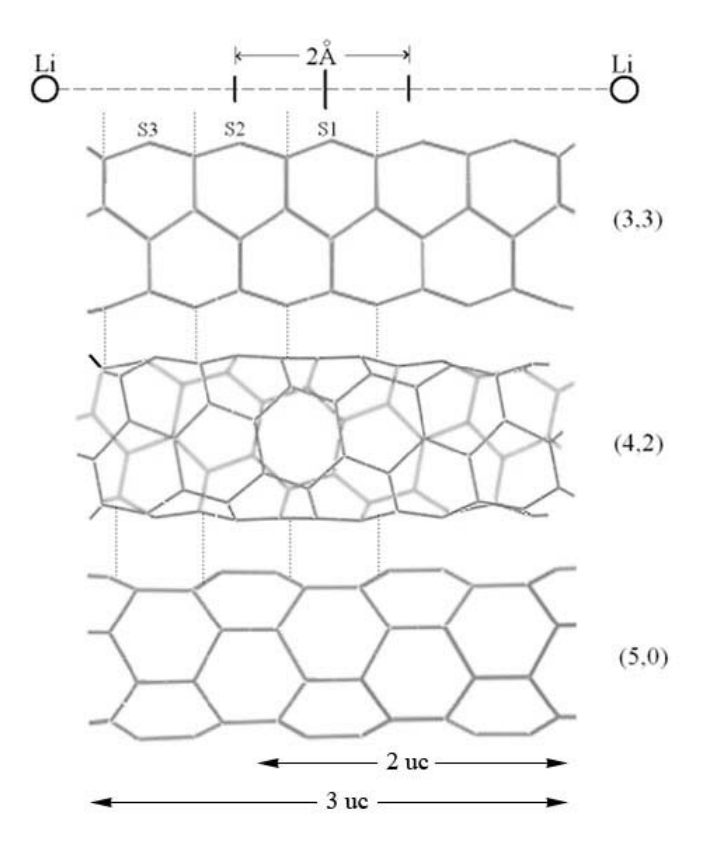
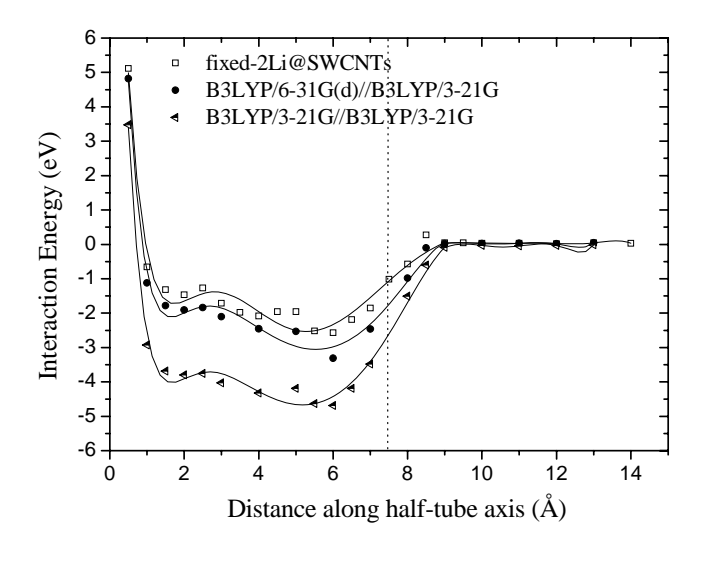
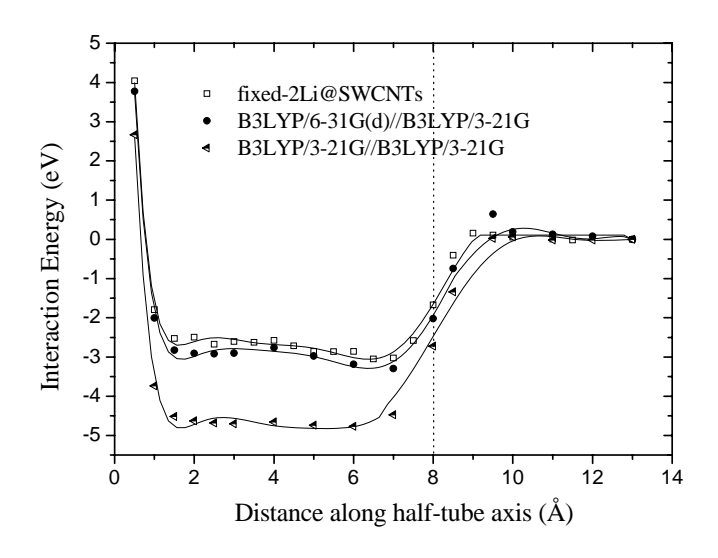


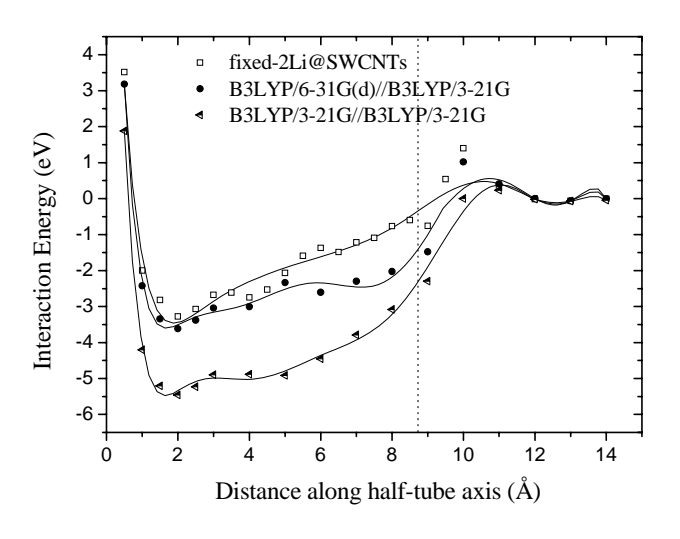
Fig. 1. Model of two Li atoms intercalated along longitudinal-axis inside the ultra-small diameter SWCNTs.



[a]

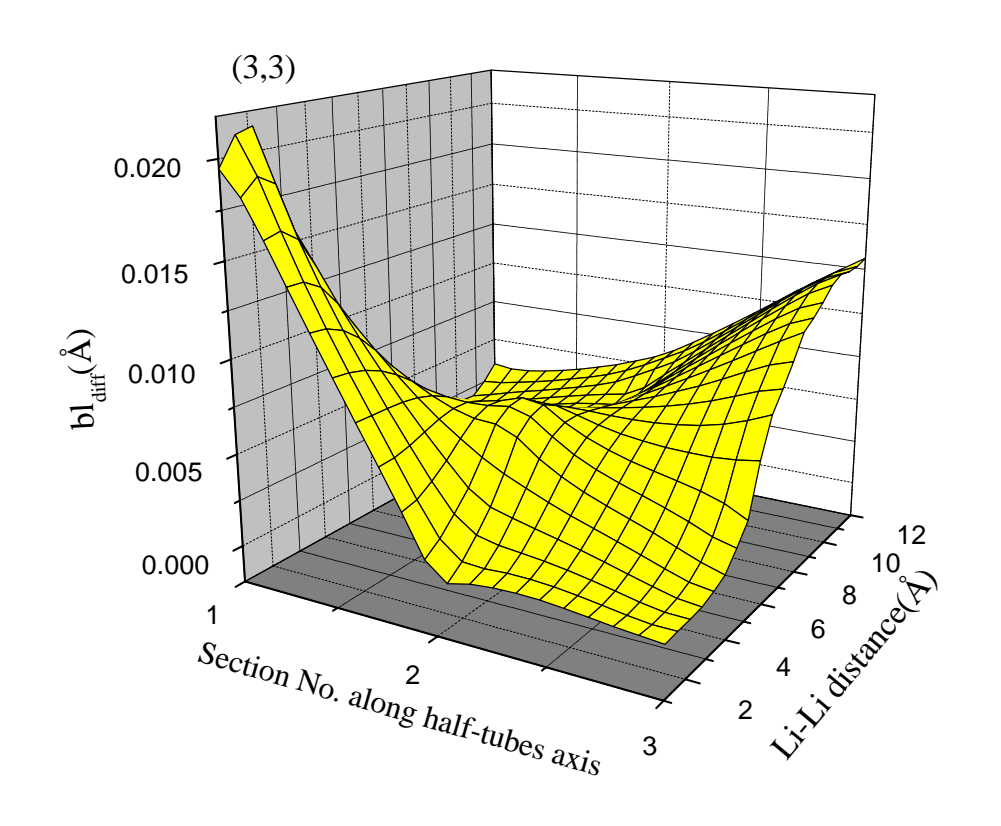


[b]

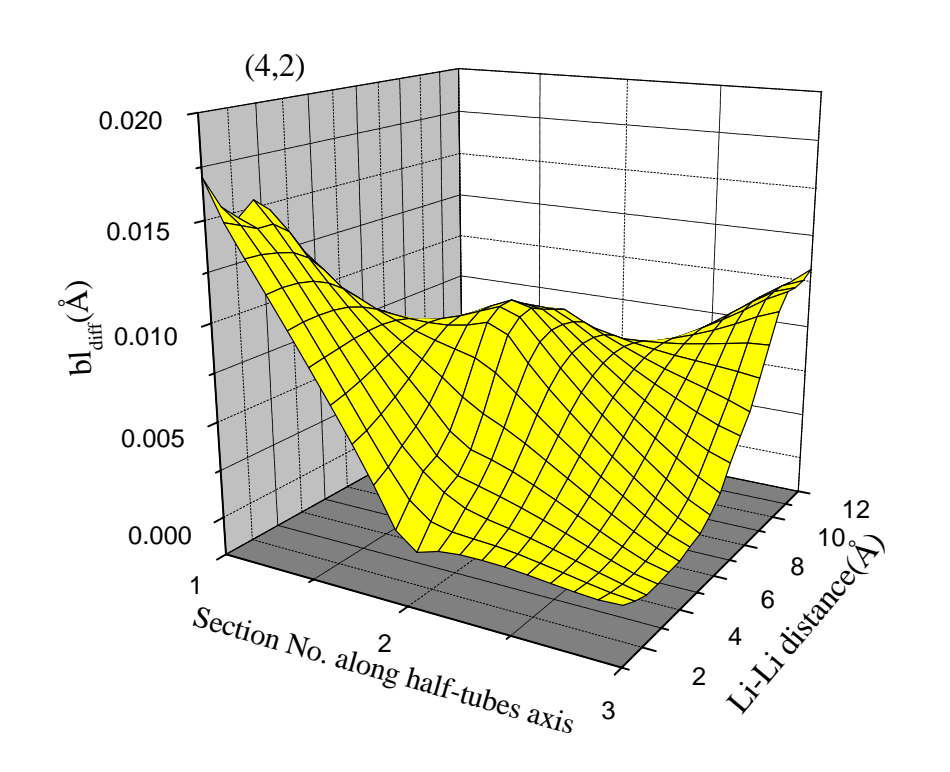


[c]

Fig. 2. Demonstration the potential energy curve of $Li_2@SWCNT$, [a] (3,3), [b] (4,2), and [c] (5,0) nanotubes. The square-dot line, circle-solid line and black-white triangle line represents the rigid-2Li@SWCNT, B3LYP/3-21G//B3LYP/3-21G and B3LYP/6-31G(d)//B3LYP/3-21G model, respectively. The vertical dash line marks the nanotube edge.



[a]



[b]

[c]

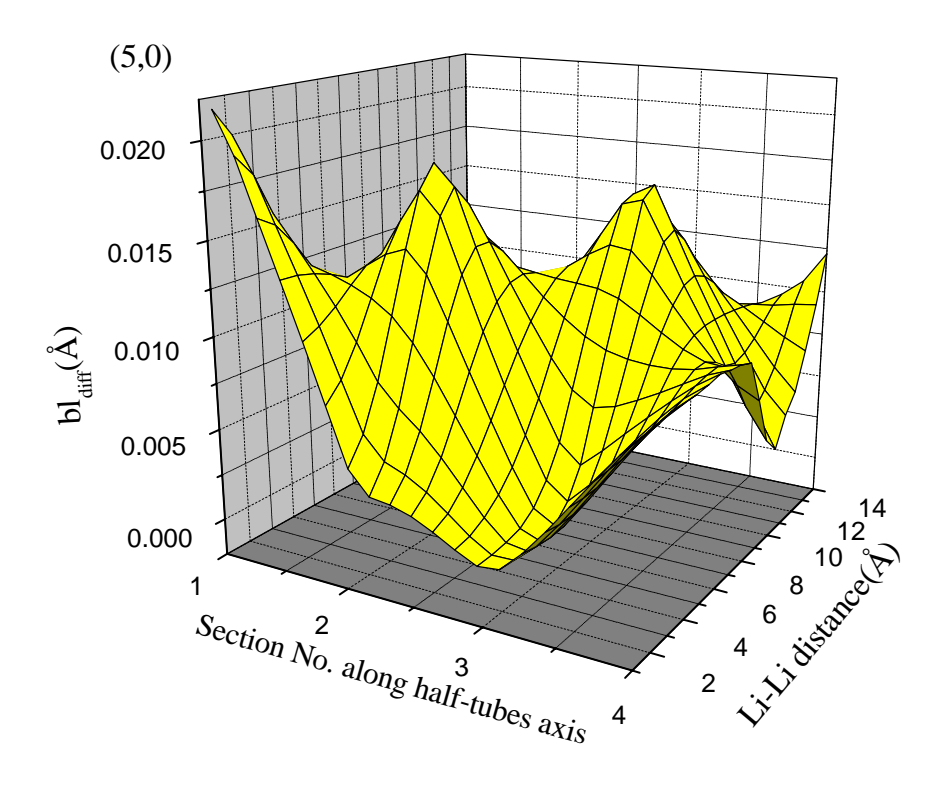


Fig. 3. The C-C bond length difference (bl_{diff}) of the intercalation two Li atoms inside SWCNTs are relatively change to the average C-C bond length (bl_{av}) of pristine [a] (3,3), [b] (4,2), and [c] (5,0) nanotubes, respectively.

Electronic structure of copolymerization of 9,9- Di (2' - ethylhexyl) 2,7 dibromofluorene (BEH-PF) and dibromo(anthracene)

Thitima Maturos*, Toemsak Srikhirin, Teerakiat Kerdcharoen and Tanakorn Osotchan

Capability Building Unit of Nanoscience and Nanotechnology, Department of Physics, Faculty of Science, Mahidol University, Rama6 road., Bangkok 10400, Thailand.

*Email address: maturos88@yahoo.com

Abstract

Copolymerization of 9,9- Di (2' - ethylhexyl) 2,7 dibromofluorene (BEH-PF) and dibromo (anthracene) can be applied as an emitting layer of the organic light emitting devices (OLED). In order to investigate the effect of anthracene composition to the electronic structure of the copolymer, geometry optimization of oligomer were performed at the AM1 level. The electronic structures of the oligomer ground state were investigated at B3LYP/6-31G* level. The energy gaps between LUMO and HOMO of the oligomers was extrapolated to the case for infinite chain length. For studying the monomer ordering effect, the same composition oligomer with different ordering were optimized and calculated the energy at the same level before. The energy gap results obtained from the ground state structure show that both the anthracene composition and the monomer ordering affect the electronic structure of the copolymer.

1. Introduction

Since organic light emitting device (OLED) was first demonstrated [1], a number of organic molecules and conjugated polymers have been fabricated for organic layer OLED. The chemical structure of conjugated polymer can be controlled, hence the emitting color are easily adjusted [2]. The color tuning is one of the advantages of organic over inorganic LED. Another advantage of the polymer light emitting devices is the case of fabrication by spin-coating deposition with polymer solution over the large areas, applied to the application on the flat panel display [3].

Polyfluorene is an interest polymer for emissive layer in OLED because of its high luminescence intensity in the blue region [4]. In order to improve the efficiency and stability of the luminescence from this polymer, the copolymerization of polyfluorene with the low band gap monomer was proposed by copolymerization with anthracene [5]. Additional, the flexible copolymerization process may lead to the color tuning of the emitting spectra due to the change of conjugation length in the polymer chain [6].

In this paper we investigated the electronic structure of the copolymerization of copolymer of 9, 9- Di (2 - ethylhexyl) 2, 7 dibromofluorene (BEH-PF) and dibromo(anthracene). The effects of anthracene composition to the electronic structure of the copolymer can be demonstrated by theoretical study and compared with the experimental results. Then the effects of the monomer ordering to the electronic structure and the conformation of the copolymer were also investigated.

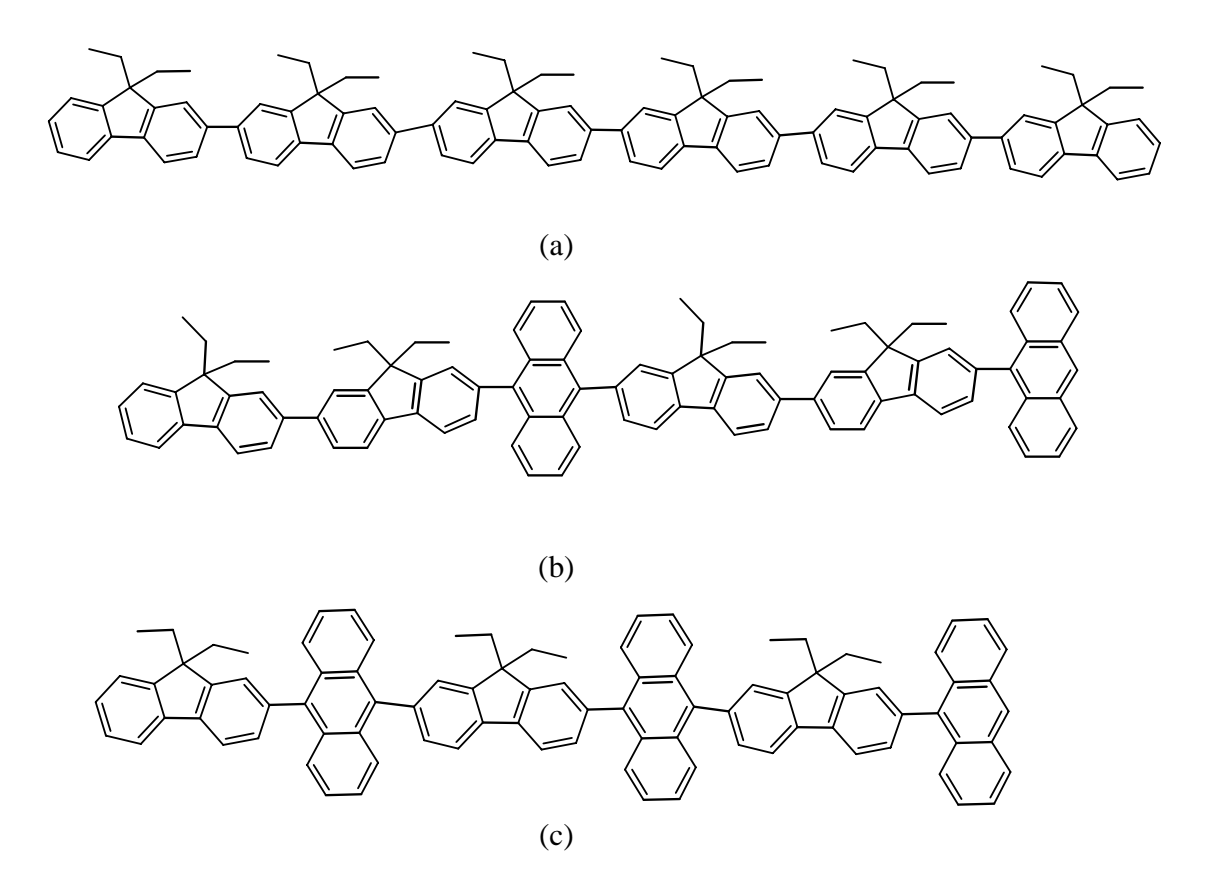


Fig. 1 Oligomer structure of modeled PF (a), 33.3% anthracene (b) and 50% anthracene (c) used in the investigation of the anthracene composition effect to the electronic structure of the copolymer.

2. Methodology

The molecular structures of the BEH-PF were modified by replacing the ethly group at the 9 position to reduce the calculation time. The oligomer geometries were optimized at the AM1 level and the ground-state energy were performed by using B3LYP/6-31G* level. The energy gap between HOMO and LUMO of the polymer were obtained by plotting the enery gap of monomer through tetramer against inverse chain lengths and extrapolating to the infinite chain length.

3. Results and discussions

In order to investigate the effect of monomer composition to the electronic structure, the monomer chemical structure with 0, 33.3 and 50 percent of anthraceneare are used in calculation

as shown in figure 1. The optimization geometry of the 6 oligomer units obtained by AM1 level is displayed in table 1. The dihedral angle between the PF (BB) is about 41.2 degree for oligomer

Percentage of anthracene (%)	Dihedral angle (degree)		E _{LUMO-HOMO}	
untiliacene (70)	BB	BA	(61)	
0	41.2	-	3.54	
33.3	41.2	71.2	3.37	
50	-	55.7	3.05	

Table 1. Average optimized dihedral angle and energy difference of the 6 oligomer units with different percent of anthracene. A represents Anthracene and B represents BEH-PF.

with all anthracene percentage. And the dihedral angle between PF and anthracene (BA) is about 71.2 and 55.7 degree for 33.3% and 50% of anthracene composition, respectively.

The energy difference between LUMO and HOMO levels ($E_{LUMO-HOMO}$) of the copolymer at various percent of anthracene was plotted as a function of inverse of number of repeating units and demonstrated in figure 2. The extrapolated energy gaps for the infinite chain length of the oligomer are about 3.2, 3.1 and 2.8 eV for 0% 33.3% and 50% of anthracene, respectively. Therefore, it indicates that the $E_{LUMO-HOMO}$ is decrease as percent of anthracene increases.

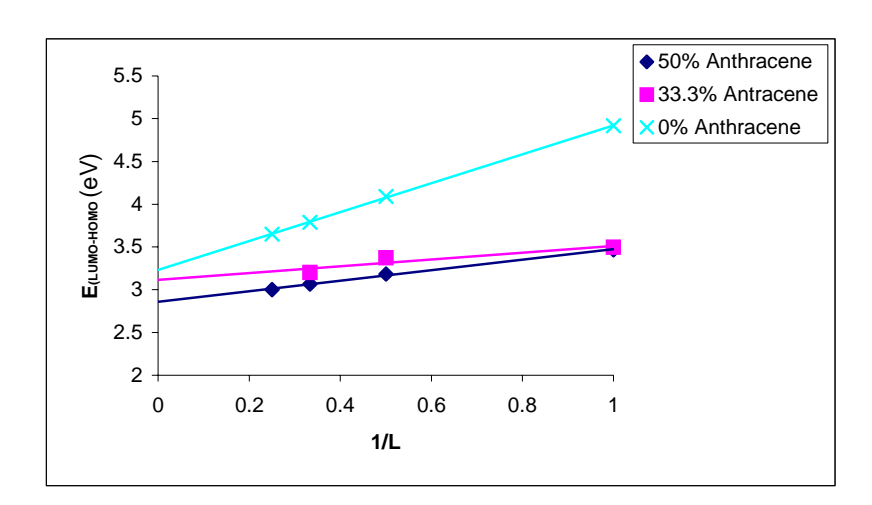


Fig 2 Energy difference between LUMO and HOMO levels of copolymer with various anthracene composition as a function of the inverse of number of repeating units

In order to study the effect of monomer ordering, the 25% anthracene oligomers with the ordering molecular arrangements of BBBABBBA, BBBAABBB and ABBBBBBA were calculated the optimum molecular structure and energy as indicated in table 2. For the optimized structure at AM1 level, the inter-ring distance between the monomer units is about 1.46 angstrom. The dihedral angle between PF rings (BB), between PF and anthracene ring (AB) and between anthracene (AA) are about 41.2, 70 and 90 degree, respectively. Additional, the total energy of the oligomer are the same for all of the oligomer ordering. The dipole moment in the symmetry molecule has less value than that in the asymmetry molecule. The electronic structure of 25% anthracene oligomer exhibits the low $E_{LUMO-HOMO}$ in the case that anthracene is normal disperse along the polymer chain. For the cases of the oligomer have an anthracene cluster in the middle of chain the $E_{LUMO-HOMO}$ is high as well as that for anthracenes are separated.

25% Anthracene		BBBABBBA	BBBAABBB	ABBBBBBA	
Inter-ring	В-В	1.46	1.46	1.46	
distance(A)	A-B	1.46	1.46	1.46	
distance(A)	A-A	-	1.47	-	
Dihedral	BB	41.2	41.2	41.2	
angles(degree)	AB	71.2	70.7	69.8	
ungres(degree)	AA	-	90.0	-	
Total energy (Kcal mol ⁻¹)		-3.15×10^{6}	-3.15×10^6	-3.15×10^6	
		3.13 × 10	3.13 × 10	3.13×10	
Dipole moment (D)		0.94	0.25	0.17	
E _{LUMO-HOMO} (eV)		3.37	3.43	3.44	

Table2. Average optimized structural parameters of the 25% anthracene oligomer with different monomer ordering. A represents Anthracene and B represents BEH-PF.

The ordering effect in 33.3% anthracene copolymers also demonstrated the similar properties, as listed table 3, as that in 25% anthracene copolymer. The inter-ring distance between the monomer units is about 1.46 angstrom. The dihedral between the PF rings (BB), between PF and anthracene rings (BA) and between the anthracene monomer (AA) are 41.2, 70 and 90 degree, respectively. For 33.3% anthracene copolymer, the oligomer with anthracene normal disperse along the polymer chain has lower $E_{LUMO-HOMO}$ than that for the cases of the oligomer have a cluster anthacene in the middle of molecule.

33.3% Anthracene		BBAABB	BBABBA	ABBBBA
Inter-ring	BB	1.46	1.46	1.46
distance(A)	AB	1.46	1.46	1.47
	AA	1.47	-	-
Dihedral angles(degree)	BB	41.2	41.2	41.2
	AB	70.8	71.2	69.7
	AA	90.3	-	-
Total energy		-2.32×10^{6}	-2.32×10^{6}	-2.32×10^{6}
(Kcal mol ⁻¹)		2.32 × 10	2.32 × 10	2.32 × 10
Dipole moment (D)		0.53	0.59	0.06
E _{LUMO-HOMO} (eV)		3.44	3.38	3.24

Table 3. Average optimized structural parameters of the 33.3% anthracene copolymer with different monomer ordering. A represents Anthracene and B represents BEH-PF.

Thus it can be indicated that the monomer ordering does not affect the molecule conformation but this affects the electronic structure of oligomer. For more understanding in this effect the molecular orbitals on the oligomer molecule are visualized near HOMO and LUMO states as displayed in Fig. 3. When anthracenes cluster in the center of chain, most electrons localize only around the anthracene rings and do not localize along the oligomer chain. Additional, the large twisting out of the plane between the anthracene rings (90 degree) is effectively interrupt the π - orbital overlap along the backbone. Thus this results in the poor electronic delocalization over the molecule. However for the case those anthracenes are dispersed along the polymer chain, electron can localize along the oligomer chain well.

It can be indicated that the dispersion of anthracene in the polymer chain leads to more localized electron along the chain and affects the long conjugation length and smaller energy gap of the copolymer. The results of 25 % anthracene copolymer are consistent with the 33.3% anthracene copolymer except for the case that anthracene is seperated far away as 6 units. This case may be due to the large distance between anthracene on the chain so the electrons localize only on the anthracene unit. The $E_{\rm LUMO-HOMO}$ value is close to that from the case that anthracene cluster in the center of the chain.

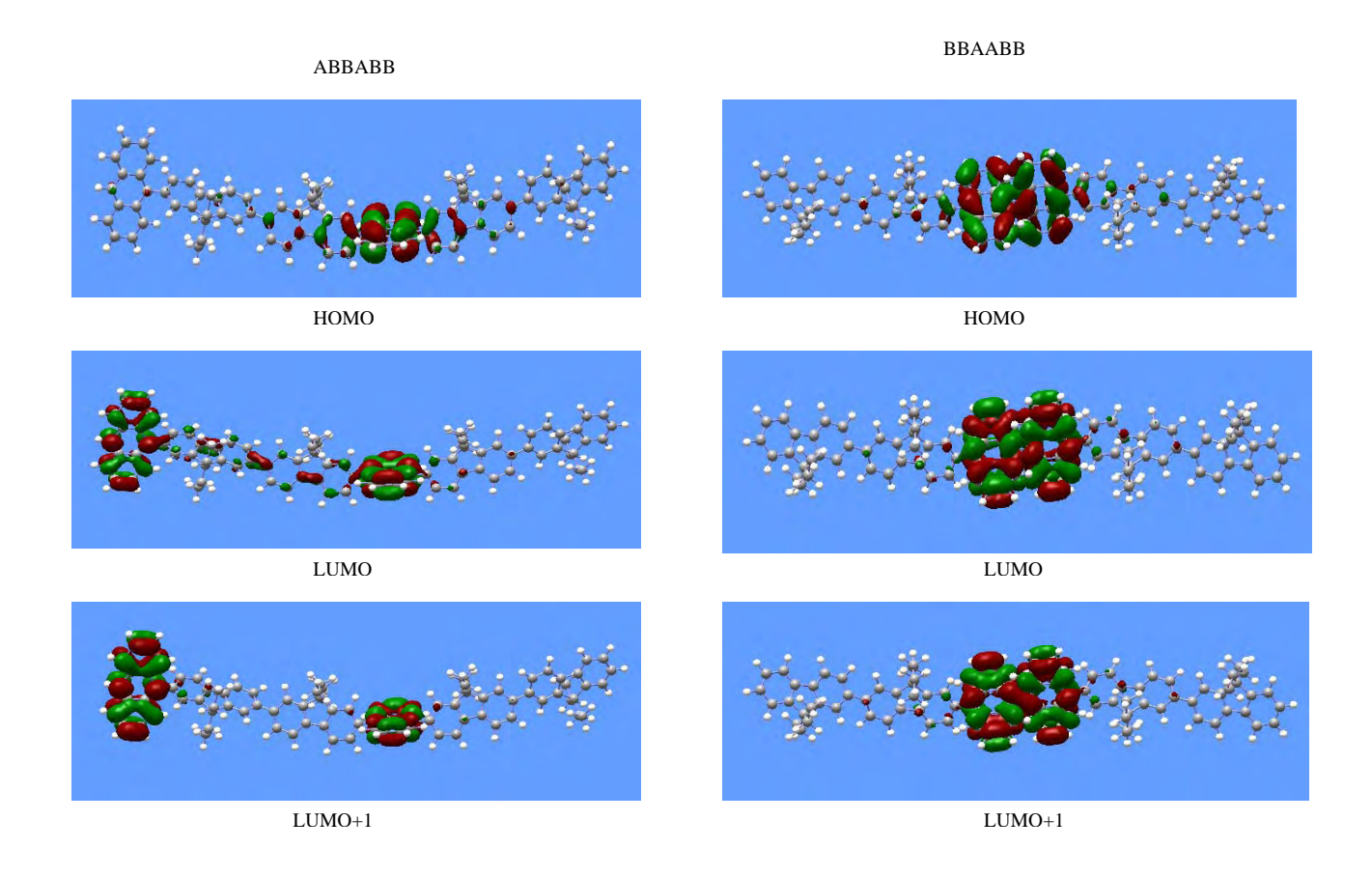


Figure 3. Molecular orbital at HOMO, LUMO and LUMO+1 levels for the 33.3% anthracene copolyemer with the ordering of ABBABB and BBAABB

4. Conclusions

The optimized molecular structures of the oligomer by AM1 level exibit that niether the anthracene composition nor monomer ordering affect the conformation of copolymer chain. The anthracene monomers play the role in decreasing the LUMO and HOMO energy difference of the copolymer. Electrons localize well between the anthracene ring and the copolymer that have disperse anthracene monomer along the chain exhibits the lower energy difference than that in the case of the polymer that have the anthracene cluster in the middle of molecule.

5. Refferences

- 1. C.W.Tang and S.A. Vanslyke, App. Phys. Lett. 1987, 51, 913
- 2. J.H. Burroughes, D.D.C. Bladley, A.R. Brown, R.N. Marks, K. MacKay, R.H. Friend, P.L. Burn and A.B.Holmes, *Nature*. 1990, 347, 539
- 3. D. Braun and A.J. Heeger, Appl. Phys. Lett., 1991, 58, 1982
- 4. M. Kreyenschmidt, G. Klaerner, T. Fuhrer, J. Ashenhurst, S. Karg, W.D. Chen, V.Y. Lee, J.C. Scott and R.D. Miller, *Macromolecules*, 1998, *31*, 1099
- 5. G. Klaerner, M.H. Davey, W.D. Chen, J.C. Scott and R.D. Miller, *Adv. Mater*, 1998, *10*, 993
- 6. G. Klaerner and R. D. Miller, Macromolecules, 1998, 31, 2007

Quantum Chemical Calculations of Electronic Structures and Electronic Properties of Polyfluorene and its derivatives

Kriengsak Sriwichitkamol¹, Teerakiat Kerdcharoen², Tanakorn Osotchan² and Supa Hannongbua¹*

Department of Chemistry, Faculty of Science, Kasetsart University, Bangkok 10900

Department of Physics, Faculty of Science, Mahidol University, Phayathai, Bangkok 10400, Thailand

Abstract

Fluorene is one of the important polymers that can be used as emitting layer on the light emitting diode (LED). Full geometrical optimization of Fluorene dimer was performed based on semiempirical AM1 method, and ab initio at the HF/3-21G* and HF/6-31G* levels. It is found that the structure shows syndiotactic conformation with the torsion angle of the dimer equals to 40 and 49 degrees. Moreover, ground-state structures and properties of fluorene oligomer and its derivatives, R = methyl, hexyl and 2-ethylhexyl, up to pentamer, were investigated at the B3LYP/6-31G*//HF/3-21G* level. Structural parameters of Fluorene are in qualitative agreement with X-ray crystallographic data. Chain length dependence of excitation energies of fluorene and its derivatives was then studied employing the time-dependent density functional theory at the TDB3LYP/6-31G*//HF/3-21G* level. Energy band gaps and effective conjugation lengths of the corresponding polymers were predicted by extrapolating vertical excitation energy of dimer through pentamer to infinite chain length. The obtained results indicated that larger substituent size from methyl to hexyl groups decreases the energy band gap as demonstrated by Eg = 2.75 and 2.55 eV, respectively. However, the limitation of the substituent size as found by R = 2-ethylhexyl group might be occurred as strong steric interaction effects to the electronic delocalization of the polymer and then, increases the energy band gap to 2.63 eV.

1. Introduction

The discovery of electroluminescence in conjugated polymers gave an impetus to the development of light-emitting devices (LEDs) for display technology. Luminescent polymers offer considerable processing adventages over the well-established inorganic electroluninescent materials and organic dye molecules as they can be deposited via spin-coating over large areas. Another important benefit of conjugated polymers is that the color and emission efficiency can be figured by manipulation of the chemical structure.

Fluorene derivatives present an interesting alternative to blue-light-emitting materials. Indeed, fluorenes and fluorene oligomers are well known as higly fluorescent compounds. These molecules contain a rigidly planar biphenyl structure in the fluorene monomer unit with facile functionalization at the C-9 position offering the prospect of controlling the polymer solubility and other physical properties. Moreover, the remote substitution at C-9 does not induce steric effects

^{*} Corresponding author

with adjacent aromatic rings. In this regard, various fully conjugated polyfluorenes have been studied for LED applications.

Derivatives polyfluorene have been synthesized by replacing atom hydrogen on methylene bridge by aliphatic substituents such as methyl group, hexyl group and 2-ethylhexyl group (Figure 1), leading to increasing both their solubility and stability. Thus, the unique structure of the polyfluorene derivative yields an attractive combination of electronic and mechanical properties that represent promising materials from an engineering viewpoint.

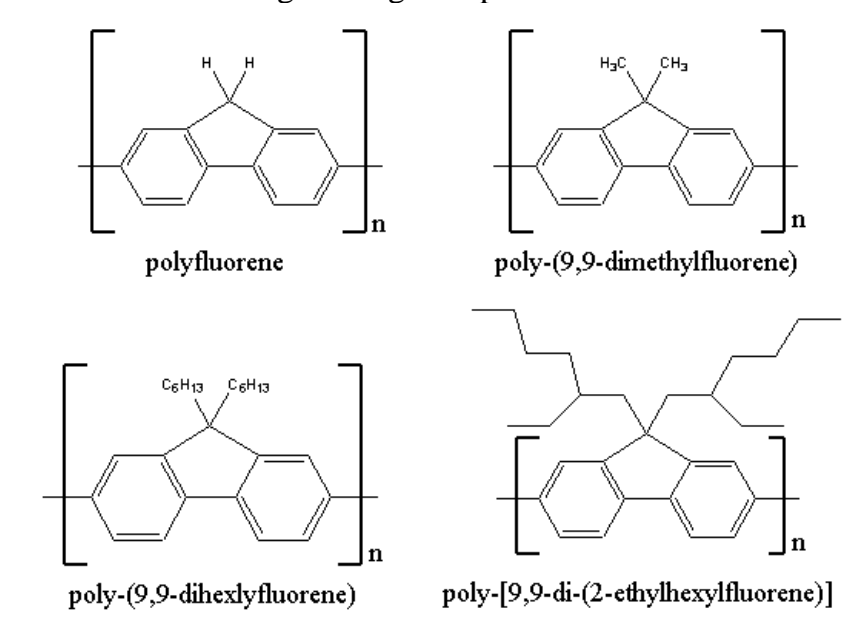


Figure 1. Illustration of chemical structure of polyfluorene and its derivatives.

There are several experimental studies of polyfluorene, poly-(9,9-dimethylfluorene), poly-(9,9-dihexlyfluorene) and poly-[9,9-di-(2-ethylhexylfluorene)] as well as theoretical studies at various level of theory. Several theoretical works can be used to investigate physical and chemical properties of these materials. Theoretical quantity for direct comparison with experimental band gap is the excitation energy from the ground state to the first dipole-allowed excited state. The implicit assumption underlying this approximation is that the lowest singlet excited state can be described by only one singly excited configuration in which an electron is promoted from the highest occupied molecular orbital (HOMO) to the lowest unoccupied molecular orbital (LUMO). In addition, the orbital energy difference between HOMO and LUMO is still an approximate to the transition energy since the transition energy also contains significant contributions from some two-electron integrals. However, the real situation is that an accurate description of the lowest singlet excited state requires a linear combination of a number of excited configurations, although the one mentioned above often plays a dominant role.

The calculated HOMO-LUMO gap agrees fairly well with the experimental band gap in many cases [4]; it may probably due to the error cancellations. Hence, it is desirable to obtain more rigorous information on the nature of the lowest singlet excited state by employing other elaborate theoretical methods. There exist a variety of theoretical approaches for evaluating this quantity for oligomers as well as infinite polymers. The crudest estimate is orbital energy difference between the HOMO and LUMO obtain from density functional theory (DFT) calculations. Among those theories, Hartree-Fock (HF)-based methods such as configuration interaction singles (CIS) and the random phase approximation usually only provide the qualitative or semiqualitative descriptions for the low-lying excited states. Time-dependent density functional theory (TDDFT) is recently developed method for calculating excitation energies. A significant quantitative improvement in the excitation energies from TDDFT over those from HF-based methods has been demonstrated, but a roughly comparable computational cost.

In this study, effect of substituent size on the geometrical structures and electronic properties of fluorene derivetives were investigated by *ab initio* and density functional theory methods. Approximate band gaps were obtained by plotting excitation energies versus inverse chain length and extrapolating to zero.

2. Methods of Calculation

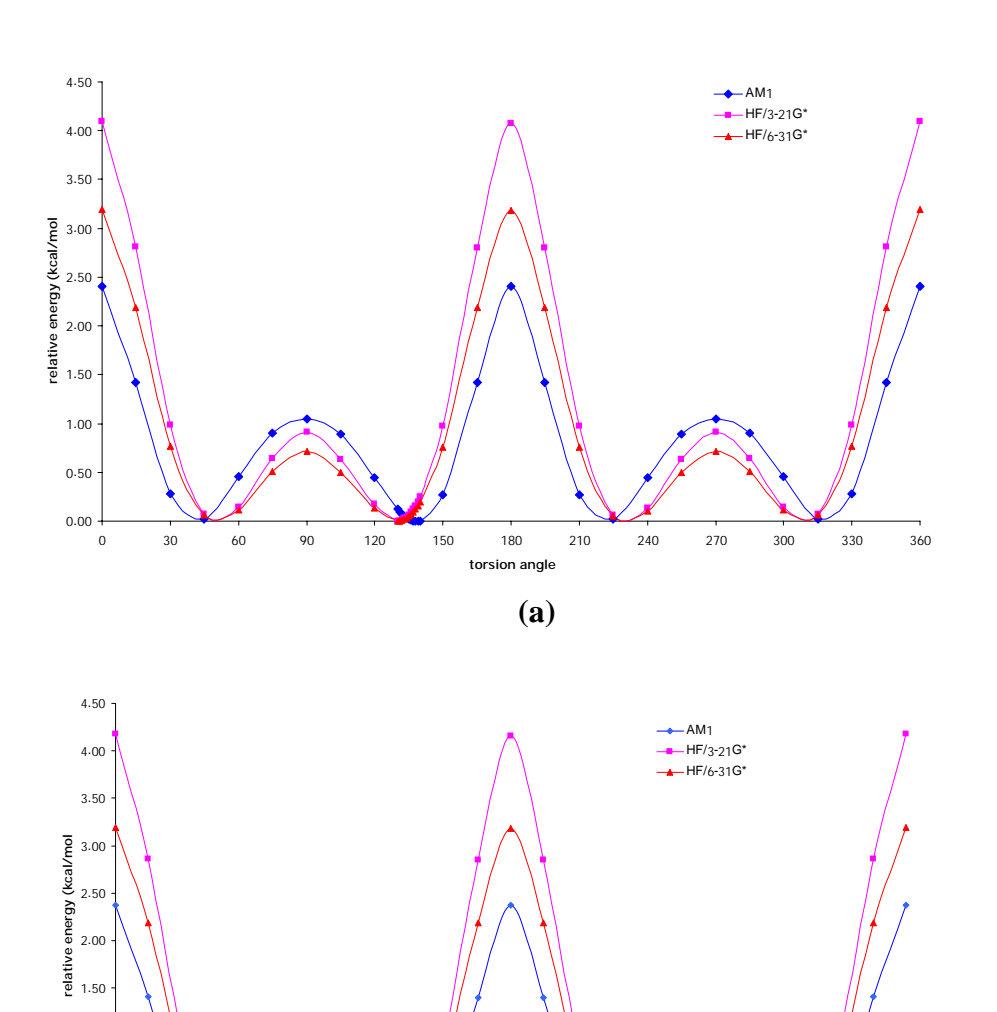
Conformational analysis of fluorene dimers and 9,9-dimethylfluorene dimers were investigated using semiempirical method Austin Model 1 (AM1) and *ab initio* calculations at the HF/3-21G* and HF/6-31G* levels. All calculations were performed by Gaussian 98 running on PC 2.4 GHz. The potential energy around the torsion angle between monomer units was also analysed. The ground-state geometries of fluorene and polyfluorene oligomers and its derivative were fully optimized at HF/3-21G* level.

TDDFT (B3LYP/6-31G*) calculations of the excitation energies were then performed at the optimized geometries of the ground states and approximate excitation energies by HOMO-LUMO differences at the B3LYP/6-31G* level. Band gaps of polymers were obtained by plotting the vertical excitation energies for the first dipole-allowed excitation energies of dimers through tetramers or pentamers against reciprocal chain lengths and extrapolating to infinite chain length.

3. Results and Discussion

3.1 Conformational analysis

Potential energy of fluorene dimers and 9,9-dimethylfluorene dimers were performed by AM1, HF/3-21G* and HF/6-31G* calculations as shown in Figure 2. It is found that the structure of fluorene and 9,9-dimethylfluorene dimers shows syndiotactic conformation with the torsion angle of the dimers equals to 49 degrees in AM1 level and equals to 40 degrees at the HF/3-21G* and HF/6-31G* levels. Based of the obtained results it is indicated that methyl group do not effect to the for conformation structure of fluorene dimers.



(b) Figure 2. Potential energy curves of polyfluorene (a) R = H (b) R = CH3

270

180

120

1.00 0.50 0.00

For the conformational analysis of poly-(9,9-dihexylfluorene), we found that the conformation structure seems to be isotactic conformation with the torsion angle of the dimer equals to 41 degree (as shown in Figure 3).

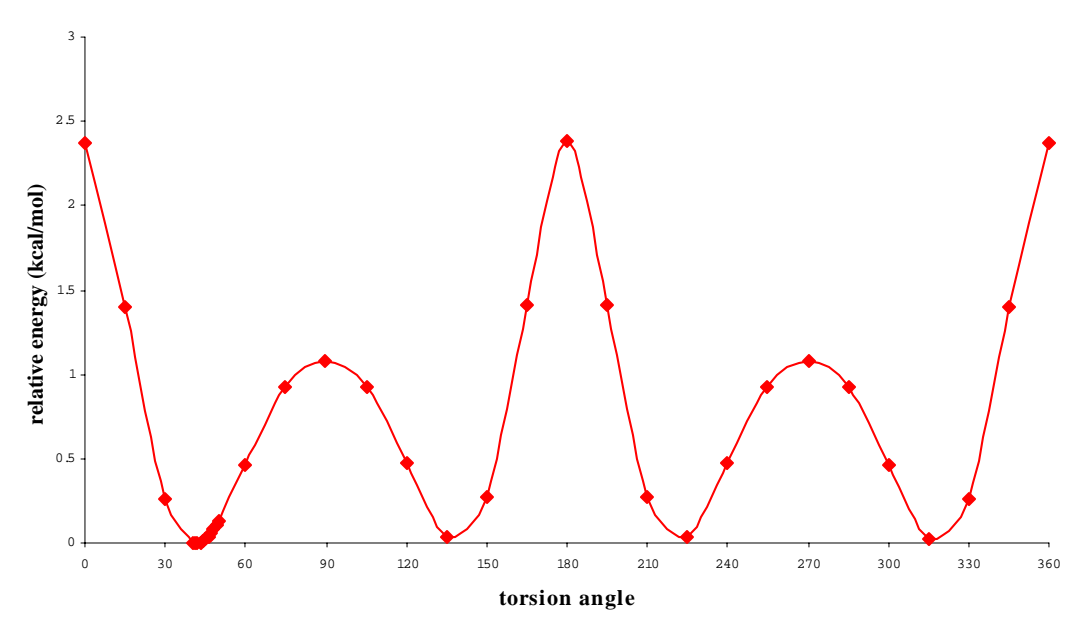


Figure 3. Potential energy curves of poly-(9,9-dihexylfluorene).

3.2 Geometries

The fluorene molecule is considered as $C_{2\nu}$ symmetry in the gas phase calculations. Atomic numbering is depicted in Figure 4. Optimized bond lengths and angles of fluorene molecule calculated with the ab initio HF/3-21G* level were displayed in Table 1. Those from MP/6-31G*, quantum chemical force field/ π electron (QCFF/PI) and X-ray study are also included for comparison.

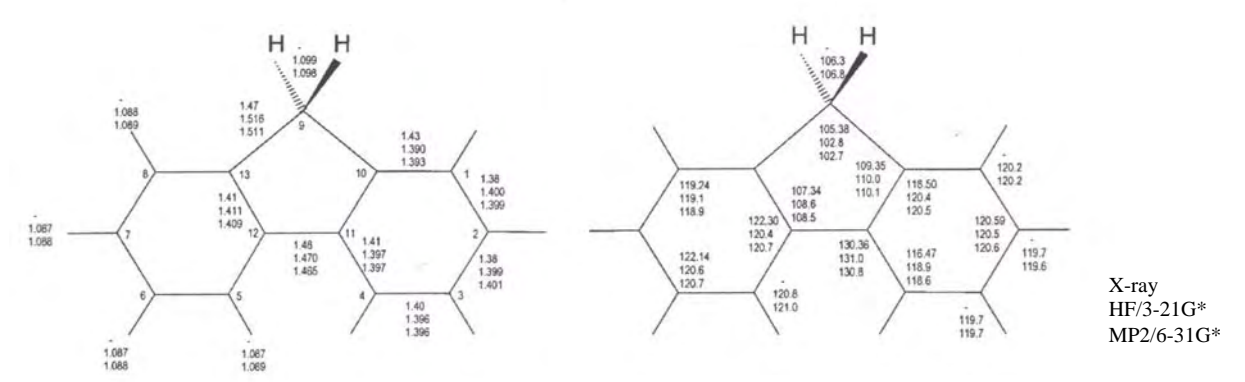


Figure 4. Comparison of the calculated and X-ray structural parameters of fluorene.

The results obtained by HF/3-21G* are very close to the corresponding MP2 ones and are in good agreement with the reported X-ray data. The calculated bond angles are similarly accurate to within a few tenths of a degree, except the QCFF/PI method, which underestimates the C_{10} - C_{9} - C_{13} angle in particular. In the X-ray Structure, C_{9} - C_{10} bond length is unusually shorter than the optimized values. The origin of this difference may be the crystal packing force.

Table 1. Equilibrium Geometrical Parameters of Fluorene in the Ground State^a

parameter	HF/3-21G*	MP2/6-31G*	QCFF/PI ^b	X-ray ^c	
Bond length					
C_1 - C_2	1.400	1.399	1.413	1.38	
C_1 - C_{10}	1.390	1.393	1.396	1.43	
C_2 - C_3	1.399	1.401	1.411	1.38	
C_3 - C_4	1.396	1.396	1.411	1.40	
C_4 - C_{11}	1.397	1.397	1.401	1.41	
C_9 - C_{10}	1.516	1.511	1.520	1.47	
C_{10} - C_{11}	1.411	1.409	1.419	1.41	
C_{11} - C_{12}	1.470	1.465	1.469	1.48	
C_1 -H	1.088	1.089			
C_2 -H	1.087	1.088			
C ₃ -H	1.087	1.088			
C ₄ -H	1.087	1.089			
C ₉ -H	1.099	1.098			
		Bond Angle			
C_2 - C_3 - C_4	120.5	120.6	120.9	120.59	
C_1 - C_{10} - C_{11}	120.4	120.5	120.5	118.50	
C_2 - C_3 - C_4	120.6	120.7	120.8	122.14	
C_2 - C_1 - C_{10}	119.1	118.9	118.5	119.24	
C_3 - C_4 - C_{11}	118.9	118.6	117.9	116.47	
C_4 - C_{11} - C_{10}	120.4	120.7	121.5	122.30	
C_4 - C_{11} - C_{12}	131.0	130.8	131.0	109.35	
C_9 - C_{10} - C_{11}	110.0	110.1	112.6	105.38	
C_{10} - C_{9} - C_{13}	102.8	102.7	99.8	107.34	
C_{10} - C_{11} - C_{12}	108.6	108.5	107.5		
C_{11} - C_4 - H	120.8	121.0			
C_2 - C_1 - H	120.2	120.2			
C_3 - C_2 - H	119.7	119.6			
C_4 - C_3 - H	119.7	119.7			
H-C ₉ -H	106.3	106.8			

^a Bond lengths in angstroms, and bond angle in degrees.

b Reference 1

^c Reference 2; standard deviation for X-ray parameters is 0.02 angstrom.

3.3 Electronic properties of polyfluorene and its derivetives

Extrapolated band gaps are obtained by excitation energies or HOMO-LUMO differences for B3LYP/6-31G*//HF/3-21G* from dimers throught pentamers of polyfluorene and its derivatives against inverse chain length and extrapolated to infinity as shown in Figure 5. Excitation energies, calculated by the TDDFT (B3LYP/6-31G*) level are presented in Table 2. We used the first excited state with significant oscillator strength (a π - π * transition), which was also the lowest excited state for all oligomers.

Table 2. Calculated Excitation energies (in eV) of polyfluorene and its derivatives at the various computational levels.

	R = H	R = methyl	R = hexyls	R = 2-ethylhexyl
TDDFT//HF/3-21G*	2.92	2.75	2.58	2.63
B3LYP/6-31G*//HF/3-21G*	3.38	3.36	3.21	3.31
E _g (Expt.) ^a	3.13	2.98	2.65	2.74

^a Reference 8.

The excitation energies are extrapolated against the reciprocal number of units, which show excellent linearity. The energies obtained from extrapolated HOMO-LUMO defferences from B3LYP/6-31G* levels are higher than the experimental band gaps (see Figure 5). The excitation energies obtained from TDDFT at B3LYP/6-31G* level is good agreement with experiment band gaps for fluorene oligomers and its derivatives. It is found that the results from TDDFT, the energy band gap of fluorene oligomers can be predicted within the range of available experimental data.

It is important to note that electronic properties of polyfluorene and its derivative strongly depend on the aliphatic substituted side chain. The energy gap values decrease and the energy band gap becomes lower in the order of polyfluorene > poly-(9,9-dimethyfluorene) > poly-[9,9-di-(2-ethylhexylfluorene)] > poly-(9,9-dihexlyfluorene). Energy band gap results indicate that derivatives of polyfluorene can be easily internally doped to vary high electrical conductivity. However, the limitation of the substituent size as found by 2-ethylhexyl group might be occurred as strong steric interaction effects to the electronic delocalization of the polymer and then, increases the energy band gap of polymer.

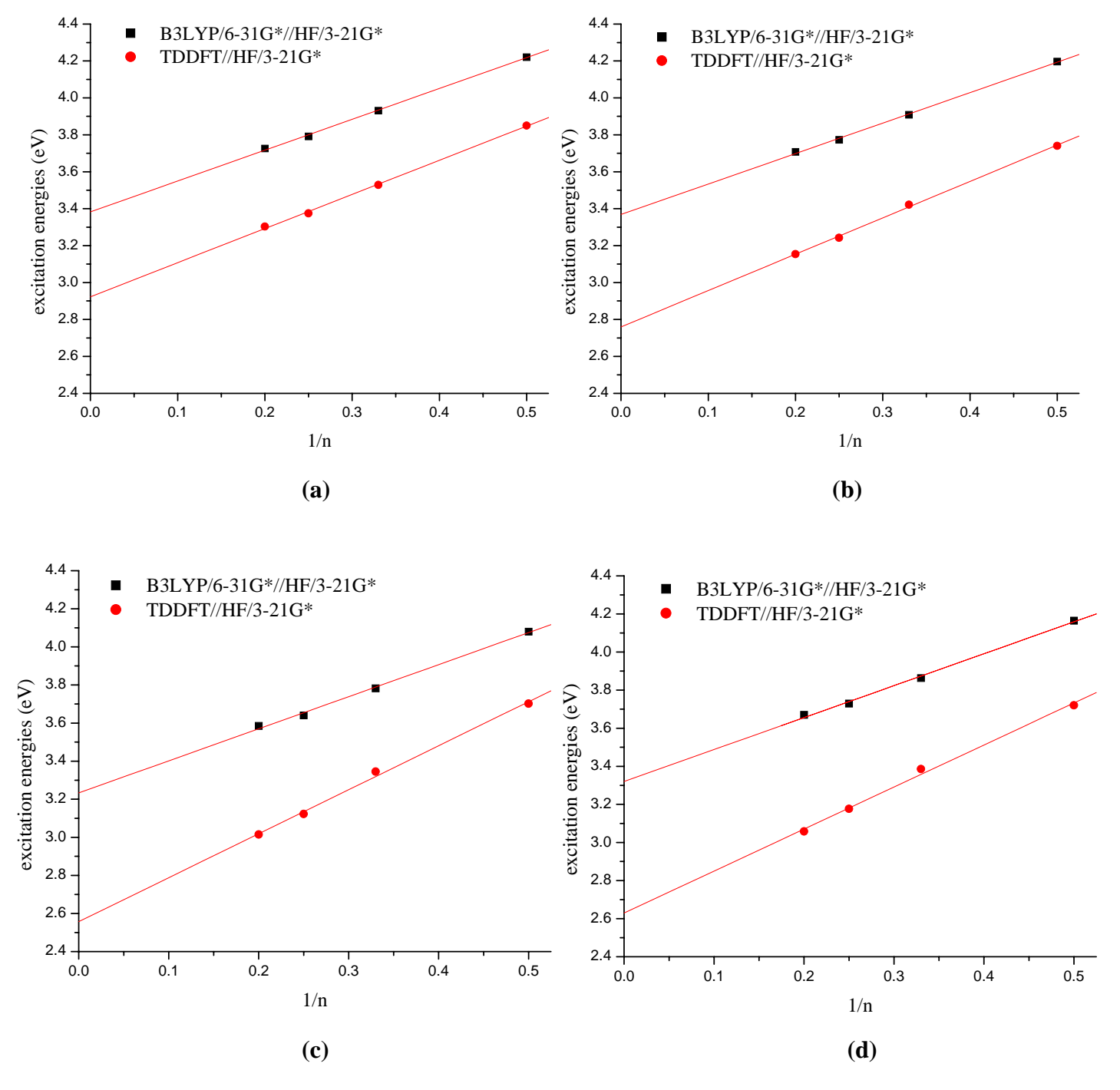


Figure 5. Plots of calculated energy band gaps versus invese chain length in oligomer units and extrapolating to infinite number of units for (a) polyfluorene (b) poly-(9,9-dimethylfluorene) (c) poly-(9,9-dihexylfluorene) and (d) poly-[9,9-(2-ethylhexylfluorene)].

4. Conclusions

Structural conformations and electronic properties of polyfluorene and its derivative were performed, based on quantum calculations. A conformational study of polyfluorene dimers by AM1, HF/3-21G* and HF/6-31G* calculations demonstrated that the structure shows syndiotactic conformation due to repulsion between the aromatic ring and methylene bridge of polyfluorene. The energy band gaps of polyfluorene and its derivative were evaluated by the extrapolation of excitation energies calculated by TDDFT (B3LYP/6-31G*) level of theory. For the polyfluorene and its derivative, the energy band gap can be pridicted within the range of available experimental data. The results indicated that larger substituent size from methyl to hexyl groups decreases the energy band gap as demonstrated by Eg = 2.75 and 2.55 eV, respectively. However, the limitation of the substituent size as found by R = 2-ethylhexyl group might be occurred as strong steric interaction effects to the electronic delocalization of the polymer and then, increases the energy band gap to 2.63 eV.

Acknowledgement

Financial support by the Postgraduate Education and Research Programs in Petroleum and Petrochemical Technology is gratefully acknowledged.

References

- [1] F. Negri, M. Z. Zgierski. J. Chem. Phys. **1992**, 97, 7124.
- [2] Burns, D. M., Iball. J. Proc. R. Soc. (London) 1955, A227, 200.
- [3] J. D. Pitts et al., and S. Wategaonkar. J. Chem. Phys. 1999, 110, 3378.
- [4] U. Salzner et al. and J. B. Lagowski. J. Phys. Chem. A. 1998, 102, 6935.
- [5] C. P. Hsu, S. Hirata and M. Head-Gordon. J. Phys. Chem. A. 2001,105, 451.
- [6] J. Rissler et al., F. Gebheard and P. Schwerdtfeger. Phys. Rev. B. 2001, 64, 45122.
- [7] J. Ma, S. Li and Y. Jiang. *Macromolecules*. **2002**, 35, 1109.
- [8] M. Fukuda, K. Sawada and K. Yoshino. *J. Polymer Science*. **1993**, 31, 2465.

Molecular electronic device from monolayer films

Rassamesard A*, Srikhirin T, Kerdcharoen T, and Osotchan T

Physics Department, Mahidol University, Rama 6 Road, Ratchathewi, Bangkok 10400 Thailand

Email: areefenmu@yahoo.com

ABSTRACT

The molecular electronic devices have gained large-scale interest in recent years, especially for future nanoscale electronic devices. The monolayer Langmuir-Blodgett films of a side chain liquid crystal copolymer with an 11-methylene spacer and a composition of 50% nitrobiphenyl and 50% methoxy ethoxy methoxy biphenyl were prepared from the air water interface.

The current-voltage characteristics of this molecule films were characterized by using scanning microscope and computerized tunnelling setup in with aluminium measurement vacuum electrodes. The local molecular conduction investigated by comparing the tunnelling current in silicon substrate, hydrophobic treated substrate, and one to four monolayer films. The tunnelling current and surface morphology for three monolayer films were also studied in the case of annealing at 100 °C for 5 minutes. It was found that the annealed surface is smoother and lower conductive due to the molecular rearrangement.

With aluminium electrodes, the electrical resistance systematically increases as number of monolayer increase from three to fifteen monolayer films as demonstrated by the linear increase of the electrical current as a function of inverse film thickness. This result shows the evidence of the main contribution in electrical conduction originated by the molecular monolayer. This result is not a consequence of the metal contact effect since the contact for all devices are equivalence. The asymmetric current-voltage relation can be observed for forward and reverse bias probably due to asymmetric of molecular structure.

Keywords: Molecular electronic devices, Scanning tunneling microscope, Monolayer films.

1. INTRODUCTION

One of the first idea of molecular electronics came from Ari Arivam and Mark A. Ratner [1] in 1974 who proposed D-σ-A molecule that construct with a donor (D) and an acceptor (A) connected with σ-bond, where D, A and σ are TTF, TCNQ and bycylooctance, respectively. The molecule aligns between metal electrodes. When potential is applied to the system, electrons flow through the molecule, resulting in a molecular rectifier (MR). For high quality MR characteristic, the sharp threshold voltage, large breakdown voltage, large current rectification ratios and large operating current are required. In theoretical

analysis of D- σ -A mechanism, the highest occupied molecular orbital (HOMO) and the lowest unoccupied molecular orbital (LUMO) are confined in two different parts of the D and A, respectively. The σ -bond prevents the orbital from spilling off the other part [2]. For applied positive potential, the Fermi level of electrode on A side aligns with the LUMO, while that on D side aligns with HOMO. At this voltage, the current increases sharply because the electrons can be loaded on the LUMO, then tunnel inelasticity [1] through the σ bond, the HOMO and pass into the second electrode. In the opposite direction, a similar process does not occur until a much higher negative voltage applied to system.

The different mechanism of a molecular rectification was described by Ellenbogen and Love [3]. The mechanism based on energy mismatch between two conducting levels localized on different parts of the molecule within the D- σ -A system. Under applied external potential, the energy levels of molecule shift with electric field. For positive applied potential the conducting level (LUMO) aligns and resonant transport of electrons between the electrodes occurs at some voltage. For negative applied potential the LUMO shifted away from each other and the current remains small. Therefore molecular rectification can exhibit.

The current rectification of Langmuir-Blodgett (LB) film of $\gamma\text{-hexadecylquinolinium}$ tricyanoquinodimethanide (C $_{16}H_{33}Q$ - 3CNQ) was studied theoretically by Krzeminski al et [4]. The active parts of this molecule (Q-3CNQ) are composed of donor and acceptor with the long insulating tail (C $_{16}H_{33}$) added to help form good LB films. The Q-3CNQ is a D- π -A molecule, the analysis confirmed that the π -bond does not sufficiently separated D and A parts and the orbital were delocalized over the Q-3NCNZ part. The rectification can be observed by asymmetric position of HOMO and LUMO with respect to Fermi levels of metal electrodes.

The numerical study of the suggested family molecules of HS-(CH₂)_m-C₆H₄-(CH₂)_n-SH was reported by P.E. Kornilovitch al et [5]. It was based on the spatial asymmetric of the molecule and require only on resonant conducting molecular level (LUMO) of π -orbital. The highest rectification achieved at m = 2 and n = 10.

In experimental, the electrical properties of MR have been mostly studied in LB film configuration which was confined between two thermally evaporated metal. The electrodes can be either the same or dissimilar metals thus the devices have the structure of metal/organic LB film/metal planar structure.

Molecular devices based on Q-3CNQ with symmetric metal electrode were shown rectifying behaviour [6]. These initial studies showed that although the molecule existed in a charged zwitterionic [7] ground state, it was believed that the conduction occurs via an uncharged excited state. This high polar molecule was, however only assembled in multilayer system. The rectification can be observed in a monolayer of Q-3CNQ between two aluminium electrodes. The rectification ratios of 26 at ± 1.5V were discovered with no temperature dependence. It has been showed that the rectification is derived from the molecular monolaver although the oxide layer usually forms on aluminium electrode. In order to verify, the aluminium electrode was replaced by gold which is free oxide metal. The deposition of top electrode was employed by cold gold evaporation [8]. The use of gold led to the increase in rectifying behaviours for most cases. It has been pointed out that there is a loss of rectification over multiple cycles of measurement [9].

Ashwell et al [10] confirmed that z-type 30 layer film of Q-3CNQ exhibited the rectification between gold electrodes. The thermal evaporation of the gold electrode may have destroyed 20 of the 30 layers, as monitored by a decreased absorbance. The current for the multilayer was three orders of magnitude smaller than that in monolayer [11], either because of inefficient electron transport between adjacent layers or current contributions from gold filaments within the LB monolayer.

The other methods are observe the electrical conduction of molecule can be performed by scanning tunnelling microscope (STM) [12-14] or the of atomic force microscope (AFM) with conductive tip [15].

The electrical resistance for the monolayer of cast film of a kind of binuclear cobalt phthalocyanic-sulphonate deposited on highly oriented pyrolytic graphite substrate demonstrated smaller value than that for the double layer [12]. The rectification of the monolayer is better than that in double layer. The STM experiments indicated that the asymmetry for current-voltage curves arise from material asymmetry. The STM was also used to studied electrical properties of complex layer of 3-marcaptopropionic acid and 3-aminopropyltri ethoxysilane [13]. The strong asymmetric of the current-voltage characteristic has been found.

The measured current-voltage characteristics of pentacosadyinoic acid deposited on flat gold substrates were correlated and discussed with gold Fermi level of the substrate, Pt/Ir Fermi level of the tip and the HOMO/LUMO energy level of the polydiacetylene molecule [14]. The conductance of a single molecule connected to two gold electrodes has been measured by using conductive tip of AFM [15]. Thousands of gold-molecule-gold junctions were formed repeatedly. Conductance histograms revealed well defined peaks at integer multiples of a fundamental conductance value, which was used to identify the conductance of a single molecule.

In this paper the current voltage characteristic of molecular film was investigated by using tips of STM as

a top electrode. These alternative methods give the possibility of measuring electrical characteristics of individual molecules through the atomic resolution. The symmetric aluminium electrode on top and bottom of the monolayer film was also investigated to study the rectifying properties of cop11 molecular film.

2. MATERIALS AND METHODS

The monolayer of the side chain liquid crystalline copolymer, cop11, as shown in the insert of Fig.1, was prepared by LB technique. A multi-monolayer film was transferred onto the silicon substrate via the horizontal deposition technique. The LB monolayer was prepared from a 150 µl of solution of 0.3 mg/ml cop11 in chloroform. Surface pressure as a function of area per molecule, isotherm, of cop11 as shown in Fig.1, exhibits a relatively steep rise, which demonstrates a close packing of the molecules. After spreading, the film was compressed at a speed of 10 mm/s until the surface pressure of 25 mN/m achieved then kept at this pressure for 1,500 second. The surface of silicon wafer was washed by acetone, methanol and chloroform in ultrasonic bath sequentially. Then cleaned silicon wafer was treated in hexamethyldisiloxane saturated vapour for 24 hours in desiccators. The monolayer LB film was deposited on hydrophobic silicon wafer substrate by horizontal dipping.

In this study multilayer films of cop11 were fabricated and characterized by X-ray diffraction technique. Before I-V characteristics were measured by STM, the surface morphology of cop11 was measured by AFM in dynamic mode. For I-V measurement with STM, an area of 100 x 100 nm² was scanned with bias voltage of 0.5 V at tunnelling current of 0.1 nA. The three layer film was then annealed at 100 °C for 5 minutes and then surface morphology was scanned by AFM. Then the I-V characteristic was measured by STM with the same bias voltage. The cop 11 film with 3, 5, 7, 10, 12 and 15 monolayers, were prepared between two aluminium coated electrodes prior to an electrical investigation. The current measurement was performed in vacuum system by applying a forward and reverse bias voltage of +1.5 to -1.5 V.

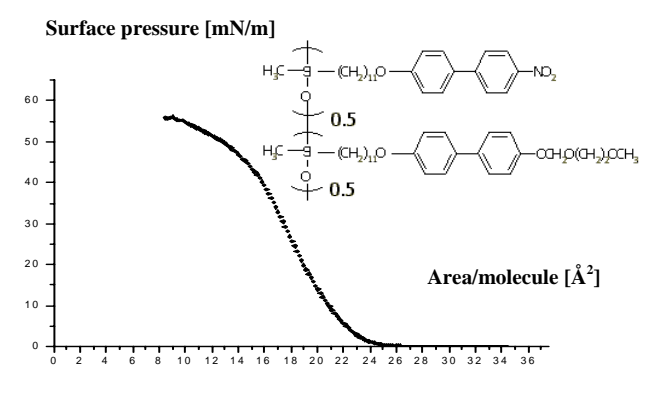


Fig. 1. Surface pressure as a function of area per molecule, isotherm, of cop11, as shown chemical structure in insert.

3. RESULTS AND DISCUSSION

The steeply inclining part of the isotherm curve as shown in Fig.1 corresponds to the formation of a solid monolayer of cop11 molecules on the water surface. The high colapse surface pressure of 55 mN/m indicates of the good film-forming behavior of the cop11 molecule monolayer. The isotherm showed mean molecular area of 23 Å 2 /molecule estimated by the x-intersection of the linear part of the isotherm. The phase transition of LB film occur at surface pressure between 4.2 and 45.3 mN/m.

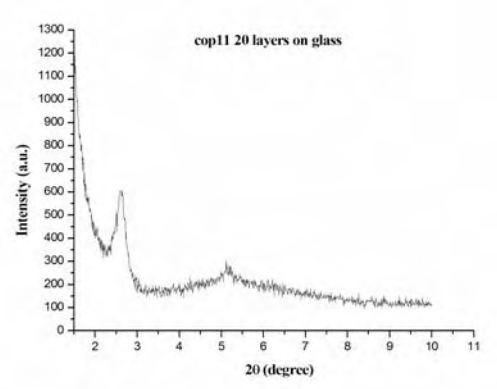


Fig. 2. X-ray diffraction pattern of 20 monolayer cop11 LB film

Two x-ray diffraction peaks were obtained at 2.61 and 5.12 degree for 20 monolayer cop11 films on hydrophobic glass slide as illustrated in Fig. 2. These values were used to estimate the d spacing of 33.87 Å the d-spacing of cop11 molecule.

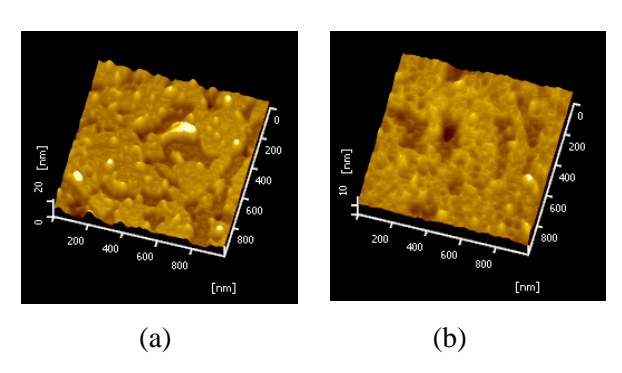


Fig. 3. Surface morphology of three layer cop11 film on silicon substrate before (a) and after (b) annealing at 100 0 C for 5 minutes measured by AFM in dynamic mode for 1000×1000 nm²

The $1\times1~\mu\text{m}^2$ AFM image of bare hydrophobic silicon is very smooth and flat. The surface of three layer cop11 LB film on silicon show some cracks probably due to the rigid film of cop11 liquid crystal film. The crack may be occurred during film transfer to the substrate.

The I-V characteristics measured by STM of bare silicon wafer, hydrophobic silicon wafer, one to four monolayer, and three monolayer annealed cop11 LB film on silicon substrates are displayed in Fig. 4.

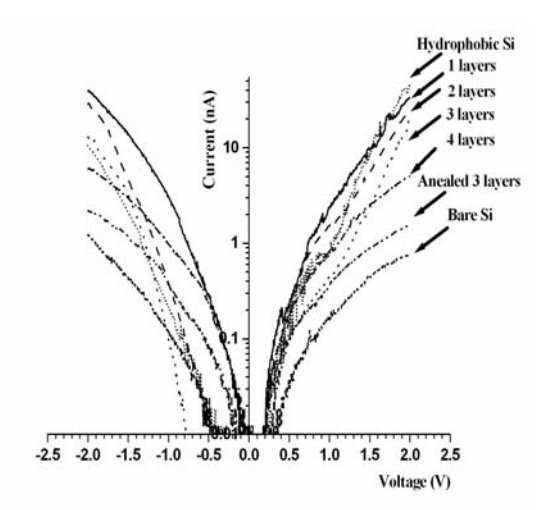


Fig. 4. I-V characteristic of bare silicon wafer, hydrophobic silicon wafer, one to four monolayer, and three monolayer annealed cop11 LB film on silicon substrates measured by STM.

Since the STM tip was set at the distance with the value of tunnelling current of 0.1 nA at 0.5 V, most of the curves pass through this point. However the current at 1.5V for one to four monolayer films become decrease as the number of monolayer increases. It indicated that the resistance of cop11 LB film is increase with the number of layers. The current in annealed film has low value while the bare silicon substrate has the lowest value. These also exhibit for those in the reverse bias cases.

The surface becomes smooth for annealed film as shown in Fig. 3. The crack propagation of annealed film is decreased. It indicated that thermal annealing affects rearrange of molecular in the film. The tunnelling current for three layer film on silicon substrate is decrease after anneal at $100\,^{0}\mathrm{C}$ for 5 minutes due to molecular rearrangement.

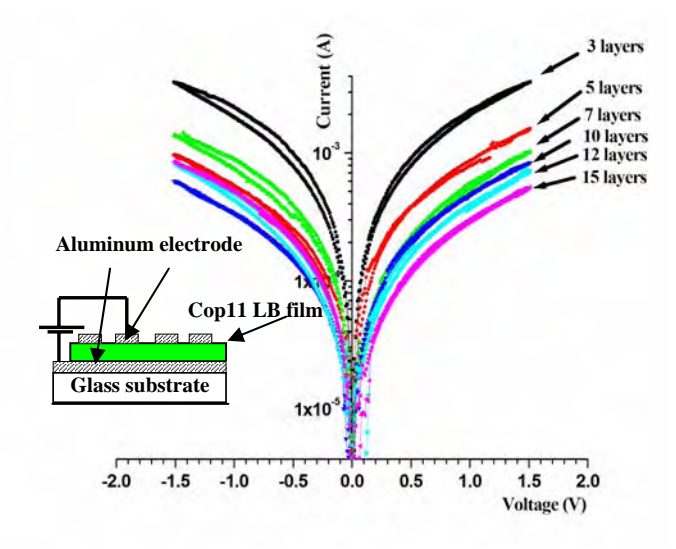


Fig. 5. I-V characteristic of 3, 5, 7, 10, 12 and 15 monolayer cop11 between aluminum electrodes.

The electrical characteristics of cop11 monolayer with aluminium metal electrodes displayed in Fig. 5, with the number of monolayer of 3, 5, 7, 10, 12, and 15. It is hard to prepare the electrode on a few monolayer film because of the pin hole and the heat damage during thermal metal evaporation. The result indicated that the current decreases when the number of layers increases with number of layers increase.

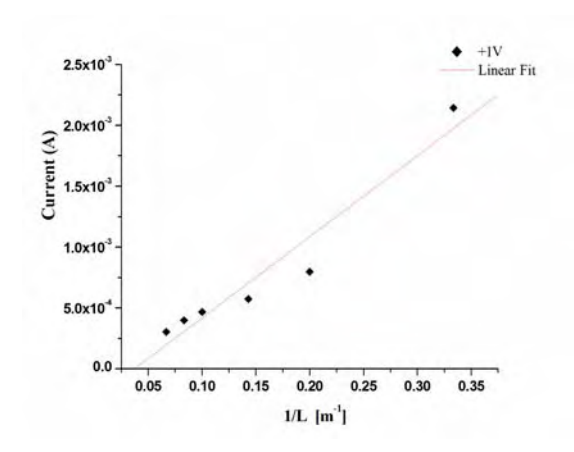


Fig. 6. Measured current at fixed apply voltage as a function of inverse of layer number.

In order to investigate the variation of current as a function of layer number, the model of simple resistance were employed. The resistance should linearly increase as the thickness increases. Therefore the measured currents at fixed apply voltage were plotted as a function of inverse of layer number as demonstrated in Fig. 6 for the case of 1.0 V.

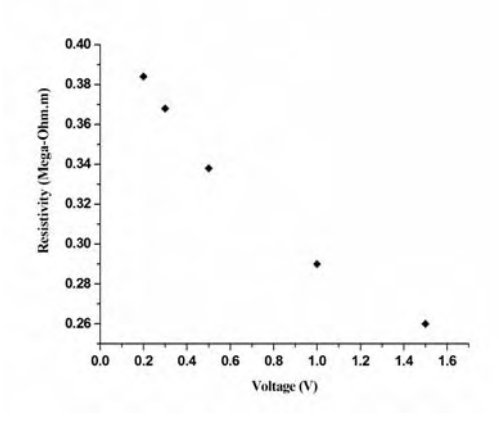


Fig. 7. Calculation result of perpendicular resistivity of molecular film as a function of applied voltage

The slope of the graph was used to estimate the perpendicular resistivity. The derived resistivity at some other apply voltages were also obtained and displays in Fig. 7. The resistivity of the film was modified by apply voltage and exhibited the decreasing value when the apply voltage increases.

4. CONCLUSSION

The side chain liquid crystal copolymer, cop 11, can form the monolayer LB films at air water interface. The conduction of this molecule films were characterized by using scanning tunnelling microscope and computerized I-V measurement setup in vacuum with aluminium electrodes. The local molecular conduction was investigated by comparing the tunnelling current in silicon substrate, hydrophobic treated substrate, and one to four monolayer films.

The tunnelling current and surface morphology for three monolayer films were also studied in the case of annealing at 100 0 C for 5 minutes. It was found that the annealed surface is smoother and lower conductive due to the molecular rearrangement. With aluminium electrodes, the electrical resistance systematically increases as number of monolayer increase from three to fifteen monolayer films as demonstrated by the linear increase of the electrical current as a function of inverse film thickness. This result shows the evidence of the main contribution in electrical conduction originated by the molecular monolayer. This should not result of the metal contact effect since the contact for all devices are equivalence.

5. REFERENCE

- 1. A. Aviram, M. A. Ratner, Chem. Phys. Lett. 29, 277 (1974).
- 2. C. Majumder et al., J. Phys. Chem. A 2001, 105, 9454-9459.
- 3. J.C. Ellenbogen, J.C. Love, Proc. IEEE 88, 386 (2000).
- 4. C. Krzeminski et al, Phys. Rev.B 64, 085405 (2001).
- 5. P.E Kornilovith et al, Phys. Rev. B, 165436 (2002).
- 6. R.M. Metzer et al, J. Am. Chem. Soc. 119, 10455 (1997).
- 7. G.J. Ashwell et al, J. Chem. Soc. Chem. Commum. 1374-1376 (1990).
- 8. R.M. Metzger, J. Mater. Chem. 10, 55-62 (2000).
- 9. T. Xu et al, Chem., Intl. Ed. 2001, 40, 1749.
- 10. G.S. Ashwell et al, J. Chem., 55, 199 (2002).
- 11. R.M. Metzger et al, J. Phys. Chem. B 2001, 108, 7280.
- 12. Y. J. Znan et al, Syn. Mater., 128, 43-46 (2002).
- 13. J.J. Langer et al, Syn. Mater., 107, 1-6 (1999).
- 14. N.G. Semaltianos et al, Chem. Phys. Let. 329, 76-83 (2000).
- 15. B. Xu, N.J. Tao, SCIENCE, 301,1221-1223 (2003).







Computational Modeling of Carbon Nanotube Based Alkali Metal Storage

Anurak Udomvech¹, Teerakiat Kerdcharoen¹ and Thanh N. Truong²

¹ Department of Physics, Faculty of Science, Mahidol University, Bangkok ² Department of Chemistry, University of Utah, Salt Lake City, USA

Abstract

The favorite materials, carbon nanotubes, are applied to several novel applications. In our study, we focus on the single-walled carbon nanotubes (SWNTs) used as anode material for storage of alkali-metal atoms. The first-principle density functional methods are utilized to explore interaction between different diameters ranging from (6,0) to (12,0). The interaction potential energy change from single-well to double-well curve when SWNTs diameter become larger. Charge transfer from alkali metals to SWNTs is found when metal bind to the side SWNTs.

Introduction

After the discovery by Iijima [1] in 1991, research on carbon nanotube (CNT) reach a critical mass in many areas of physics and chemistry. Synthesis methods have been rapidly improved to produce large amount of size-controlled CNT for commercial applications [2, 3, 4]. CNT has two types of structure: (1) single walled carbon nanotube [5] (SWNT) which is a single rolled graphene sheet; (2) multi-walled carbon nanotube (MWNT) in which each CNT is encapsulated by the others based on the Russian-Doll model. Carbon nanotube can adsorb a number of atomic and molecular species, for instances alkali metals (i.e. Li [6], K [7], Rb [8] and Cs [9]) and hydrogen [10], nitrogen [11], oxygen [12] and methane [13] gases. The adsorption properties provide the opportunities for applications such as hydrogen and other gases storage [14, 15], gas sensor [16], catalyst [17] and Li-ion batteries.

Binding of atoms and molecules to the sidewall of carbon nanotube modifies the conductivity of the nanotube. For instances, oxygen [18] and fluorine decrease the conductivity, whereas alkali metals do the opposite. Field emission property is also affected by the adsorption. Oxygen gas is found to degrade the field emission of carbon nanotube, whereas hydrogen helps to clean the defects on the nanotube [19]. Doping carbon nanotube with Cs atoms was found to reduce the work function from 4.8 to 2.4 eV [20]. Wadhawan et al. found that deposition of Cs on the single-walled carbon nanotube (SWNT) bundles dramatically improve the field emission efficiency [9].

Recently, nano-structured materials for anode has drawn interest from the battery industry because engineering limit has been reached for the conventional materials







such as carbonaceous materials and metal oxides.^{1,2,3} The idea is that optimization of the device performance, i.e. charge-discharge cycles and reversibility, based on nanoscale properties could bring the development process out of the trial-and-error cycles. Carbon nanotube becomes a prospect candidate for uses in Li-ion batteries because it can provide large numbers of nanoscale sites for intercalant atoms that exceed the ideal capacity of commonly used graphite electrode of LiC₆.

In this work, we have investigated Li⁺-doped CNT by first principles calculations (B3LYP/6-31G). All of CNT employed in this study is of the zigzag type, denoted by the chiral vector (m,0). Since the CNTs in this study are finite-sized, hydrogen atoms are used to cap the dangling carbon atoms at the open ends of a nanotube. The potential energy surface of Li⁺-SWNT system is investigated by insertion of Li⁺ into CNT from the sidewall and plotting the binding energy as a function of distance along the cross section.

The shape of Li⁺-SWNT potential energy surface was investigated for model SWNT varying diameters from (6,0) to (12,0), as illustrated in Figure 1. The cluster model of these nanotubes has only 1 unit cell length (1UC). For small diameter SWNTs such as (6,0) and (7,0), the potential energy surface has single minimum inside the nanotube. As the tube's diameter becomes larger, as found for (8,0) and up, the double-welled shape is developed inside the nanotube. The binding energy depends on the tubule diameter slightly, having values between 1.7-2.2 eV. It was found that Li⁺ tends to bind to both internal and external of SWNT sidewalls, whereas binding at the exterior is slightly stronger. For instances, binding energies to the interior and exterior of nanotube are -1.9 and -2.1 eV for SWNT(6,0) and -1.9 and -2.0 eV for SWNT(9,0), respectively.

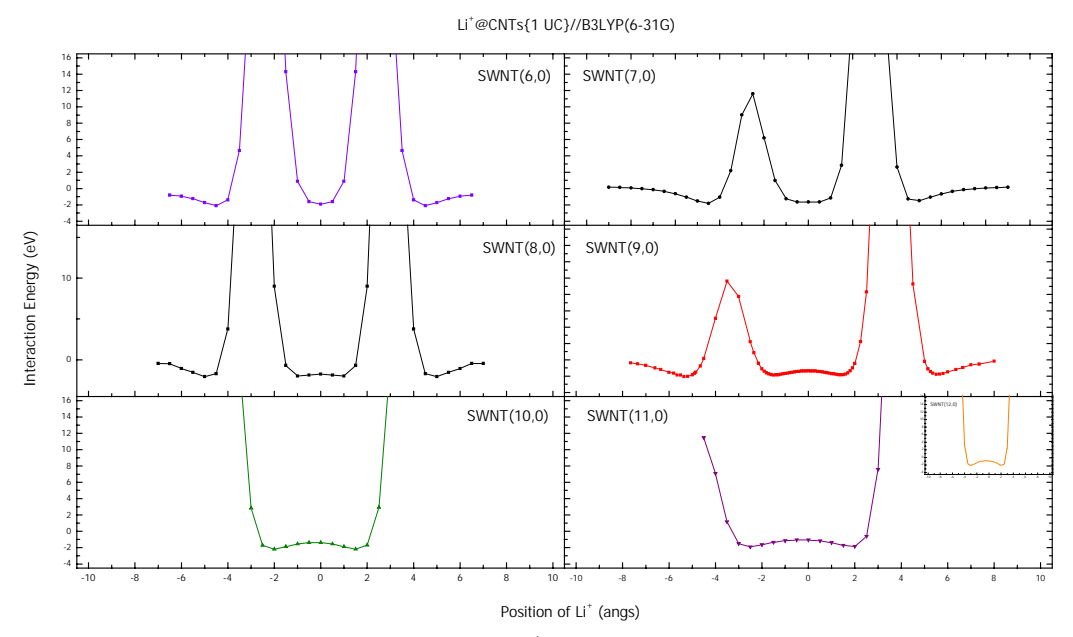


Figure 1 Potential energy profile of the Li^+ -CNT systems based on 1 unit-cell cluster model. Li^+ is placed along the cross section of the CNT. For the SWNT(m,0) and m is







the even number, Li^+ passes through C-C bonds on both sides, whereas it passes through hexagon (C_6) center on the left side when m is odd number.

From the above results, one can conclude that CNT provides adsorption site for Li^+ and the adsorption strength originates from local interaction between Li^+ and the adsorption site. It is still not clear whether local adsorption site is the bond (C₂), the trigonal (C₃) or the hexagon (C₆). We examined the Li^+ -C₂ and Li^+ -C₆ PES minima located at the external wall of SWNT(7,0) and SWNT(9,0) and found that binding of Li^+ at the C₆ hexagon (1.83 eV and 2.04 eV respectively) is preferred over the C₂ bond (1.49 eV and 1.76 eV respectively).

It is necessary to investigate whether the 1UC cluster model is sufficient to represent Li-CNT PES. SWNT(6,0) and SWNT(9,0) were extended up to 4UC and 3 UC structures, respectively. It was found that the PES obtained from the longer nanotube retains the same shape of the shorter one but has deeper energy minimum. In the SWNT(6,0), the energy minima in the interior of CNT are -1.9, -1.9, -2.6 and -2.7 eV for 1UC, 2UC, 3UC and 4UC structures, respectively. Likewise, these minima are -1.86, -2.34 and -2.34 eV in the case of SWNT(9,0).

Mulliken population analysis has been done for Li⁺-CNT systems and the charge on Li is displayed in Figure 3. It is clear that when the metal ion is far away from CNT, the charge reaches the ideal value of +1. As the ion gets closer to the nanotube, its positive charge becomes smaller due to the electron transfer to the metal, even to the extent that the metal becomes negatively charged when the metal is too close to nanotube (i.e. when it passed through the sidewall, charge on Li is between -0.4 to – 0.5). When Li ion locates inside the nanotube, its positive charge reach maximum when it locates at the center. The charge maximum increases when the tube's diameter is larger, i.e. from +0.43 in SWNT(6,0) to +0.88 in SWNT (12,0).

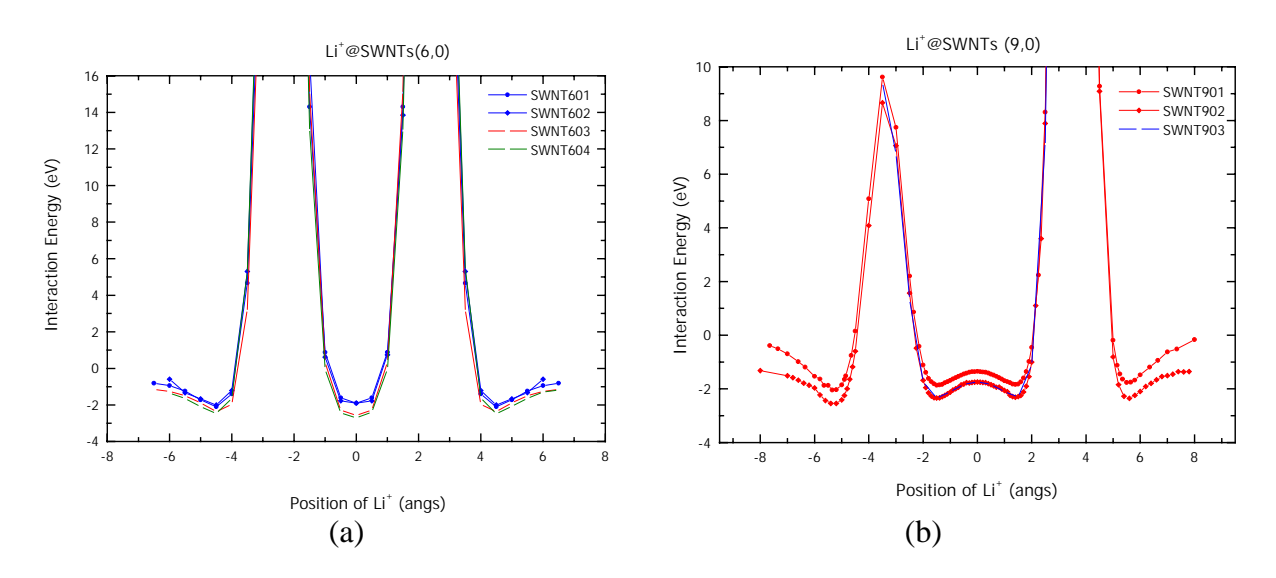


Figure 2 Potential energy profile of the Li⁺-CNT systems upon increasing tubule length, (a) SWNT(6,0) and (b) SWNT(9,0).

ANSCSE6 2002







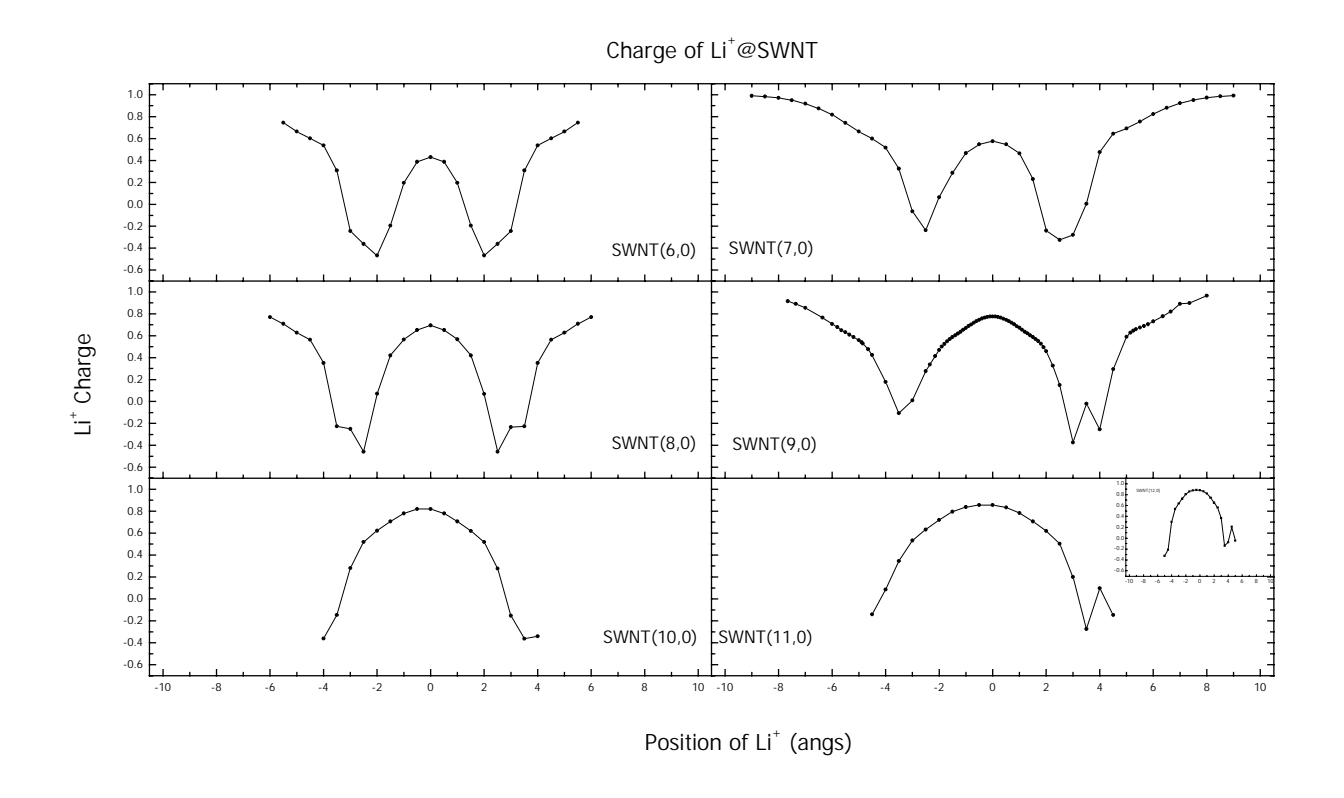


Figure 3 Mulliken charge on the Li ion versus the distance from the center of 1UC cluster model of CNT.

This study reveals that Li⁺ can adsorb to both internal and external sidewalls of CNT. Binding energy is dominated by local interaction of the metal ion with the C₆-hexagon of the CNT. Electron transfer from CNT to Li⁺ is observed, which means the interaction is not purely electrostatic. The "ion-pi" interaction (or bonding) may explain why a short CNT can be used to model the PES of longer or infinite CNT since this interaction is "local" in nature.

Acknowledgements

A. U. expresses his gratitude to Ministry of University Affairs and the Shell Centenary Foundation for graduate research grant. Support to T. K. from Basic Research Grant of the Thailand Research Fund is gratefully acknowledged.

References

- [1] Iijima, S. 1991. Nature 354, 56.
- [2] Ajayan, P. M. & Ebbesen, T. W. 1997. Rep. Prog. Phys. 60, 1025.
- [3] Ajayan, P. M. 1999. Chem. Rev. 99, 1787.
- [4] Rao, C. N. R., Satishkumar, B. C., Govindaraj, A. & Nath, M. 2001. ChemPhysChem 2, 78.

ANSCSE6 2002







- [5] Iijima, S. & Ichihashi, T. 1993. Nature 363, 603.
- [6] Bendiab, N., Anglaret, E., Bantignies, J. L., Zahab, A., Sauvajol, J. L., Petit, P., Mathis, C. & Lefrant, S. 2001. Phys. Rev. B 64, 245424.
- [7] Claye, A. S., Nemes, N. M., Janossy, A. & Fischer, J. E. 2000. Phys. Rev. B 62, R4845.
- [8] Rao, A. M., Eklund, P. C., Bandow, S., Thess, A. & Smalley, R. E. 1997. Nature 388, 257.
- [9] Wadhawan, A., Stallcup, R. E. & Perez, J. M. 2001. Appl. Phys. Lett. 78, 108.
- [10] Cao, A., Zhu, H., Zhang, X., Li, X., Ruan, D., Xu, C., Wei, B., Liang, J. & Wu, D. 2001. Chem. Phys. Lett. 342, 510.
- [11] Yang, Q. H., Hou, P. X., Bai, S., Wang, M. Z. & Cheng, H. M. 2001. Chem. Phys. Lett. 345, 18.
- [12] Zhu, X. Y., Lee, S. M., Lee, Y. H. & Frauenheim, T. 2000. Phys. Rev. Lett. 85, 2757
- [13] Talapatra, S. & Migone, A. D. 2002. Phys. Rev. B 65, 045416.
- [14] Schlapbach, L. & Zuettel, A. 2001. Nature 414, 353.
- [15] Dillon, A. C. & Heben, M. 2001. J. Appl. Phys. A 72, 133.
- [16] Peng, S. & Cho, K. 2000. Nanotechnology 11, 57.
- [17] Nisha, J. A., Yudasaka, M., Bandow, S., Kokai, F., Takahashi, K. & Iijima, S. 2000. Chem. Phys. Lett. 328, 381.
- [18] Rochefort, A. & Avouris, P. 2000. J. Phys. Chem. A 104, 9807.
- [19] Lim, S. C., Choi, Y. C., Jeong, H. J., Shin, Y. M., An, K. H., Bae, D. J., Lee, Y. H., Lee, N. S. & Kim, J. M. 2001. Adv. Mater. 13, 1563.
- [20] Suzuki, S., Bower, C., Watanabe, Y. & Zhou, O. 2000. Appl. Phys. Lett. 76, 4007.
- [21] Tarascon, J. M. & Armand, M. 2001. Nature 414, 359.
- [22] Poizot, P., Laruelle, S., Grugeon, S., Dupont, L. & Tarascon, J. M. 2001. J. Power Source 97-98, 235.
- [23] Li, N., Martin, C. R. & Scrosati, B. 2001. J. Power Source 97-98, 240.







Electron quantum transport simulation in nanoelectronic devices

Noparit Jinuntuya^{1, 2} and Tanakorn Osotchan²

¹Department of Physics, Faculty of Science, Kasetsart University,
Bangkok 10900, Thailand
²Capability Building for Nanoscience and Nanotechnology, Department of Physics,
Faculty of Science, Mahidol University, Bangkok 10400, Thailand

Abstract

Electron transport in one dimensional nanoscale n⁺⁺ - n⁺ - n⁺⁺ system is simulated by non-equilibrium Green's function formalism. The total length of the device used in the calculation is only 30 nm, in which the quantum mechanics is needed for fully implementation. Therefore Schrödinger and Poisson equations are required to be solved self consistently. However in order to equip the open boundary at the contacts and Fermi energy difference between two contacts, the non-equilibrium Green's function formalism with self-energy matrix is used to solve Schrödinger equation in this system. In equilibrium condition the comparisons between using the Green's function formalism and directly solving Schrodinger equation with fix boundary are examined in term of the accuracy and speed of computation. Using the directly solve solution for the initial guess of self-consistence is proposed for an effective transport simulation for this nanoelectronic systems.

Introduction

Progress in semiconductor fabrication technology has led to smaller and faster electronic devices. The theoretical description of transport in these devices has become more complex. The active length of those devices is probably comparable to a mean-free path. Therefore the simple drift-diffusion approach is not valid any more. It is clear that quantitative simulation tool for such devices require atomic level quantum mechanical models [1].

In this paper the electrical property of n^{++} - n^{+} - n^{++} nanoscale device structure was simulated with the n^{++} , n^{+} and n^{++} region length of 4.5, 21.0 and 4.5 nm, respectively. The total length of the device is only 30.0 nm, so the full implementation of quantum mechanic is needed. Our propose is to illustrate some of the unusual issues that arise in the numerical procedure of this device simulation. The non-equilibrium Green's function (NEGF) formalism was used to handle the open boundary at contacts with the concept of self-energy matrix [1-3]. The applied voltage at both contacts leads the system to non-equilibrium condition with different Fermi energy. Only coherent case was considered in this study, therefore the scattering term in the Hamiltonian was ignored. The quantum electron transport was considered only along the structure (x)







direction) while electrons freely move in transverse direction (y and z directions) under periodic boundary condition. This device structure is uniform over the cross section area therefore this structure can be accounted as a quantum electron transport in one-dimensional device structure.

Calculation

The main task in our calculation is to calculate the density matrix ρ from which various quantities can be obtained. In equilibrium condition the density matrix is simply the Fermi function of the Hamiltonian matrix but it cannot be used in non-equilibrium case. Therefore in order to derive the non-equilibrium condition, the density matrix can be calculated in NEGF scheme by the defined Green's function $G = [EI - H - \Sigma_1 - \Sigma_2]^{-1}$. Here H is the longitudinal Hamiltonian matrix of the isolated device, Σ_1 and Σ_2 are the self-energy matrices representing the coupling between the device and left and right reservoirs respectively, and E and E are the electron energy and identity matrix [1-3].

When bias voltage is applied, the two contacts will have different Fermi level μ_1 and μ_2 . The density matrix can be calculated by assuming the 'reflectionless' contacts at both ends [3]. Electrons from the device can enter into the reservoir without suffering reflection. Therefore the +k and -k states are occupied only by electron originating in the left and right contacts, respectively. For non-equilibrium transport the density matrix can be given by

$$\boldsymbol{\rho} = \frac{1}{2\pi} \int_{-\infty}^{\infty} dE \left[F_0 \left(E - \mu_1 \right) \mathbf{A}_1 \left(E \right) + F_0 \left(E - \mu_2 \right) \mathbf{A}_2 \left(E \right) \right], \tag{1}$$

where F_0 is summation of Fermi function of states in the transverse modes. From Eq. 1 electrons fill up proportionally to the left and right spectral function A_1 and A_2 according to the Fermi function in the left and right contacts, respectively. These spectral functions can be transformed by $A_{1,2} = G\Gamma_{1,2}G^+$ where $\Gamma_{1,2} = i (\Sigma_{1,2} - \Sigma^+_{1,2})$ [3].

The description of our device can then be obtained by calculating electron density n(x) and potential U(x) self-consistently. The electron density can be obtained from the diagonal element of the density matrix in discrete real space representation, $n(x_i) = \rho_{i,i}[3]$. The potential relates to the charge distribution by Poisson equation

$$\frac{d}{dx} \left(\varepsilon \frac{dU(x)}{dx} \right) = q^2 [N_D(x) - n(x)], \qquad (2)$$

where $N_D(x)$ is the doping concentration profile. In order to solve the differential equations, the boundary conditions must be imposed both to the Hamiltonian matrix and Poisson equations. In the latter case, the zero field boundary condition would be implemented on both ends. However, to avoid the singular matrix, the zero-field







condition was applied only at one end while the varied potential at the other end can be obtain from the electrical neutralize condition.

For the finite difference implementation of Hamiltonian matrix, the boundary condition can be obtained from the self-energy matrix which representing the coupling between the device and the reservoirs. Since there is no reflection along the longitudinal direction, the continuity of plane wave at both contacts was assumed to derive the value of self-energy.

In order to achieve I-V characteristic, the current density through the device length L can be calculated by the relation J = -q Trace $(\rho J_{\rm op})$ where the current operator $J_{\rm op}$ in the real space representation can be written in the following form [3]

$$J_{\rm op} = \frac{\hbar}{2mL} \begin{bmatrix} 0 & -i & 0 & \cdots \\ +i & 0 & -i & \cdots \\ 0 & +i & 0 & \cdots \\ \vdots & \vdots & \vdots & \ddots \end{bmatrix}.$$
(3)

Calculated results

In the calculation we use the numerical integration to evaluate density matrix and finite difference scheme to solve Poisson equation numerically. The device structure was divided into 100 discrete sections. The following parameters were used in our calculation, $m = 0.25m_0$, $\varepsilon = 10\varepsilon_0$, $N_D = 1\times10^{26}$ m⁻³ in n++ regions with 4.5 nm long and $N_D = 5\times10^{25}$ m⁻³ in n+ region with 21.0 nm long.

1 Equilibrium case

When there is no voltage applied to the structure, the device is in equilibrium with the same Fermi energy levels on both sides of the contact. In this case the spectra functions on both sides are also identical since the wave vectors of the plane wave in both reservoirs are determined by the same relative energy. The total spectral function was proven to be equal the sum of the left and right spectral functions. By simplify Eq.1, the density matrix can be derived by the total spectral function.

In the self-consistent calculation the potential relative to the Fermi energy was initially guessed by the asymptotic values derived from the doping concentration of two regions of n⁺ and n⁺⁺. The potential as a function of distance was initially estimated by these values. The potential was used in Hamiltonian to calculate density matrix and electron density. Then the result electron density was substituted in Poisson Equation and new potential profile can be obtained. In order to prevent the divergence of the iteration, the weight factor was employed to multiple the result potential before used in the next iteration.







The electron density n(x) and potential U(x) was numerically solved self-consistently and the calculated profiles are presented in Figure 1. In equilibrium the Fermi level as indicated by dashed line is constant over the entire structure and the value relative to potential equals 0.31 and 0.29 eV in the n^{++} and n^{+} regions, respectively. The depletion regions of about 4.0 nm extended equally into both sides from the n^{+} / n^{++} junctions. The values of the relative potential and electron density at the interface equal half of deviation value i.e. 0.06eV and 7.5×10^{25} m⁻³, respectively.

The electron density in equilibrium condition was also directly solved from Schrödinger equation with periodic boundary conditions to examine the accuracy and speed of computation. It was found that both methods achieved the same rate of convergence and give the identical result if the energy division used in the numerical integration is sufficient. This is due to the delta function like feature of spectral function at energy around the relative Fermi energy. Therefore the computational time for direct solved Schrödinger equation method is very much shorter. The numbers of the floating-point operations per iteration for direct Schrödinger-Poisson solver and NEGF method are 4.71×10^7 and 1.04×10^{10} flops, respectively. When solving on the same machine, the computational time per iteration for the NEGF scheme is about 70 times longer than that for directly solving Schrodinger equation. However this direct method cannot be employed for the non-equilibrium case.

2 Non-equilibrium cases

In non-equilibrium case the spectral functions on the left and right sides are different since the relative electron energy, used in determining the self-energy and wave vector, is shifted by bias voltage. The fixed-point boundary condition used in solving Poisson Equation on the left side was varied after the convergence of both functions in order to ensure that the electron concentration at the left edge is equal to the doping concentration. It is found that after adjusting the left relative potential value, the electron density at the right edge also approximately equals the doping concentration on the right region. Since the iteration is very sensitive to the initial function, the small step of the applied voltage was employed until it reaches the desired voltage.

The calculation results of potential profile and electron density for an applied bias voltage of 0.20 V are presented in Figure 2(a) and (b) respectively. The electron density slightly changes under the bias voltage. The carrier concentration on the left end of the $\rm n^+$ region is slight lower with the deviation value of $1.18\times10^{25}~\rm m^{-3}$, while the carrier density on the right end is slightly increase so that the depletion region in the right hand side is wider.

Under applied bias of 0.20 V the relative potential at the left contact is pulled down with the value of 0.043 eV while the right potential is pulled up of about 0.035 eV. Thus the Fermi energy relative to the potential at the left and right side is extend to 0.355 and 0.277eV. The potential difference between the left and right is 0.122 V that is less than the value of applied voltage by 0.078 V. Therefore there is the voltage value of 0.043 V and 0.035 V dropped at the left and right contact respectively.







The dropped voltage between the structure and at the left and right contacts as a function of applied voltage was calculated and showed in Figure 3(a). The dropped voltage is approximately linear dependent to the applied voltage. The current density was calculated from density matrix including diagonal and off-diagonal elements. In order to obtain the I-V characteristic the current density was examined as a function of bias voltage and the results is shown in Figure 3(b). The I-V characteristic is approximately linear with the conductance value of $7.6 \times 10^6 \,\Omega^{-1}$ at the device area of 1 mm².

Since there is the voltages dropped at left and right contacts, we calculated the conductance of the device by the only part of the voltage dropped at the device and the conductance value of $12.6\times10^6~\Omega^{-1}$ was obtained. The contact conductance was calculated from the voltages dropped at the left and the right contacts and the conductance values of 36.3×10^6 and $39.7\times10^6~\Omega^{-1}$ were obtained respectively.

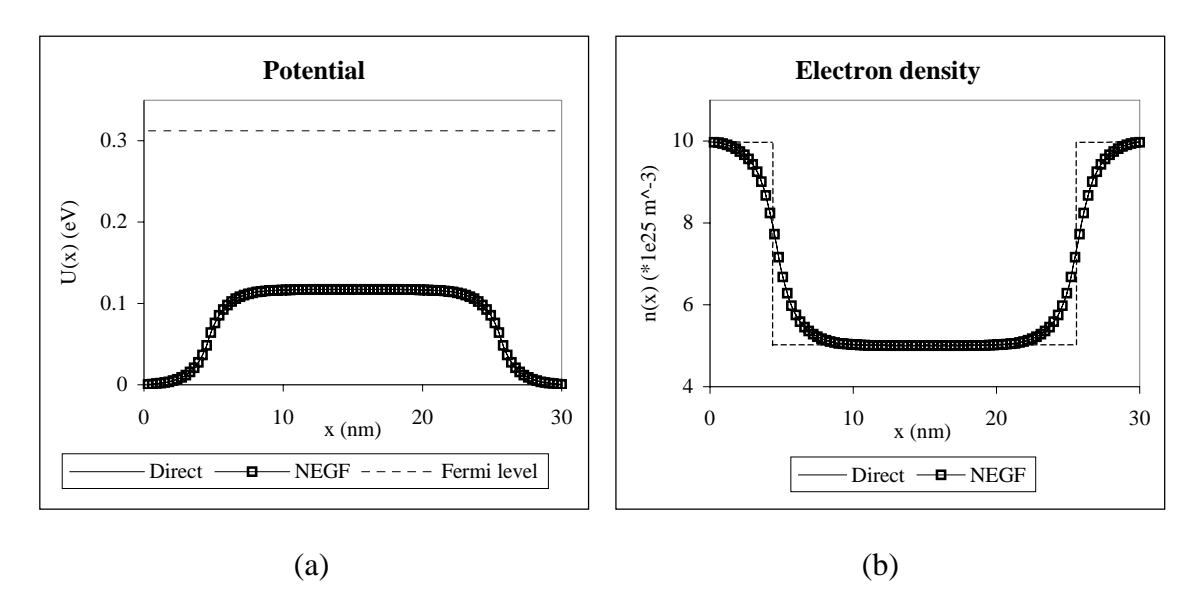
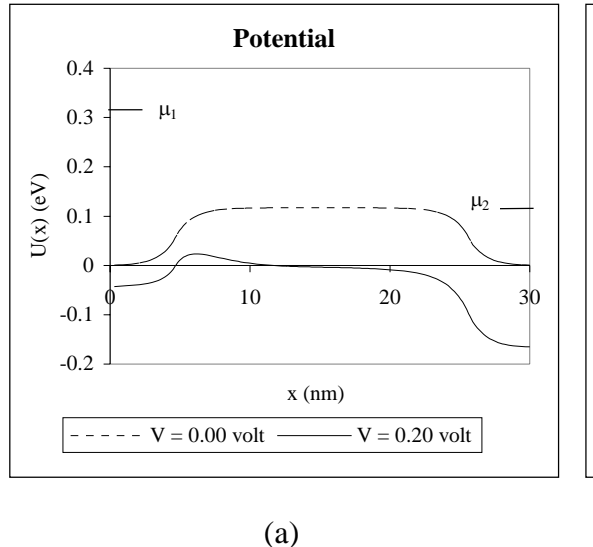


Figure 1 Calculated profiles of (a) equilibrium potential and (b) electron density in the n^{++} - n^{+} - n^{++} nano-structure by direct solving Scrhödinger equation (solid line) and NEGF methods (square). Dash lines in (a) and (b) indicate the Fermi energy level and doping profile, respectively.









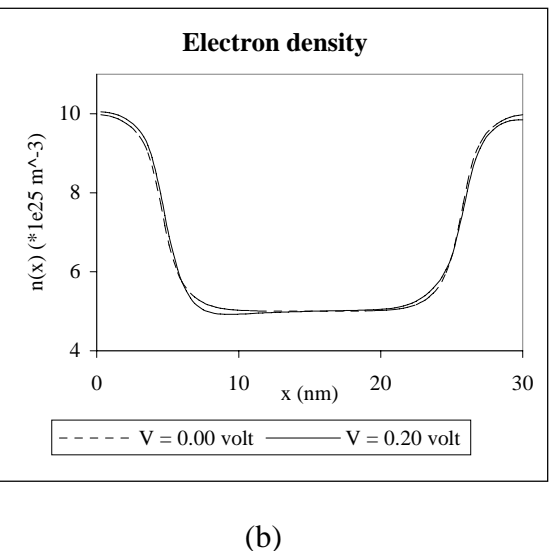
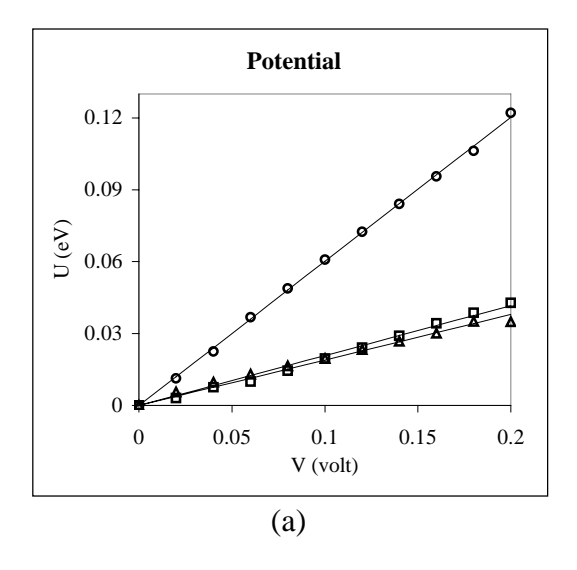


Figure 2 Calculated profiles of (a) potential and (b) electron density at applied voltage of 0.20 V (solid line) and equilibrium case (dash line) in the n^{++} - n^{+} - n^{++} nanostructure. The Fermi energy levels (μ_1 and μ_2) are displayed at the left and right side in the potential profile.



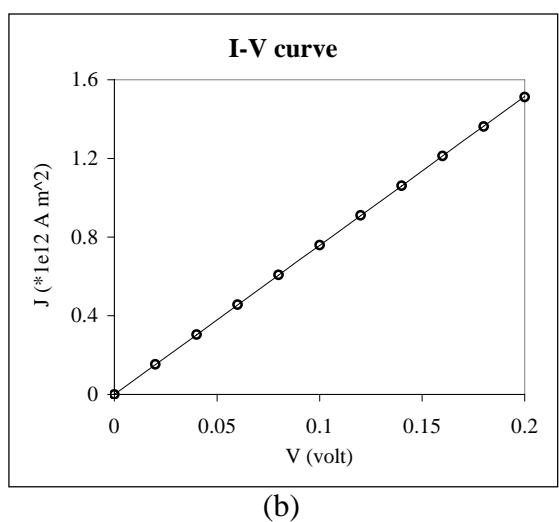


Figure 3 Calculated values of (a) relative potential drop on the left (square) and right (triangle) contacts and potential difference (circle) and (b) current density as a function of applied voltage. The solid lines are drawn by linear least square fit.







Conclusions

In this paper the NEGF formalism was employed to simulate the transport properties of a one-dimensional n^{++} - n^{+} - n^{++} ballistic resistor to corporate the quantum transport that arise in the simulation of this nanoscale device. The self-consistent potential profile inside the structure tends to flat in the interior layer, indicating that the voltage drop is primarily at the interface. A significant fraction of the voltage is dropped at both contacts and can be associated with the contact resistance [3, 4].

This computing procedure for self-consistent solutions of NEGF and Poisson equation should be able to capture the essential physics of quantum transport in some other nano-structure for example nanotube and molecular wire. However, the scattering process may occur in the device and leads to the non-coherent transport. The quantum transport including the scattering can be evaluated by adding self-energy terms inside the device and further development will be conducted.

References

- [1] Bout, F. A. 1993. Mesoscopic physics and nanoelectronics: nanoscience and nanotechnology. Phys. Rep. 234, no. 2&3. 73.
- [2] Danielewicz, P. 1984. *Quantum theory of nonequilibrium process*. I. Ann. Phys. 152, 239.
- [3] Datta, S. 1995. *Electronic Transport in Mesoscopic Systems*. Cambridge University Press.U.K.
- [4] Imry, Y. 1997. *Introduction to Mesoscopic Physics*. Oxford University press, Inc. New.

The Geometry and Electronic Structure of Nanotubes and their Application as Charge Storage and Transport Devices

Anurak Udomvech

Graduate Student at Department of Physics, Faculty of Science, Mahidol University, Rama 6 Road, Bangkok 10400 Thailand g4137694@student.mahidol.ac.th

Teerakiat Kerdcharoen¹, Vudhichai Parasuk² and Yuthana Tantirungrotechai³

¹Department of Physics, Faculty of Science, Mahidol University

²Department of Chemistry, Faculty of Science, Chulalongkorn University

³Department of Chemistry, Faculty of Science, Mahidol University

Abstract

Carbon nanotubes are seamlessly rolled single shells of graphene sheet, only a few nanometer across. This research focuses on single-wall carbon nanotubes (SWNTs) that have a zigzag shape. Geometry and electronic structure of open- and closed-ended (9,0) zigzag nanotubes were studied. The consequence of geometrical stability, the HOMO-LUMO gaps and charge distribution on the SWNTs were investigated using several ab-initio and semiempirical quantum computational techniques. It was found that geometry of SWNTs is effected by how the tube ends is capped. The characteristic transition of a zero-dimension (0-D) to that characteristic of a delocalized one-dimensional (1-D) for geometry takes place when the length of the tube increases up to 40 Å. Calculation shows that the electronic charge density accumulated at the two-end cap of closed SWNTs.

1. Introduction

A cylindrical carbon nanotubes, so called "buckytube", are chosen as a nanostructured system being investigated. The nanotubes structure proceeds its strength from the carbon-carbon bonds. The carbon atoms are bonded in hexagonal arrays as a graphene sheet. Nanotubes derive unique properties from their dimension and topology. A single-wall nanotube (SWNT) can be considered as resulting from rolling up a single shell of graphite to cylindrical form. The tube's orientation is denoted by a roll-up a chiral vector:

$$C = na + mb \equiv (n, m)$$

where a and b are the unit vectors of the hexagonal arrays and n and m are integers.² These orientation can bulid three type of SWNTs, are armchair, zigzag and chiral nanotubes respectively.

Zigzag nanotubes are formed when either n or m are zero and the chiral angle is 0° . Armchair nanotubes are formed when n=m and the chiral angle is 30° . All other nanotubes, with chiral angles intermediate between 0° to 30° , are known as chiral nanotubes. The theoritical prediction, the (n,0) zigzag tubes are expected to be metallic by n/3 is an integer and semiconducting otherwise. While the resulting of the (n,m) tubes are chiral, are expected to be metallic if (2n+m)/3 is an integer. Otherwise, they are semiconductors. But all the armchair tubes are metallic. The theory predicts that individual SWNT can considered as a

quantum wires. The prediction assume nanotubes as a semi-infinitely long tube that corresponding with STM studied electronic structure of nanotubes several microns in length. Then, it's very nessecities to study a confinement behaviour in finite long tubes. The electronic structure of finite length armchair nanotube has been studied. The additional confinement of the electrons along the tube axis leads to the opening of a band-gap in short armchair tubes. Moreover, when the tube length increase they found the transition from 0-D structure (quantum dot) to 1-D structure (quantum wire). Even so the zigzag tube have not studied. Because of it can be both the metallic and semiconductor and geometrical differ clearly from armchair tube. Currently, little is known about the effect of finite length on the properties of (n,0) zigzag tube. Understanding quantum size effect in carbon nanotubes is essential in device application of nanoelectronic devices.

We determined geomerty and electronic structure calculation on different-length (9,0) zigzag nanotubes that have open-end and closed-end by one-half bucky ball. The quantum chemical calculation are used to learn about HOMO-LUMO energy level and energy gap as function of the length of the tube unit cell and charge distribution on nanotube. Resulting found that geometry of SWNTs is effected by how the tube ends is capped. The characteristic transition of a zero-dimension (0-D) to that characteristic of a delocalized one-dimensional (1-D) for geometry takes place when the length of the tube increases up to 40 Å. Calculation shows that the electronic charge density accumulated at the two-end cap of closed SWNTs.

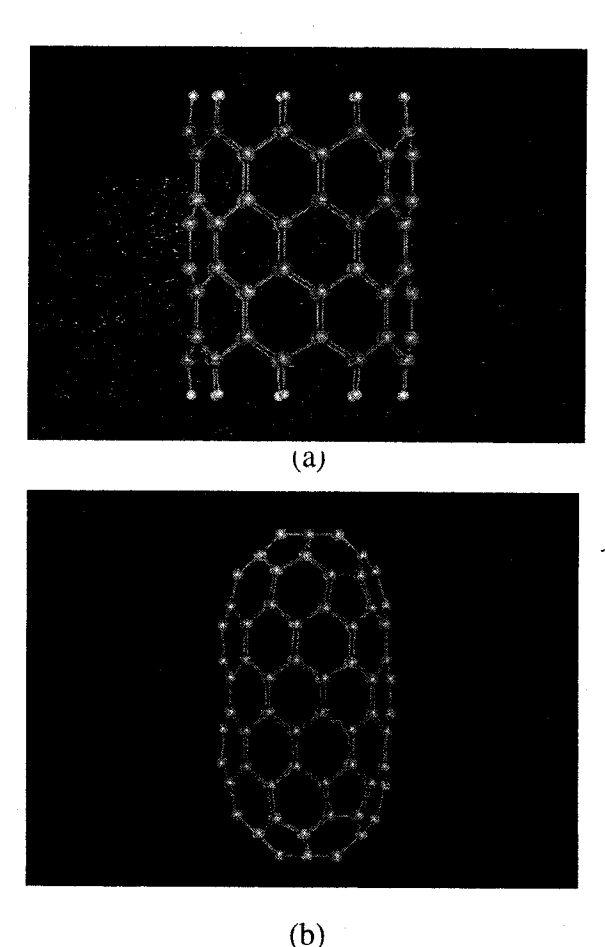


Fig.1. The initial geometry structures of (9,0) zigzag shape SWNTs with Molecular Mechanic calculation. (a) (9,0) open-end shape with 2-unit cells. (b) (9,0) closed-end or fullerene capped.

2. Computational Details

In order to study the geometry and electronic structure of nanoscale systems, we needed useful quantum chemical calculations⁹, molecular modeling¹⁰ and computational nanotechnolgy¹¹ to be solved. Molecular mechanics, that have perform the calculation by employing the HyperChem 6.0 package, is used to generated all primary tubes fixed diameter with increase nanotubes length along the tubes axis. (9,0) zigzag tubes are generated (Fig.1), we denoted the increasing length of tubes by adding various cyclacene to increase length along the tube axis. We have been considered theoritically by performing the semiempirical AM1 (Austin Model)⁹⁻¹⁰ to obtain geometrical stability and electronic behaviour of zigzag tubes. In the study the (9,0) zigzag sigle-wall open- and closed-end models are investigated. The first principle calculation (Hartree-Fock: HF)⁹⁻¹⁰ and Density Functional approximation (DFT) are useful applied to be comparison the difference of the resulting of another level of theory. In the Hartree-Fock and semiempirical calculation, we employed a GAMESS program in which 6-31G* basis set and by Gaussian 98 program¹² are performed HF in which ECP basis set and DFT/B3LYP functional which ECP basis.

All calculations were performed by optimizing the initial open- and closed-capped structures in which open-capped mean that the both end-sides are added hydrogen atoms for close shell system. Closed-end are capped both sides with one-half of fullerene C_{60} . The diameter was fixed at ~0.7 nm and vary the length along tubes axis to ~40 Å. The energy gap was obtained as the difference between the HOMO and LUMO energies, while the fermi energy ($E_F = 0 \text{ eV}$) was taken as the mean energy between HOMO and LUMO.

3. Results and Discussion

To evaluate the influence of finite length on the geometrical and electronical properties of the zigzag shape nanotubes, we optimized to test the quality of the geometry structure and electronic structure of a cyclacene (Fig.2). The result is demonstrated in Table 1. Semipmpirical method are shown in which the geometry and electronic structure of nanotubes satisfied when compared with first principle (HF) method. Thus the different-length of (9,0) nanotubes are calculated by semiempirical method that sufficiently optimization several atoms on SWNTs. The calculations shown the optimization all structures that achieved to a length ~40-~45 Å or about 10-unit cells as show in table 2. The Table 2 and 3 shown the differene bond lengths between structures open- and closed-end by quantum calculation (AM1) and molecular mechanic (MM2). We found that the middle cyclacene-rings and leftright end-rings are completely converged the bond length by 4-unit cells. The comparison of molecular machanical model with semiempirical model demonstrate explicitly different-bond length value. Molecular mechanic, shown crude result between capped and uncapped structure, demonstrated bond lengths as well. Semiempirical displayed different-bond value of open- and closed-end structures. Therefore closed-end are capped with one-half fullerene but open-end are added by hydrogen atoms. The left-right end-rings in Table 3, the MM2 calculation shown bond structure to be similar to middle-ring, while the AM1 calculation demonstrated unlikely bond values both uncapped and capped structure when compare by middle-ring. The calculation from MM2 displayed all structure of nanotubes have been bond values as well, but AM1 shown the structrues that each unit cell have differentiate bond values.

The electronic structure calculation are performed by AM1-RHF type semiempirical

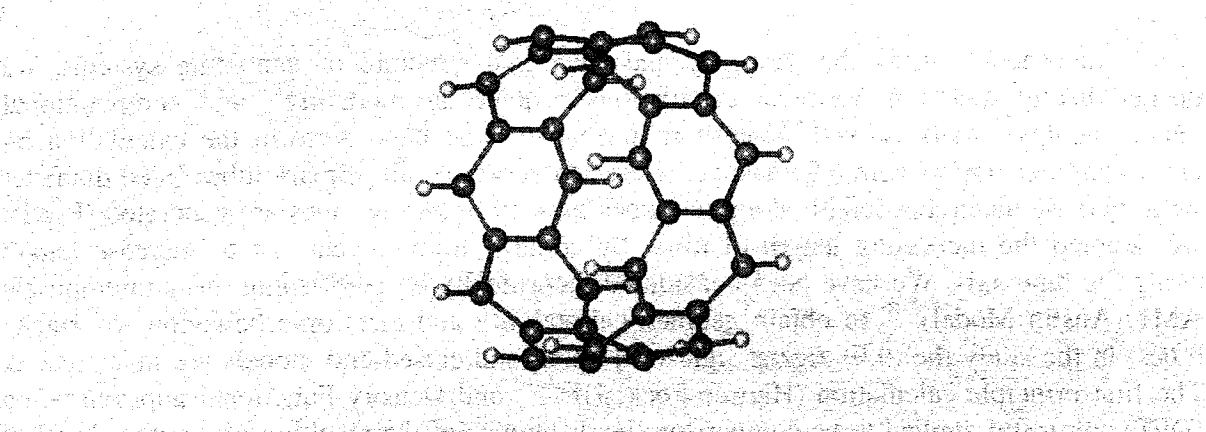
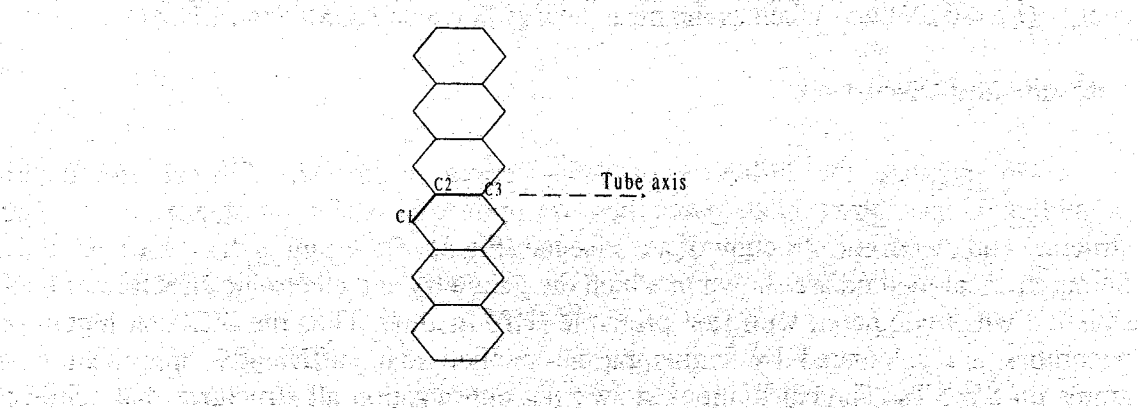


Fig.2. Show the cyclacene structure of (9,0) zigzag shape generated by Molecular Mechanics

Third that whe

Table 1. Testing quality of level of theory with Geometry and electronic structure of (9,0) zigzag shape 1-unit cell (cyclacene)

a) Comparison of the average bond length of (9,0) zigzag shape that defined



Bond MM2	AM1 HF/6-	31G* HF/CEI	2-31G B3LYP/6-	31G* B3LYP/CEP-31G
C_1 - C_2 1.402 Å	1.408 Å 1.40	3 Å 1.422	! Å 1.410	Å 1.436 Å
C_2 - C_3 1.399 Å	1.452 Å1.46	2 Å 1.477	'Å 1.470	열맞고 말리다는 아이들이 가장 독자 생산이다. 이 사람은 가지 않면서 가지 하는 것은 이 글로만 연하는데 그 모든 그는데

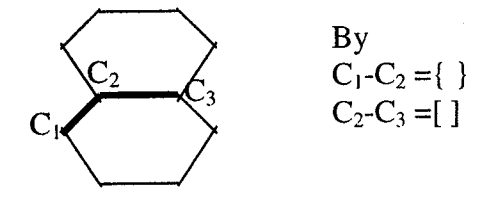
b) Mulliken population, HOMO-LUMO energy level and energy gap (AE)

. Water Laboration	AM1	HF/6-31G*	HF/CEP-31G	B3LYP/6-31G*	B3LYP/CEP-31G
C ₁ (a.u.)	-0.103	-0.167	-0.348	-0.252	-0.499
C ₂ (a.u.)	-0.035	-0.033	0.0797	0.121	- 0.194
HOMO (eV)	-6.820	-4.8082	-4.8344	-3.9228	-4:1977
LUMO (eV)	-2.117	-0.1632	-0.6580	-2.7905	-3.0999 *
ΔE (eV)	4.703	4.6450	4.1764	1.1323	1.0978

parties from the first first factor and the first factor of the fi

nara d<u>alaka 10. katika k</u>ati anara sala wiki dalah katika katika katika katika katika katika dalah katika kati

Table 2 comparison of geometry's closed- and opened-end with change numbers of unit cell located middle cyclacene ring. By AM1//AM1 method



Unit	Opened-end		Closed-end	
Cells	MM2	AM1	MM2	AM1
2	{1.407}	{1.420}	{1.422}	{1.432}
,	[1.400]	[1.431]	[1.399]	[1.421]
4	{1.399}	{1.425}	{1.399}	{1.428}
	[1.397]	[1.426]	[1.397]	[1.420]
6	{1.399}	{1.425}	{1.399}	{1.428}
	[1.397]	[1.425]	[1.397]	[1.420]
8	{1.399}	{1.425}	{1.399}	{1.428}
	[1.397]	[1.425]	[1.398]	[1.420]
10	{1.399}	{1.425}	{1.400}	{1.428}
	[1.397]	[1.425]	[1.398]	[1.420]

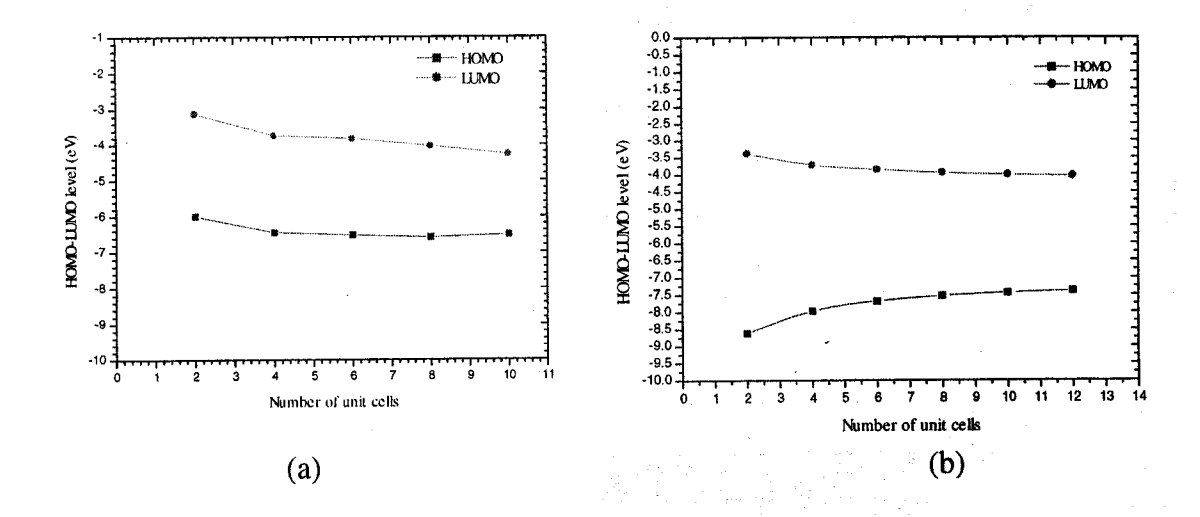


Fig.3 Demonstrate the variation of the HOMO-LUMO levels of a (9,0) nanotubes as function of its number of unit cells (a) open-end structures and (b) closed-end structures.

Table 3. comparison of geometry's closed- and opened-end with change numbers of unit cell at the end-rings (left and right). By AMI//AMI method

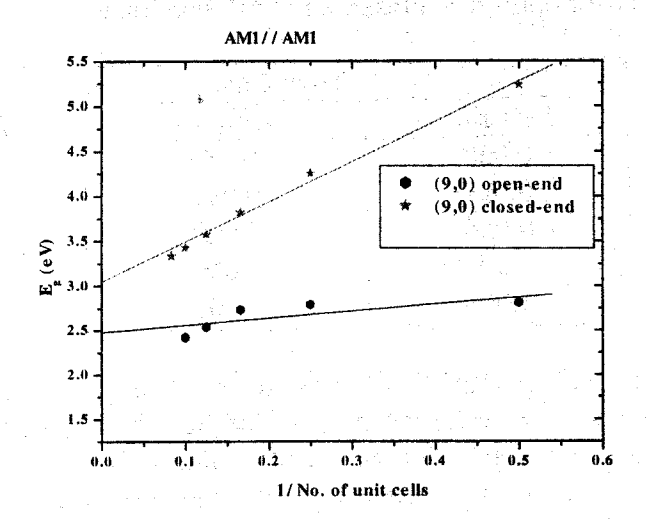


Fig.4 Show the variation of energy gap of (9,0) nanotube compare by inversion of a number of unit cells.

molecular orbital calculations. We found the electronic structure of a variation length along a tube axis of (9,0) nanotubes are convergence pattern, as Figure 3 shows. The Fig. 3a is openend (9,0) nanotubes shape that demonstrated HOMO-LUMO energy of a variation unit cells along tube axis. The energy reveled the HOMO-LUMO state of nanotubes are slowly narrowed parallel. The convergence scheme are pattern of exopential both HOMO and LUMO. The Fig. 3b shown HOMO-LUMO level of closed-end structure by vary unit cells as well open-end structures. We found the HOMO level as exponentially inversion with openend structures, but LUMO level is as well. This result, we can predict the transition of a zero-dimension (0-D) to that characteristic of a delocalized one-dimensional (1-D) for geometry takes place when the length of the tube increases up. We found that the energy gap, E_g , of the both shapes should concentrated to constant value for infinite-long length structure, as Figure 4 shows.

Table 3 a) Total charge density for optimized open-end (9,0) nanotubes

No. CNTs	Total Charge density			
unit cells	Left-ring	middle-ring	Right-ring	
2	-1.268	-0.234	-1.268	
4	-1.220	-0.055	-1.222	
6	-1.211	-0.036	-1.211	
8	-1.205	-0.025	-1.206	
10	-1.201	-0.020	-1.201	

b) Total charge density for optimized closed-end (9,0) nanotubes

No. CNTs			
unit cells	Left-ring	middle-ring	Right-ring
2	0.030	0.084	0.030
4	0.021	0.032	0.021
6	0.006	0.020	0.006
8	0.006	0.006	0.006
10	0.006	0.006	0.006

The electronic total charge distribution on nanotubes are also considered, as the average charge located middle-cyclacene ring, including left- and rigth-end ring. There are demonstrated by open-end negative charge density while closed-end are positive charge, as shown Table 3. We found each ring decreasingly accumulated charge density when including unit cells length. Otherwise, the capped of closed-end shape are accumulated charge density negatively, we can predicted the one-half of fullerene, as capped, have like to accumulate charge density more than all cyclacene tubes.

References

- [1] S. Iijima, *Nature* **354**, 56 (1991).
- [2] M. S. Dresselhuas, G. Dresselhuas, and P. C. Eklund, Science of Fullerene and Carbon Nanotubes (Academic Press, San Diego, CA 1996.)
- [3] P. M. Ajayan, S. Iijima, and T. Ichihashi, Phys. Rev. B 47, 6859 (1993).
- [4] S. J. Tans, M. H. Devoret, H. Dai, A. Thess, R. E. Smalley, L. J. Geerling, and C. Dekker, Nature 386, 474 (1997).
- [5] T. Ando, Semicond. Sci. Technol. 15, R13-R17 (2000).
- [6] J. W. G. Wildöer, L. C. Venema, A. G. Rinzler, R. E. Smalley, and C. Dekker, *Nature* 59, 391 (1998).
- [7] T. W. Odom, J.-L. Huang, P. Kim, and C. M. Lieber, *Nature* 62, 391 (1998).
- [8] A. Rochefort, D. R. Salahub, and P. Avouris, J. Phys. Chem. B 103, 641-646 (1999).
- [9] P. W. Atkin, Molecular Quantum Mechanics
- [10] A. R. Leach, Molcular Modelling: Principles and applications (Addison Wesley Longman Limited., England, 1996.)
- [11] K. Eric Drexler, Nanosystems: Molecular Machinery, Manufacturing and Computation (John Wiley & Sons Inc., New York, 1992).
- [12] A. Frisch, M. J. Frisch, Gaussian 98 User's Reference (Gaussian Inc., Pittsburgh, USA.).

The equilibrium distance, the zero-point frequency of the ground state structure, and the electronic structure of Fe₂

Viwat Vchirawongkwin and Vudhichai Parasuk
Department of Chemistry, Faculty of Science, Chulalongkorn University
Phyathai Rd., Patumwan, Bangkok 10330, Thailand.
yods@atc.atccu.chula.ac.th

Abstract

The ground state of Fe₂ molecule ($^7\Delta_u$) was calculated using multiconfiguration self-consistent-field (MCSCF) and multireference configuration interaction (MRCI) methods with various basis sets. The equilibrium nuclear distance (R_e) of 4.27 and 4.14 Bohr and the zero-point frequency (ω_e) of 212.0 and 309.7 cm^{-1} were obtained at MRCI level with ANO's [17s12p9d4f]/(4s3p2d1f) and [17s12p9d]/(8s7p7d) basis, compared to the experimental value of 3.53 - 3.82 Bohr for R_e and 299.6 cm^{-1} for ω_e . The f functions seems to weaken the bond in Fe_2 . Furthermore, adding the Davidson's correction (Q) to the CI energy, the calculated bond distance is shorten to 4.01 Bohr for [17s12p9d4f]/(4s3p2d1f) basis and 3.99 Bohr for [17s12p9d]/(8s7p7d) basis while increasing the ω_e to 324.5 and 406.6 cm^{-1} for both basis respectively. This implies the considerable error caused by the lack of size-extensivity of the CI method to the bond distance. For the electronic structure, our calculations yielded the natural occupations of $3d^{7.5}4s^{0.5}$ which is different from the previous study of $3d^74s^1$ (Tomonari's).

1. Introduction

The interesting property of transition metal dimers is the equlibrium nuclear distance, since it is shorter than the internuclear distance between the nearest neighbors in the corresponding metal. In solid Fe metal, the internuclear distance is 4.69 Bohr [1]. For Fe₂ dimer, the nuclear distance (R_e) was found to be 3.54 Bohr in argon matrix [2] and 3.82 Bohr in neon matrix [3]. The isomer shift of Mössbauer spectroscopy [4, 5, 6] indicates a smaller number of 4s electrons, $4s^{2-x}$, and larger number of 3d electron, $3d^{6+x}$ in Fe₂, as compared to $3d^64s^2$ in Fe. The resonance Raman spectrum shows a fundamental frequency for ground state of 299.6 cm^{-1} [4, 7].

The smaller 4s population of Fe₂ was discovered by Shim and Gingerich [8]. They performed ab initio SCF and configuration interaction (CI) calculations and reported the R_e of 4.54 Bohr which is too long and $^7\Delta_u$ state for the ground state. Later, Harris and Jones [9] using DFT and LSD approximation found the shorter R_e of 3.97 Bohr and the ground state is $^7\Delta_u$. Tomonari and Tatewaki [10] using SCF and CI calculations gave the best R_e result of 3.82 Bohr which agrees within experimental error. All previous calculations suggested that the Fe-Fe bond is dominated by electrons in 4s orbital. Because there exists many low-lying electronic states for Fe₂ dimer, using a single-determinantal method might not be suitable for describing the electronic state of Fe₂ system. Here, the multiconfiguration self-consistent field (MCSCF) method together with multi-reference configuration interaction (MRCI) were suggested to investigate the electronic ground state, R_e ,

QUANTUM TRANSPORT THROUGH SINGLE MOLECULE WITH N-ELECTRON MODEL

A. Chantasri*, T. Osotchan
Center of Nanoscience and Nanotechnology,
Physics Department, Faculty of Science, Mahidol University, Bangkok
and National Nanotechnology Center, Thailand Science Park, Pathumthani

Abstract

Calculation of current flow through a single molecule in three-terminal field effect transistor device was expanded from two-electron transport to N-electron picture. For self-consistent method the number of electron in the iterative procedure was modified and the current can be derived by non-equilibrium Green's function formalism. This current-voltage result was compared with that using master equation. The number of electron states in the channel was increased to 2^N states and then the current was calculated by the probability rate between these states. With two approaches, the current-voltage curves have small difference when the level-splitting energy is less than 0.05 eV. In addition, the higher splitting energy causes explicitly N steps in the current-voltage curves obtained by the master equation. Moreover, the relative energy level with respective to the electrode Fermi energy determines the threshold voltage of saturate current. The fraction of gate voltage is also shifted this relative energy levels and gains the similar feature of the drain current. The saturate current calculated by both techniques exhibit the same values as a result of the equal probability for all state-transitions.

Keyword: Quantum transport, Molecular conduction, Self-consistent method, Master equation, I-V characteristics

1. INTRODUCTION

Currently there are many studies on the conduction of single molecule not only to understand the system in atomic level, but also to implement future device unctionalities. Since 30 years ago, the experimental efforts have been improved in techniques of measuring current-voltage characteristics of molecules [1-3]. The images of single molecule can be investigated by scanning tunneling microscope including that for organic molecule on a metal contact [4-5]. The current-voltage of metal-molecule(s)-metal junction was measured by different techniques, such as mechanically controllable break junction [6], contact to self-assembled monolayers [7-9] and molecule-bridged gold nanoparticle dimmers [10].

There are a number of theoretical approaches to describe these measured I-V characteristics [11-12]. The fundamental theorem is normaly base on quantum mechanics or statistical mechanics. The system can be described by the molecule coupled with the metal contacts. The metal performs as a reservoir of electrons for passing through molecular states. Thus, electron transport through molecule can be prospected as the open systems which described by non-equilibrium Green's function (NEGF) in term of

density of state (DOS) [13-17]. Furthermore, the other effort is to model molecular conduction with weakly coupled molecules by using the probabilities at different discrete states [18-19]. The results of these calculations exhibited the step feature in I-V curve [18, 20, 21].

In this work, there are two approaches used in calculation of I-V characteristics for single molecule in device with three terminal contacts. The first method is base on self-consistent procedure for finding the self-consistent potential with NEGF formalism [22-23]. The channel (molecule) potential is modified by the density of electron in the molecule and also relatively adjusted by gate voltage. Moreover, the other technique is used master equation to calculate in term of probability between energy states and extended this model to multielectron case [24-26]. The current is derived by a rate constant of electron comes in and out together with the probabilities of such states.

2. CALCULATION DETAIL

2.1 Self-consistent method with NEGF

General formalism of NEGFF normally used in molecular conduction [27] can be generated by

[.]

molecular Hamiltonian matrix together with the selfenergy matrices. These self-energy matrices are derived from the coupling between source and drain contacts. Actually in one-energy level molecule, the matrix formulas can be simplified by pure constant.

The coupling between the molecule energy level \mathcal{E} and metal contacts can cause the broadening of energy level. Broadening factor is defined the sum of the strength of coupling parameters of source (γ_1) and drain (γ_2) contacts as $\gamma = \gamma_1 + \gamma_2$. In this work, the symmetry contacts are assumed thus $\gamma_1 = \gamma_2$. The DOS for the single broaden level can be written as

$$D(E-\varepsilon) = \frac{\gamma/2\pi}{(E-\varepsilon)^2 + (\gamma/2)^2}.$$

The electron density at energy E in middle channel can be calculated from the product of DOS and Fermi functions of incoming electron from the source and outgoing electron to the drain contacts. Thus the total electron density can be calculated by

$$n = \int\limits_{-\infty}^{\infty} dE \cdot D_{\varepsilon}(E-U) \frac{\gamma_1 f_1(E) + \gamma_2 f_2(E)}{\gamma_1 + \gamma_2} \, ,$$

where U is the relative potential of the molecule. The applied voltage across drain and source adjusts this relative potential. In addition the applied gate voltage is shifted this potential with the factor evaluated from the capacitance of each terminal.

This relative potential has to be modified after new electron density obtained according to Possion equation. Thus the electron density is calculated iteratively with the Possion equation until the self consistently potential can be achieved.

In this approach, the electron transport for N-electron model can be approximated by considering them independent with equal DOS but the effect of potential on the increase of the number of electron is taken into account. Therefore the current can be approximated by the N times of one-electron current.

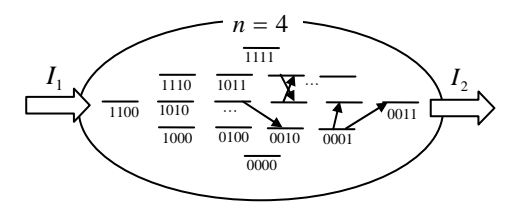


Fig. 1. Diagram of current through the N-electron single molecule with an example of N=4. All possible states are $2^N=16$ with five energy levels according to the number of electron occupying in that state. Six states at the neural level are placed in the middle with $N_0=2$ and x=0. The x=1 and x=2 are the case of number of occupied electron $N_1=3$ (1110, 1011, ...) and $N_2=4$ (1111), respectively. The arrows present a possible adding and removing electron from that state.

2.2 Master equation

The electron current through single molecule can be resolved under consideration of the discrete electron states. The energy levels of multielectron states depend on the electron configuration in that state. The state in the configuration with equal number has the same energy level while the configuration state with large number of electron has higher energy level.

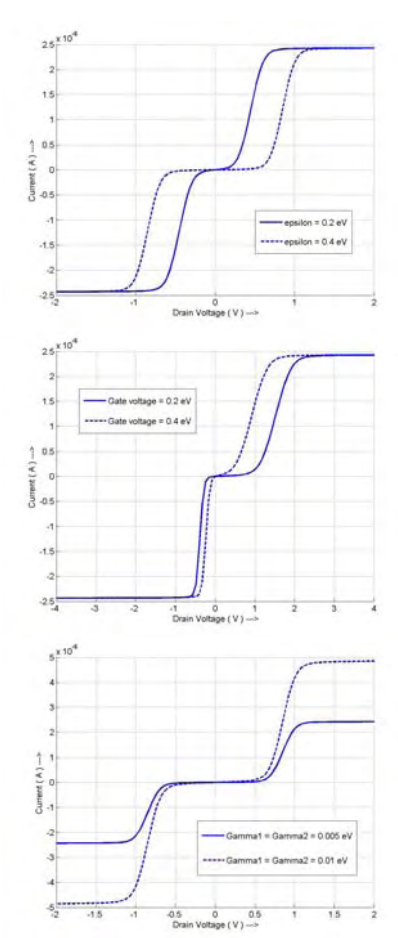


Fig. 2. Calculated drain current as a function of applied drain voltage by SCF technique for N-electron model with N=4 with relative energy of a) 0.2 and 0.4 eV, applied gate voltage of b) 0.2 and 0.4 eV and broadening value of c) 0.005 and 0.01 eV.

For N electron model, the number of all possible configuration state equals 2^N states. The energy levels of these configuration states are separated into N+1 levels. For even number of N, the number of occupied electron in the neural state corresponds to the one half of N and defined as N_0 . In two degenerate states with spin up and down and either be filled or empty, the electron-electron interaction energy for a collection of N electrons can be described by the proportional to the number of distinct pairs as

$$U_{ee}(N) = U_0 \binom{N}{2} = \frac{U_0 N(N-1)}{2},$$

where U_0 is the interaction energy per pair. The corresponding one-electron level can be defined by the bare energy ($\widetilde{\mathcal{E}}$) plus the self-consistent potential:

$$\varepsilon = \widetilde{\varepsilon} + \left[\frac{\partial U_{ee}}{\partial N}\right]_{N=N_0} = \widetilde{\varepsilon} + \left(U_0 N_0 - \frac{U_0}{2}\right).$$

After the neural state of N-electron level defined, the higher energy state level can be determined by considering the affinity potential. The affinity potential can be derived from the interaction energy difference between the case of number of occupied electron equal $N_x\!+\!1$ and that for N_x by

$$\begin{split} \boldsymbol{U}_{Affinity} &= \boldsymbol{U}_{ee}(\boldsymbol{N}_x + 1) - \boldsymbol{U}_{ee}(\boldsymbol{N}_x) \\ &= \boldsymbol{U}_0 \boldsymbol{N}_x \end{split}$$

Thus, energy difference for the next higher state can be written as

$$\begin{split} E_{xf} - E_{xi} &= \widetilde{\varepsilon} + U_{Affinity} \\ &= \varepsilon + \frac{U_0}{2} + U_0 (N_x - N_0) \\ &= \varepsilon + \frac{U_0}{2} + U_0 x \end{split}$$

Where the index x is used for defining the energy levels relative to the neural level by -N/2, -N/2+1, ..., -1, 0, 1, ..., N/2 as shown for example case of 4-electron model in Fig. 1.

In the case of determine the lower energy state, the ionization energy can be derived by the interaction energy difference between the case of number of occupied electron equal N_x and that for N_x -1 by

$$U_{lonization} = U_{ee}(N_x) - U_{ee}(N_x - 1)$$
$$= U_0(N_x - 1)$$

So, the energy different for lower energy level can be written as

$$E_{xf} - E_{xi} = -\tilde{\varepsilon} - U_{Ionization} = -\varepsilon + \frac{U_0}{2} - U_0 x$$

The rate of change for occupation probability of the given multielectron state can be determined by the probability rate of in coming to this state and the rate of out going from those states. Each probability can be solved using the rate-equation by treating the probability for each N-electron state as an independent variable. The time evolution of the probability of arbitrary state is given by master equation

$$\frac{dP_{\alpha}}{dt} = \sum_{\beta} R_{\beta \to \alpha} P_{\beta} - R_{\alpha \to \beta} P_{\alpha}$$

where the rate constant R can be derived by the coupling constant and the electron occupation for that energy state with Fermi function. The rate constant of incoming electron is accounted for occupied state of Fermi function while the outgoing rate is defined for vacant states.

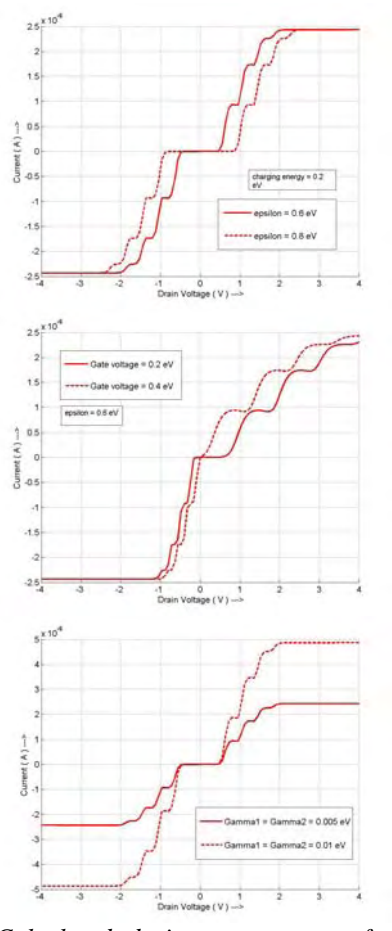


Fig. 3. Calculated drain current as a function of applied drain voltage by master equation for N-electron model with N=4 with relative energy of a) 0.2 and 0.4 eV, applied gate voltage of b) 0.2 and 0.4 eV and broadening value of c) 0.005 and 0.01 eV.

In steady-state system, the evolution rate of the occupation probability of state equals zero. The exact value of N-electron state probabilities can be solved by using linear algebra to these 2^N system equations. The trivial solution can be defined with constrain of the total summation of all probabilities equal one. For steady-state, the tunneling current through the left source equals to that to the right drain contact and the contribute current from only one side (source) can be evaluated by the summation of all N-electron state probability rates as

$$I_1 = e \sum_{\alpha,\beta} (\pm) \gamma_{\alpha \to \beta}^{source} P_{\alpha}$$
.

3. RESULT AND DISCUSSION

The conduction of single molecule can be illustrated by calculated I-V characteristics of single molecule device between two metal electrodes as a source and drain with varying the controlled gate voltage. For each drain voltage bias, the current was calculated by self-consistent method with NEGF formalism. At low applied voltage, the energy level is relatively far from Fermi levels of the metal contact therefore in energy space there is only small intercept part of DOS and Fermi distribution. This leads to small current and the current increases as the bias voltage increases due to the shift of relative energy level as indicated in Fig. 2. The current rapidly increases at the applied voltage in which Fermi level aligns close to energy level of the molecule. At higher than this threshold voltage, the current becomes saturated due to the energy level lies above Fermi level.

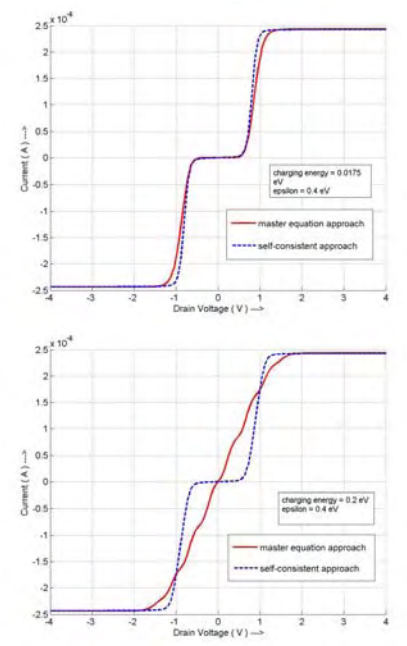


Fig. 4 Calculated drain current as a function of applied drain voltage by SCF and master equation for N-electron model with N=4 with relative energy of 0.4 eV and charging energy of 0.0175 eV and b) 0.2 eV.

The threshold voltage is strongly depend on the relative position of energy level to the Fermi level which determined by parameter ε. The higher ε gives the higher threshold voltage as shown in Fig. 2a. Actually this relative energy can also be modified by gate voltage with the factor derived from the capacitance on each terminal. The applied gate voltage makes the entire IV curve shift to higher voltage. This results in the asymmetric of IV curve as illustrated in Fig. 2b. The higher gate voltage also modifies the IV curve no equally for the forward and reverse bias cases.

The broadening parameters are used to determine the strength of coupling with two contacts and the higher broadening factor leads to higher saturated current as seen in Fig. 2c. This is due to high electron flow rate across the barrier between molecule and contact. Since the coupling factor is also determined the broadening of the energy level, the slope of the IV curve is slightly change.

The N-electron current was also calculated by the master equation and the calculated results for N=4 are

shown in Fig. 3. Since the sixteen energy levels for N=4 can have in five energy levels, the calculated IV curve present the four current steps for forward and reverse bias. By setting the pair interaction energy of 0.2 eV, the IV curve for relative energy level ϵ of 0.6 and 0.8 eV are compared in Fig. 3a. These result in the difference of the threshold voltage for the first step. For N-electron transport through the device, the theoretical result shows N current steps maximum and less number of steps can be observed in the case of large electron charging energy exceeding the value of energy level ϵ . The width of each step satisfies the splitting energy between the levels of electron state.

The gate voltage is modified the relative energy and provides the asymmetric IV curve as illustrated in Fig. 3b. This also affects the slope of IV step. While the coupling factor enhances the magnitude of calculated current as shown in Fig. 3c.

In order to compare the calculated result from two methods, the small pair interaction energy of 0.0175 eV (comparing to the relative energy level of 0.4 eV) was used to calculate the current from the master equation. This current as illustrated in Fig. 4 indicates no step like due to relative small charging energy and has about the same feature as that from the SCF calculation. The saturated current from both method exhibits the same value. However as the pair energy increases, the IV curve shows step like current and deviates form that calculated by SCF.

4. CONCLUSION

Two approaches including self-consistent procedure and master equation approach were used to calculate the current through the single molecule device with N-electron model. Both approaches provide the same maximum current but the latter approach presents the current steps in the I-V characteristics because of discrete electron states. However this step behavior is reduced as the pair interaction energy becomes relative small comparing to the difference between the energy level and Fermi level of contact.

The gate voltage can shift the energy level of the molecule and make an asymmetric IV characteristic. The coupling constant determines the broadening of the molecular level and the flow of current. So higher coupling constant leads to the higher saturated current. The threshold voltage is a result of the alignment of molecular energy level and Fermi level which derived by this relative energy level. The N-electron model can be extended by considering the variation of coupling strength to these multielelctron states.

5. ACKNOWLEDGMENT

The first authors would like to thank Department of Promotion Science and Technology for scholarship. This research work is partially support by National Nanotechnology Center

REFERENCES

- [1] R.P. Feynmann, Eng. Sci. 23 (1960) 22.
- [2] A. Aviram, M.A. Ratner, Chem. Phys. Lett. 29 (1974) 277.
- [3] J.K. Gimzewski, C. Joachim, Science 283 (1999) 1683.
- [4] M.A. Reed, Proc. IEEE. 87 4 (1999) 652.
- [5] W. Tian, S. Datta, S. Hong, R. Reifenberg, J. I. Henderson, and P. Kubiak, J. Chem. Phys. **109** (1998) 2874
- [6] C. Kergueris, J.-P. Bourgoin, S. Palacin, Phys. Rev. B, **59** 19 (1999) 12505.
- [7] M.A. Reed, C. Zhou, C.J. Muller, T.P. Burgin, J.M. Tour, Science **278** (1997) 252.
- [8] J. Chen, M.A. Reed, A.M. Rawlett, J.M. Tour, Science **286** (1999) 1550.
- [9] B. Xu, N.J. Tao, Science 301 (2003) 1221.
- [10] T. Dadosh, Y. Gordin, R. Krahne, I. Khirvrich, D. Mahalu, V. Frydman, J. Sperling, A. Yacoby, I. Bar-Joseph, Nature 436 (2005) 677
- [11] S. Datta, W. Tian, Phys. Rev. Lett. 79 13 (1997) 2530.
- [12] F. Zahid, A. W. Ghosh, M. Paulsson, E. Polizzi, S. Datta, Phys. Rev. B 70 (2004) 24537.
- [13] R. G. Endres, C. Y. Fong, L. H. Yang, G. Witte, Ch. Woll, Computational materials Science **29** (2004) 362.
- [14]Y. Wang, M. Lieberman, IEEE Transactions on Nanotechnology, **3** 3 (2004) 368.

- [15] J. Fransson, O. M. Bengone, J. A. Larsson, and J. C. Greer, IEEE Transactions on Nanotechnology, **5** 6 (2006) 745.
- [16] K. Hirose, N. Kobayashi, Journal of Physics: Conference Series 38 (2006) 65.
- [17] G. Speyer, R. Akis, D.K. Ferry, Superlattices and Microstructures **34** (2003) 429.
- [18] B.Muralidhatan, A. W. Ghosh, S. Datta, Phys. Rev. B **75** (2006) 155410
- [19] E. Bonet, M. M. Deshmukh, D. C. Ralph, Phys. Rev. B **65** (2002) 045317
- [20] J. Park, A. N. Pasupathy, J. I. Goldsmith, C. Chang, Y. Yaish, J. R. Petta, M. Rinkoski, J. P. Sethna, H. D. Abruna, P. L. McEuen, and D. C. Ralph, Nature London **417** (2002) 722.
- [21] C. J. Muller, J. M. Krans, T. N. Todorov, M. A. Reed, Phys. Rev. B **53** 3 (1996) 1022.
- [22] R. Venugopal, Z. Ren, S. Datta, M. S. Lundstrom, D. Jovanovic, J. Appl. Phys **92** 7 (2002) 3730.
- [23] M. Brandbyge, J. L. Mozos, P. Ordejo, J. Taylor, K. Stokbro1, Phys. Rev. B **65** (2002) 165401.
- [24] E. Bonet, M. M. Deshmukh, and D. C. Ralph, Phys. Rev. B **65** (2002) 045317.
- [25] M. H. Hettler, W. Wenzel, M. R. Wegewijs, H. Schoeller, Phys. Rev. Lett. 90 (2003) 076805.
- [26] J. M. Kinaret, Y. Meir, N. S. Wingreen, P. A. Lee, and X.-G. Wen, Phys. Rev. B **46** (1992) 4681.
- [27] S. Datta, "Quantum Transport: Atom to Transistor", Cambridge University Press, 2005.

การสืบค้นเชิงทฤษฎีของการบรรจุลิเธียมใอออน ลิเธียมอะตอมและกลุ่มของลิเธียมอะตอมเข้าไปในท่อนาโน คาร์บอน

THEORETICAL INVESTIGATION OF Li $^+$ /Li and Li CLUSTERS INSERTION INTO SINGLE-WALLED CARBON NANOTUBES

<u>อนุรักษ์ อุดมเวช</u>^{1,2}*, ธนากร โอสถจันทร์ 1,2 และ ธีรเกียรติ์ เกิดเจริญ 1,2

Anurak Udomvech^{1,2}, Tanakorn Osotchan^{1,2} and Teerakiat Kerdcharoen^{1,2}

¹Department of Physics, Faculty of Science, Mahidol University, Bangkok 10400, Thailand;

บทคัดย่อ: งานวิจัยนี้ใช้การคำนวณเชิงทฤษฎีด้วยคอมพิวเตอร์เพื่อจำลองแบบการเจือและยึดติดของไอออนและ อะตอมของลิเธียมบนพื้นผิว รวมถึงการเคลื่อนผ่านผนังและปลายเปิดของท่อนาโนคาร์บอน โดยใช้ระเบียบวิธีการ คำนวณทางกลศาสตร์ควอนตัม แบบจำลองแสดงพื้นผิวพลังงานศักย์ที่ไอออนและอะตอมของลิเธียมเคลื่อนผ่าน ผนังตามทิสทางภาคตัดขวางของท่อนาโนคาร์บอนเป็นผลให้สามารถใช้ท่อนาโนคาร์บอนเพิ่มขนาดความจุของ แบดเตอรี่แบบลิเธียมเนื่องจากลิเธียมไปยึดติดกับท่อนาโนคาร์บอนทั้งภายในและภายนอก สำหรับแบบจำลองของ การเคลื่อนผ่านสิเธียมมากกว่า 1 อะตอมผ่านปลายเปิดของท่อนาโนคาร์บอนแบบ(6,0) ที่มีไฮโดรเจนอะตอมยึดติด พบว่าไม่ปรากฏกำแพงศักย์ขวางการเคลื่อนผ่านลิเธียมอะตอมเข้าสู่ภายในท่อนาโนคาร์บอน และพบกำแพงศักย์ เล็กๆเมื่อเคลื่อนลิเธียมอะตอมภายในท่อนาโนคาร์บอนตามทิศทางของแนวแกนท่อซึ่งแสดงให้เห็นว่าลิเธียม อะตอมชอบอยู่ภายในท่อนาโนคาร์บอน แต่เมื่อลิเธียมอะตอมเคลื่อนผ่านเข้าไปในท่อนาโนคาร์บอน (9,0) ซึ่งมีเส้น ผ่านศูนย์กลางที่ใหญ่กว่าท่อนาโนคาร์บอน (6,0) พบว่าพลังงานศักย์ของลิเธียมอะตอมเคลื่อนภายในท่อนาโน กร์บอนตามทิศทางแนวแกนท่อแบบ(9.0) แตกต่างจากแบบ (6.0) อย่างชัดเจน

Abstract: Theoretical investigations on single-walled carbon nanotubes (SWNTs) have been performed using first-principles total energy calculations to explore feasibility of doping Li⁺/Li through the sidewall and open-end of nanotubes. The first model elucidates the potential energy surface between Li⁺/Li and SWNTs as function of distance along a cross section by inserting Li⁺/Li through the nanotube's sidewall. These investigations have revealed that Li⁺/Li@tube systems could enhance the capacity of lithium batteries by using both interiors and exteriors of nanotubes. Second model, the insertion of Li atoms pass through opening mount of (6,0) single-walled carbon nanotubes have shown no insertion barrier in which the tube's mouth is passivated by hydrogen. The diffusion barrier is small inside the nanotube and Li atoms prefer to reside along the tube axis. For the larger diameter tube, (9,0), it has shown different interaction characteristic if lithium is located at tube axis.

Methodology: In this study, the calculations have been carried out using the density functional formalism with a self-consistent manner. The insertion process is performed using a real-space cluster scheme with Becke's 3-parameter hybrid functional where the correlation functions is provided by the functional of Lee-Yang-Parr, which includes both local and non-local terms. We use a standard all-electron basis set of 6-31G to represent orbitals of C, H, and Li atoms and ion in all calculations. Spin-unrestricted wave functions are employed for different orbitals and spins. All of SWNT structures employed in this study are of the zigzag type with chiral vector (m,0). The study of Li⁺/Li inserted sidewall of SWNT using structure in which m = 6-12 and plotting the potential energy surface as a function of distance along the cross section. Penetration of Li⁺/Li through the nanotube sidewall has been done based on two trajectories: C2 for which the metal/ion penetrates through C-C bond and C6 where the metal/ion passes through the middle of the hexagon.

²Capability Building Center of Nanoscience and Nanotechnology, Faculty of Science, Mahidol University, Bangkok 10400, Thailand,

^{*}E-mail address: giganu@hotmail.com and g4636510@student.mahidol.ac.th

The SWNT in this study are finite-sized by varying unit-cell cylinder along the tube-axis and hydrogen atoms are used to cap the dangling carbon atoms at the two open-ends of the nanotube. The structures of nanotube have employed non-relaxing atomic coordinates, in order to save computational effort with point group symmetry. For Li clusters, the symmetry properties have also played in which D_{6h} and C_{2v} of (6,0) and (9,0) nanotubes, respectively. Penetration of Li atoms through the two open-ends of nanotube has been done in tube-axis trajectory. The binding energy profile of the system was defined by subtracting the total energy of the whole from the sum of the total energy of nanotube structures and the energies of the isolated Li atoms.

Results, Discussion and Conclusion: We have found that, for single Li⁺/Li insertion, the energy minimum locates at the center of small diameter (6,0) nanotube and PES of (7,0) nanotube is not clear whether it is double-well or flat. For (8,0) to (12,0), the barrier height inside tube has emerged clearly enough to identify the double-well PES. The adsorption of Li⁺/Li at C6 and C2 sites in the tube's interior differ only slightly, while preferential adsorption on C6 site gains more contrast for the exterior of the nanotube as depicted in Figure 1.

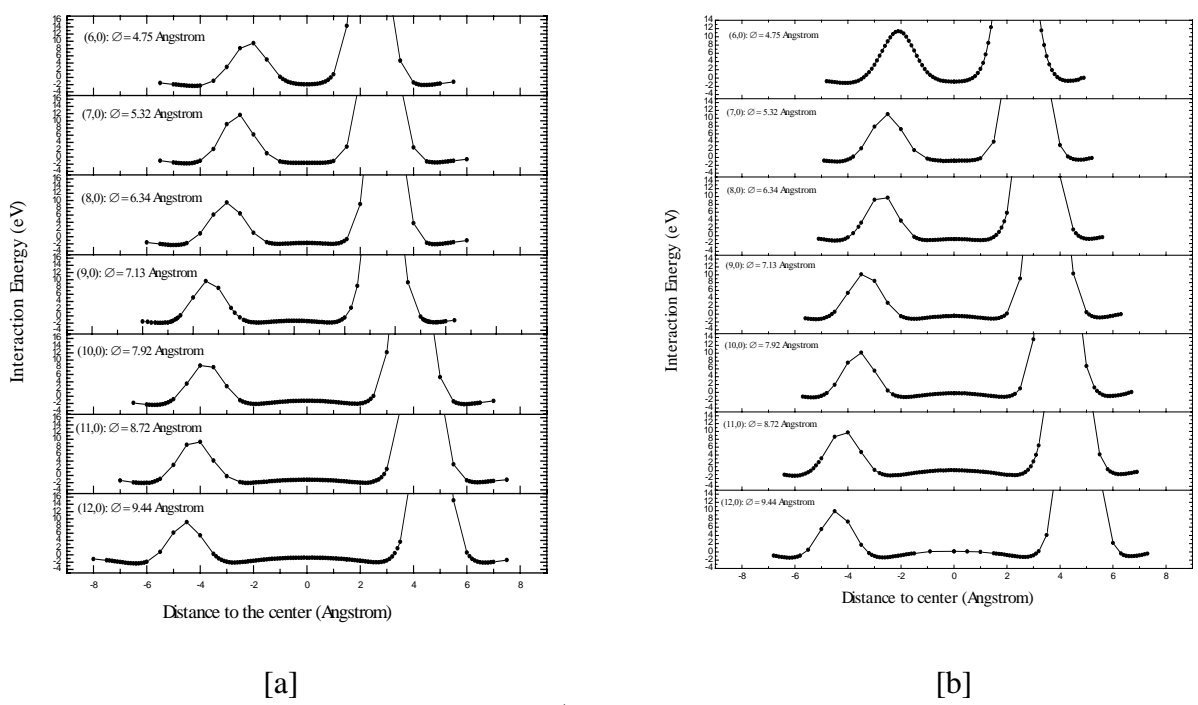
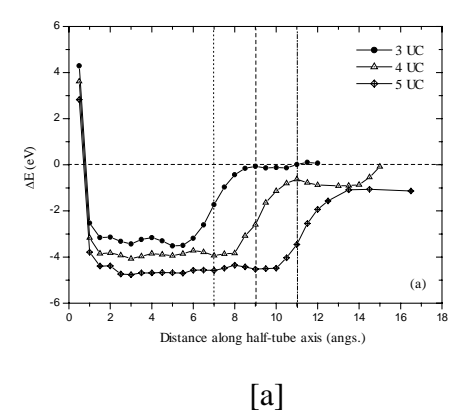


Figure 1. The potential energy surface of Li⁺/Li and zigzag SWNT, (m,0) in which m=6-12, as a function of distance along the cross section direction. [a] Li⁺@SWNT [b] Li@SWNT.

Single cylindrical potential well is formed along the internal sidewall, whereas a cluster of local minima covers the external sidewall and each minimum is separated from other minima by C2 sites. It could be visually elucidated that surface diffusion can easily take place along the internal wall, while being hindered for the external. SWNT doped by Li or Li⁺ can be expected that the atom or ions will localize on the hexagons along the nanotube's external wall, while freely moving along the sidewall for the inside. For rechargeable Li-ion battery, nanotubes can be made opened to allow intercalation of Li⁺/Li to migrate into and out of the tubes.

For more concentration, Li atoms prefer to locate at situations along the tube-axis in (6,0) nanotube but not in (9,0) as shown in Figure 2. The insertions of Li atoms to SWNT have no energy barrier when the open-mount is passivated by hydrogen atoms. The diffusion barrier is small inside the nanotube indicating that Li atoms prefer to reside along the tube axis. The Li atoms have lower energy inside the nanotube than outside the nanotubes. In larger diameter of nanotube, the interaction curve shows that Li atoms do not prefer to locate at the tube-axis direction.



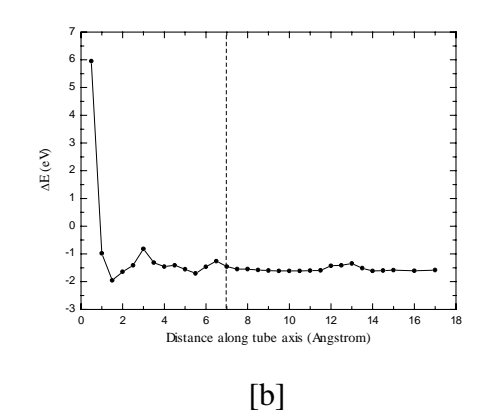


Figure 2. The binding energy as a function of the distance from the geometric center of the (6,0) and (9,0) SWNT of finite-size structures. [a] 2 Li atoms-(6,0) [b] 2 Li atoms-(9,0).

Acknowledgement: The author expresses gratitude to the Center of High Performance Computing, University of Utah and Capability Building Center for Nanoscience and Nanotechnology, Mahidol University for Computation.

References: [1] Becke A. D., J. Chem. Phys. **1993**, 98, 5648.

- [2] Lee C., Yang W., Parr R. G., Phys. Rev. B. 1998, 38, 785.
- [3] Miehlich B., Savin A., Stoll H., Preuss H., Chem. Phys. Lett. 1989, 157, 200.
- [4] Udomvech A., Osotchan T., Kerdcharoen T., unpublished.
- [5] Yang J., Liu H.J., Chan C.T., Phys. Rev. B. 2001, 64, 08542.
- [6] Liu H.J., Chan C.T., Solid State Com. 2003, 125, 77-82.
- [7] Agrawal B.K., Agrawal S., Srivastava R., J. Phys.: Condens. Matter **2004**, 16, 1467-1488.

Keywords: First-principle, Density functional theory, Single-walled carbon nanotube, Lithium insertion, Adsorption

เร็คติไฟร์จากโมเลกูล

Molecular rectifier

<u>อารีเฟ็น รัศมีศาสน์^{1,2}, ธนากร โอสถจันทร์^{1,2}, เติมศักดิ์ ศรีคิรินทร์¹,พัชรินทร์ ธรรมสิริอนันต์²</u>

<u>Areefen Rassamesard^{1,2}</u>, Tanakorn Osotchan^{1,2}, Toemsak Srikhirin¹, Phatcharin Thamasirianunt²

Department of Physics, Faculty of Science, Mahidol University, Bangkok 10400, Thailand

²Center of Nanoscience and Nanotechnology, Faculty of Science, Mahidol University, Bangkok 10400, Thailand

E-mail address:fenmu@hotmail.com

บทคัดย่อ: การเร็คติไฟร์ คือการที่ควบคุมกระแสไฟฟ้าให้ไหลผ่านแค่ทิศทางเคียว โดยทั่วไปแล้วอุปกรณ์เร็คติไฟร์มี ส่วนประกอบที่สำคัญคือ ไดโอด ซึ่งผลิตมาจากสารกึ่งตัวนำ จากแนวความคิดของ Aviram กับ Ratner ในปี 1974 ที่ได้ กล่าวถึงความเป็นไปได้ทางทฤษฎีในการนำโมเลกุลของสารอินทรีย์มาทำหน้าที่เป็นอุปกรณ์เร็คติไฟร์ ซึ่งโมเลกุลที่มาทำ หน้าที่แทนไดโอดนั้นต้องมีคุณสมบัติคล้ายกับรอยต่อฟี-เอ็นของไดโอด คือ โมเลกุลนั้นมีส่วนประกอบที่สำคัญ 3 ส่วนคือ ส่วนที่สามารถให้อิเล็กตรอนได้ดี(D) อีกส่วนหนึ่งของโมเลกุลสามารถรับอิเล็กตรอนได้ดี(A) โดยทั้งสองส่วนนั้นเชื่อมกัน ผ่านพันธะพาย(π) เป็นโมเลกุล D-π-A ในงานวิจัยนี้ได้ศึกษาโดยใช้โมเลกุลของสารโคพอลิเมอร์ (Fig.1) ซึ่งในการเตรียม เร็คติไฟร์จากโมเลกุลนั้นเตรียมด้วยเทคนิคของ Langmuir - Blodgett ได้การศึกษาความหนาของฟิล์มจากสารโคพอลิเมอร์ ด้วยเทคนิคของ การสะท้อนรังสีเอ็กซ์ และ ทำการศึกษาสมบัติความเป็นวงจรเร็คติไฟร์ของสารที่ใช้ โดยการวัดความสัมพันธ์ ระหว่าง กระแสไฟฟ้าที่ไหลออกจากโมเลกุล กับ ความต่างศักย์ที่ป้อนให้แก่วงจรเร็คติไฟร์จากโมเลกุล ในระบบสุญญากาศ ซึ่งพบความไม่สมมาตรของกระแสที่ไหลเมื่อให้แรงดันไบแอสตรง และไม่ไหลกับไบแอสกลับ

Abstract: A molecular rectifier, followed a prediction by Aviram and Ratner(Ref.1), is a molecule which allows the current to flow in a specific direction. This organic molecule behaves in a similar manner as the p-n junction in diode. The molecule consists of an electron donor (D) connected to an electron acceptor (A) through a π bridge (π). This is categorized as a "D- π -A" molecular rectifier. A polar monolayer of a side chain liquid crystal polymer containing the "D- π -A" rectifier component on the side chain was prepared at the gas-water interface. This film was subsequently being transferred onto a metal electrode was by horizontal deposition. X-ray reflectivity technique was revealed that the film was successfully transferred. Our preliminary study shows an asymmetry characteristic I-V curve

$$H_{3}C \xrightarrow{q} - (CH_{2})_{1}O \xrightarrow{} - ND_{2}$$
 0.5
 $H_{3}C \xrightarrow{q} - (CH_{2})_{1}O \xrightarrow{} - CH_{2}O$
 0.5
 0.5
 0.5

Fig 1. Molecule structure of employed copolymer.

Methodology: The monolayer of the side chain liquid crystalline polymer, cop11, was prepared by Lagmuir – Blodgett (LB) technique. The film was transferred onto the substrate via the horizontal deposition technique. A sandwiched film of cop11 with a very thickness, 5-20 layers, was prepared between two aluminum coated electrodes prior to an electrical investigation. The measurement was performed by applying a forward bias form 0 to 0.900 Volt and a reverse bias from 0.900 to –0.900 Volt with 0 0.001 Volt/step while the current passes through the polymer film was recorded.

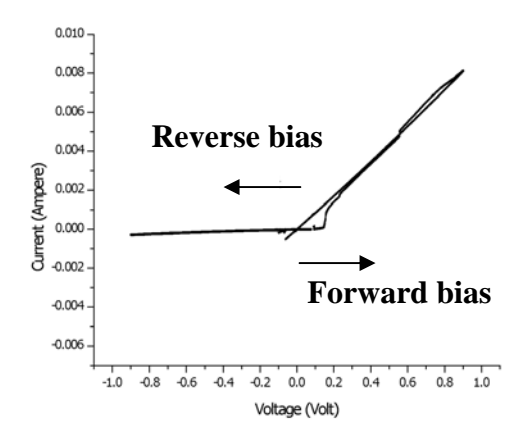


Fig 2. Typical measured current and applied voltage of Al |cop11|Al structure.

Results, Discussion and Conclusion: The measured current through the polymer film are increased linearly when applied forward bias is increased. The current is constantly decreased during the decrease forward bias with about the same rate and almost constant current exhibited for reversed bias. This probably dues to asymmetry of the molecular structure since the same metal contacts were used for electrical electrodes.

References: 1. Aviram and M. A. Ratner, Chem. Phys. Lett. 29, 277(1974).

- 2. R.M. Metzger, Mat. Sci and Eng C3, 277(1995).
- 3. Chen, W. Wang, App. Phys. Lett. 78, 3735(2001).
- 4. A. S. Martin, J. R. Sambles, Phy. Rev. Lett. 70, 218(1993).
- 5. Micheal C. Petty, Langmuir-Blodgett films an introduction, Cambridge University Press 1996.

Keywords: Molecular rectifier, diode, p-n junction

Acknowledgement: Research Project has been supported by Thailand Research Fund.

การศึกษาพฤติกรรมทางไฟฟ้าของฟิล์มบางโมเลกุลโคพอลิเมอร์ด้วยกล้องจุลทรรศน์แบบแรงอะตอมและกล้องจุลทรรศน์แบบ กระแสทันเนล

Electrical characteristic of monolayer film of a side chain liquid crystal copolymers studied by scanning tunneling microscopy and atomic force microscopy

อารีเฟ็น รัศมีศาสน์, ธนากร โอสถจันทร์, เติมศักดิ์ ศรีคิรินทร์ Areefen Rassamesard, Tanakorn Osotchan, Toemsak Srikhirin

Capability Building Unit of Nanoscience and Nanotechnology, Department of Physics, Faculty of Science, Mahidol University, Bangkok 10400, Thailand

E-mail address: fenmu@hotmail.com

บทคัดย่อ: ฟิล์มชั้นเดี่ยวของโมเลกุลโคพอลิเมอร์ (cop11) ที่ประกอบด้วยหมู่เมททิลีน 11 หมู่ โดยโมเลกุลมีอัตราส่วนของใน โตร ใบฟีนิล (NBP) และ เมท็อกซี อีท็อกซี เมท็อกซี ใบฟีนิล อย่างละ 50% เตรียมบนแผ่นผลึกซิลิกอนที่ทำให้เป็นไฮโดรโฟ บิก ด้วยเทคนิคของ เลงเมียร บลอดเจท (LB) บนผิวน้ำ โดยทำการเคลือบฟิล์มแบบแนวราบ ได้ศึกษาพื้นผิวของฟิล์มที่เตรียม มาด้วยกล้องจุลทรรศน์แบบแรงอะตอม(AFM)ในไดนามิกโมด ได้วัดสมบัติไฟฟ้าของฟิล์มโดยใช้กล้องจุลทรรศน์แบบ กระแสทันเนล (STM) โดยเข็มของ STM จะวางตัวอยู่เหนือผิวฟิล์มเล็กน้อยและจากผลการวัดความสัมพันธ์ระหว่าง กระแสไฟฟ้ากับความต่างศักย์ที่ป้อนเข้าไปพบว่าความต้านทานทางไฟฟ้าของฟิล์มชั้นโมเลกุลเดียวมีค่าน้อยกว่าฟิล์มสองชั้น ส่วนการใช้เครื่อง AFM วัดการนำไฟฟ้านั้นเข็มนำไฟฟ้าจะสัมผัสกับผิวฟิล์มโดยตรง จากการวัดคุณสมบัติทางไฟฟ้าของฟิล์ม 5 ชั้นโมเลกุลบนแผ่นผลึกซิลิกอน พบว่าความไม่สมมาตรของกระแสไฟฟ้าที่ความต่างศักย์ไฟฟ้าแบบตรงและแบบย้อนกลับ

Abstract: The monolayer Langmuir-Blodgett (LB) films of a side chain liquid crystal copolymer (cop11) with an 11-methylene spacer and a composition of 50% nitrobiphenyl (NBP) and 50% methoxy ethoxy methoxy biphenyl (MEMBP) were prepared from the gas water interface. This film was subsequently being transferred onto a hydrophobic silicon wafer substrate by horizontal deposition technique. The surface morphology of monolayer film was imaged by atomic force microscope (AFM) in dynamic mode. The current-voltage (I-V) characteristics of monolayer and double layers films were characterized by using scanning tunneling microscope (STM). It should be noticed that the STM tip stays with small distance on the film surface. The electric resistance for the monolayer is smaller than that for the double layer. For measuring the conductance by AFM, the AFM tip has to contact to the film surface. Then the conductive tip was biased by external voltage and current through the tip was measured to extract I-V characteristics from molecules at the local area of the surface. The electric characteristic for the 5 layer film by using conductive AFM exhibits the antisymmetric current between forward and reverse bias.

Methodology: The monolayer of the side chain liquid crystalline copolymer, cop11 as shown in Fig.1., was prepared by LB technique. A multilayer film was transferred onto the substrate via the horizontal deposition technique. The LB monolayer was spread from a solution of 0.3 mg/ml cop11 in chloroform. Isotherm of cop11 as shown in Fig.2., exhibits a relatively steep rise, which demonstrates a close packing of the molecules. The mean molecular area of 23 nm^2 was estimated. After spreading the film was compressed at a speed of 10 mm/s until the surface pressure of 25 mN/m achieved then kept at this pressure for 1500 second. The surface of silicon wafer was washed with acetone, methanol and chloroform in ultrasonic bath respectively, and then cleaned silicon wafer was treated in hexamethyldisiloxane saturated vapor for 24 hours in desicators. The monolayer LB film was deposited on hydrophobic silicon wafer substrate by horizontal dipping. Before I-V characteristics were measured by AFM, the surface morphology of cop11 was measured in the area of $100 \times 100 \text{ nm}^2$. The I-V characteristics were measured at each point on the film surface with gold coated conductive tip. For I-V measurement with STM, an area of $100 \times 100 \text{ nm}^2$ was scanned with bias voltage of 0.5 V and tunneling current of 0.1 nA. The electrical properties of the cop11 LB films can examined with conductive AFM tip. The applied voltage can be varied form -10 to +10 volt and the measured current has been limited at $\pm 100 \text{ nA}$.

$$H_{\mathcal{C}} = (0+)_{11}0$$
 0.5
 $H_{\mathcal{C}} = (0+)_{11}0$
 0.5
 0.5
 0.5
 0.5
 0.5

Fig.1. Chemical structure of cop11.

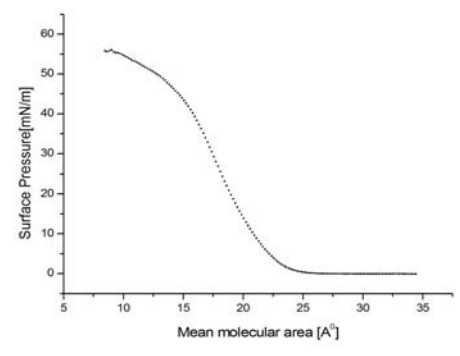


Figure.2. Surface pressure – area per molecule of cop11 at the air-water interface on water (150 µl of 0.30 mg/ml in chloroform with pure water subphase).

Results, Discussion and Conclusion:

The surface morphology of monolayer cop11 LB film compared with hydrophobic silicon wafer were showed in Fig.3. and Fig.4. For hydrophobic silicon wafer there are small valleys. The morphology of bare silicon is similar to that of hydrophobic silicon wafer.

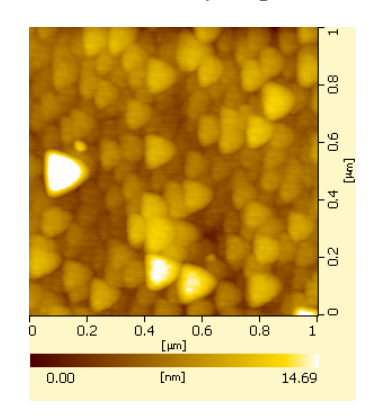


Fig.3. AFM images of hydrophobic silicon wafer substrate.

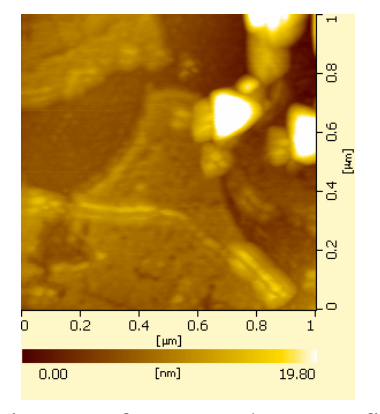


Fig.4. AFM images of am monolayer LB film of cop11 deposited on hydrophobic silicon wafer substrate.

In isotherm of cop11 on pure water as shown in Fig.2., the steeply inclining part of the curve corresponds to the formation of a solid monolayer of cop11 molecules on the water surface. The isoterm showed area per molecule about 23 nm^2 and phase transition of LB film occur at surface pressure of 4.2 and 45.3 mN/m.

The I-V characteristics of bare silicon wafer, hydrophobic silicon wafer, cop11 LB film monolayer and cop11 LB film 2 layers showed in Fig.5. For applied voltage of +1 volt the measured current through bare silicon wafer, hydrophobic silicon wafer, cop11 LB film monolayer and cop11 LB film 2 layers, are 0.174, 0.925, 1.81, 0.529 nA, respectively. For STM measurement the electrical resistance for the monolayer is smaller than that for the double layers.

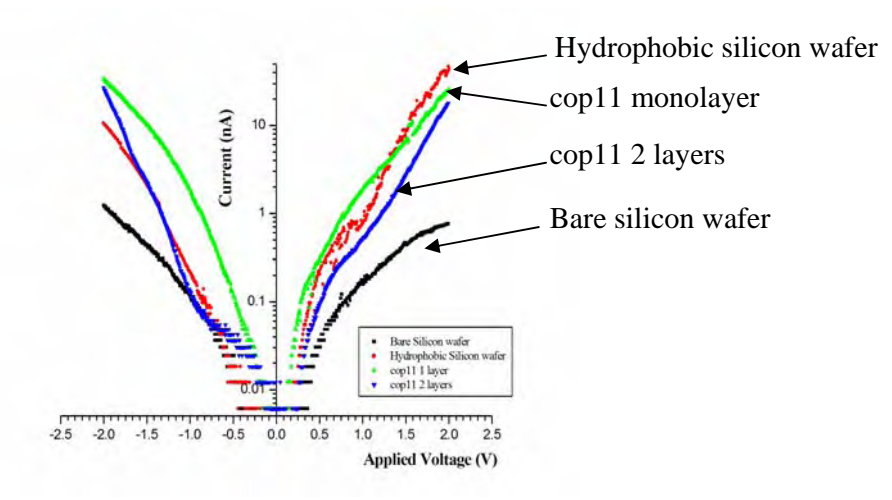


Fig.5. I-V plot for bare silicon wafer, hydrophobic silicon wafer, cop11 LB film monolayer and cop11 LB film 2 layers, respectively, measured by STM.

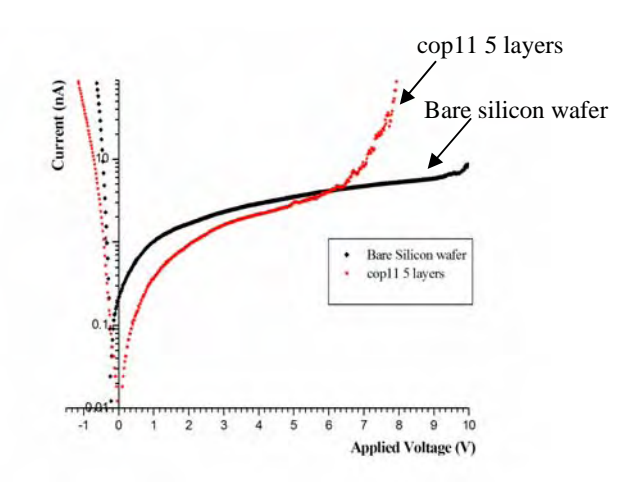


Fig.6. I-V characteristic of cop11 5 layers and bare silicon wafer measured by using conductive tip of AFM.

By using conductive AFM tip the I-V characteristics of bare silicon wafer and 5 layers cop11 LB film showed in Fig.6. . The current at +7.5 volt are 4.84, 21.8 nA for bare silicon wafer and cop11 5 layer film, respectively. The conductive AFM tip measurement indicates the strong asymmetric for the I-V curve of cop11 LB film.

References:

- 1. Aviram and M. A. Ratner, Chem. Phys. Lett. 29, 277(1974).
- 2. N.G Semaltianos, Chem. Phys. Lett 329, 76-83(2000).
- 3. Y.J. Zhang et al., Syntetic Metals, 128, 43-46(2002).

Keywords: Molecular rectifier, LB, AFM, STM

Acknowledgement: Project has been supported by Thailand Research Fund.

ความสัมพันธ์ของโครงสร้างและสมบัติทางอิเล็กทรอนิกส์ต่อการเปล่งแสงของโพลิเมอร์ผสมของโพลิ ฟลูออรีนและแอนทราซีน

CONFORMATION AND ELECTRONIC STRUCTURE RELATE EMISSION SPECTRA FOR POLYFLUORENE AND ANTHRACENE COPOLYMER

ริติมา มธุร a^1 , ประฐากรณ์ ศรีสงคราม 1 , สมพร มณีทูล 1 , อนุรักษ์ อุคมเวช 1 , ธีรเกียรติ์ เกิดเจริญ 1 , เติมศักดิ์ ศรีคิรินทร์ 1 และ ธนากร โอสถจันทร์ 1

<u>Thitima Maturos</u>¹, Prathakon Srisongkam¹, Somporn Maneetoon¹, Anurak Udomvech¹, Teerakiat Kerdcharoen¹, Toemsak Srikhirin¹ and Tanakorn Osotchan¹

¹Capability Building Unit in Nanoscience and Nanotechnology, Department of Physics, Faculty of Science, Mahidol University, Bangkok 10400, Thailand;

E-mail address: maturos88@yahoo.com

บทคัดย่อ : โครงสร้างที่สถานะพื้นของโพลีฟลูออรินและโพลิเมอร์ผสมของโพลีฟลูออรินและแอนทราซิน ได้คำนวณด้วยวิธี senienpinical และ ab initio พบว่าสายโซ่โของพลิเมอร์ผสมมีลักษณะที่บิดมากกว่ากรณี ของสายโซ่ของโพลีฟลูออริน ซึ่งมีผลทำให้การเข้ามาเกาะกันระหว่างสายโซ่ของโพลิเมอร์ข้างเคียงเป็นไปได้ ยากขึ้น ดังนั้นการผสมแอนทราซินในโพลีฟลูออรินจึงเป็นการลดการเปล่งแสงที่เกิดจากเกาะกันของสายโซ่ โพลิเมอร์ ได้คำนวณสมบัติทางอิเล็กทรอนิกส์ที่สถานะพื้นโดยแบบจำลองโมเลกุลที่ใช้ทฤษฎีฟังก์ชันความ หนาแน่น โดยพบว่าเมื่อเพิ่มสัดส่วนของแอนทราซินในโพลิเมอร์ผสมค่าช่องว่างระหว่างแถบพลังงานจะมีค่า ลดลงซึ่งสอดคล้องกับผลการทดลอง

Abstract: The conformation and the ground-state electronic structure of 9, 9 Di (2' ethylhexyl) 2, 7 dibromofluorene (BEH-PF) and copolymer of BEH-PF and dibromo(anthracene) were studied by semiempirical and *ab initio* at various levels of calculation. The conformational analysis results show that the copolymer chain are more twisting than in the case of homopolymer due to the out of plane of anthracene unit. This leads to the reducing of excimer emission from the copolymer. The calculated electronic structure of the copolymer by density functional theory shows that the increasing of anthracene composition leads to the lowering of energy gap which is consistent with the experimental results.

Introduction: Polyfluorene is one of the interesting polymer for its application in organic light emitting devices (OLED) because of its high luminescence intensity in the blue region [1]. However, the important drawback for this polymer is the long wavelength emission at about 500 nm upon heating or passing the current. These long wavelength emissions were defined as an excimer emission which is the result of the polymer chain packing [2]. Copolymerization of polyfluorene with anthracene is one approach that can be used to suppress these excimer emissions and to improve the stability and emission color [3]. By-product of copolymerization process may lead to the color tuning of the emitting spectra due to the change of conjugation length in the polymer chain [4].

In this paper we investigated conformation of 9, 9- Di (2 - ethylhexyl) 2, 7 dibromofluorene (BEH-PF) and copolymer of BEH-PF and dibromo(anthracene). The relation of the conformation and the emission spectra from the experimental results were compared. The electronic structure of the polymer were examined and also compared with the experimental results.

Methodology: The molecular structures of the BEH-PF were modified by replacing the ethyl group at the 9 position to reduce the calculation time. Conformational analysis of PF dimers and BEH-PF-co-ANT was obtained by using semiempirical Austin Model 1 (AM1) and *ab initio* calculation at HF/3-21G* and HF/6-31G* levels. The AM1 optimized structure were used to find the ground-state energy by using B3LYP/6-31G* level. The energy gap between HOMO and LUMO of the polymer were obtained by plotting the LUMO-HOMO energies of monomer through tetramer against inverse chain lengths and extrapolating to energy gap at the infinite chain length. All the calculations were performed by using Gaussian 98 program.

Results and discussions: The conformational analysis of PF dimers from fig.1 shows the suitable conformation with the torsion angle of the dimer equal to 42 degrees in AM1 level and equals to 50 and 45 degrees at HF/3-21G* and HF/6-31G* levels, respectively. For PF-co-ANT the preferable torsion angle between PF and ANT at AM1 levels is in the range 60-115 degrees and equal to 90 degrees at the HF/3-21G* and HF/6-31G* levels. The conformational analysis indicates that when anthracene is incorporated to the polyfluorene chain it tends to lie in the out of plane structure. Therefore, with comparing to the homopolymer chain, the packing of the neighbour copolymer chain is more difficult. Comparing this calculated result with the emission spectra from the spin cast film, it shows that the excimer peaks from the PF-co-ANT are located at the shorter wavelength compare with the PF spectra. These can be infered that the out of plane of anthracene unit encourage the reduction of the excimer emission. The electronic structure obtained by B3LYP/6-31G*//AM1 shows that the increasing anthracene composition leads to the lowering of energy gap as shown in table 1. This result is consistent with the experimental red shift emission of the PF-co-ANT.

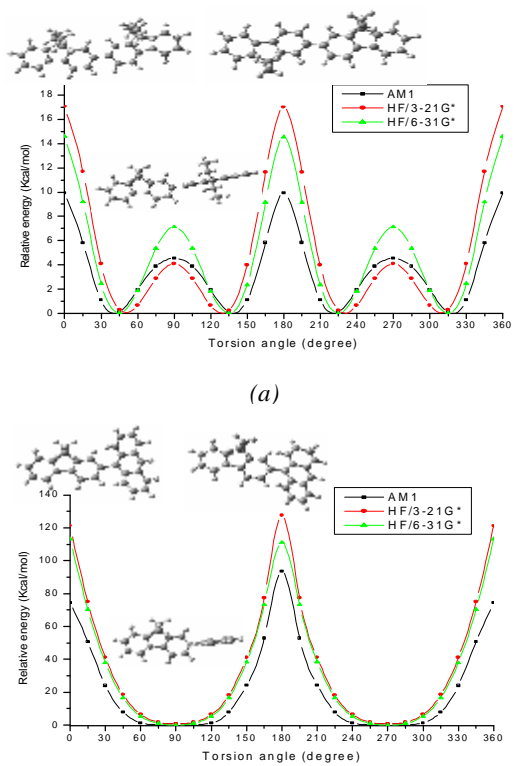


Fig.1 Potential energy curves of (a) PF and (b) PF-co-Anthracene at AM1 and ab initio with HF/3-21G* and HF/6-31G* basis sets

% Anthracene	Extraporated energy gap (eV)	1 _{max emission} (solution)	I _{excimer emission} (film)
0	3.54	415 nm	500
30	3.37	443 nm	490
50	3.05	-	-
60	-	443 nm	490

Table 1 Extraporated calculated energy gap and measured emission spectra for BEH-PF and dibromo(anthracene) copolymer

Reference:

- 1. M. Kreyenschmidt, G. Klaerner, T. Fuhrer, J. Ashenhurst, S. Karg, W.D. Chen, V.Y. Lee, J.C. Scott and R.D. Miller, *Macromolecules*, 1998, *31*, 1099
- 2. Do-Hoon Hwang, Nam Sung Cho, Byung-Jun Jung, Hong-Ku Shim, Jeong-Ik Lee, Lee-Mi Do, Taehyoung Zyung, *Optical Materials*, 2002, *21*, 199
- 3. G. Klaerner, M.H. Davey, W.D. Chen, J.C. Scott and R.D. Miller, Adv. Mater, 1998, 10, 993
- 4. Wei Yang, Qiong Hou, Chuanzhen Liu, Yuhua Niu, Jian Huang, Renqiang Yang and Yong Cao, *J. Mater. Chem.*, 2003, 13, 1351

Keywords: Polyfluorene, OLED, conformational analysis

Acknowledgement: The research has been supported by National Metal and Materials Technology Center (MTEC).